



National Library
of Canada

Bibliothèque nationale
du Canada

Canadian Theses Service

Services des thèses canadiennes

Ottawa, Canada
K1A 0N4

CANADIAN THESES

THÈSES CANADIENNES

NOTICE

The quality of this microfiche is heavily dependent upon the quality of the original thesis submitted for microfilming. Every effort has been made to ensure the highest quality of reproduction possible.

If pages are missing, contact the university which granted the degree.

Some pages may have indistinct print especially if the original pages were typed with a poor typewriter ribbon or if the university sent us an inferior photocopy.

Previously copyrighted materials (journal articles, published tests, etc.) are not filmed.

Reproduction in full or in part of this film is governed by the Canadian Copyright Act, R.S.C. 1970, c. C-30. Please read the authorization forms which accompany this thesis.

**THIS DISSERTATION
HAS BEEN MICROFILMED
EXACTLY AS RECEIVED**

AVIS

La qualité de cette microfiche dépend grandement de la qualité de la thèse soumise au microfilmage. Nous avons tout fait pour assurer une qualité supérieure de reproduction.


S'il manque des pages, veuillez communiquer avec l'université qui a conféré le grade.

La qualité d'impression de certaines pages peut laisser à désirer, surtout si les pages originales ont été dactylographiées à l'aide d'un ruban usé ou si l'université nous a fait parvenir une photocopie de qualité inférieure.

Les documents qui font déjà l'objet d'un droit d'auteur (articles de revue, examens publiés, etc.) ne sont pas microfilmés.

La reproduction, même partielle, de ce microfilm est soumise à la Loi canadienne sur le droit d'auteur, SRC 1970, c. C-30. Veuillez prendre connaissance des formules d'autorisation qui accompagnent cette thèse.

**LA THÈSE A ÉTÉ
MICROFILMÉE TELLE QUE
NOUS L'AVONS REÇUE**

 National Library
of Canada

Bibliothèque nationale
du Canada

0-315-24865-3

Canadian Theses Division

Division des thèses canadiennes

Ottawa, Canada
K1A 0N4

PERMISSION TO MICROFILM — AUTORISATION DE MICROFILMER

- Please print or type — Écrire en lettres moulées ou dactylographier

Full Name of Author — Nom complet de l'auteur

Varadaraja Sarma. VORUGANTI.

Date of Birth — Date de naissance

August 11, 1940

Country of Birth — Lieu de naissance

INDIA

Permanent Address — Résidence fixe

7144-178 Street
Edmonton, Alberta
T5T 3E9

Title of Thesis — Titre de la thèse

Corrosion of a Steel in Aqueous $H_2O + CO_2$ Systems from 100 to 300°C

University — Université

University of Alberta

Degree for which thesis was presented — Grade pour lequel cette thèse fut présentée

M.Sc

Year this degree conferred — Année d'obtention de ce grade

1984

Name of Supervisor — Nom du directeur de thèse

Dr. S.A. Bradford

Permission is hereby granted to the NATIONAL LIBRARY OF CANADA to microfilm this thesis and to lend or sell copies of the film.

The author reserves other publication rights, and neither the thesis nor extensive extracts from it may be printed or otherwise reproduced without the author's written permission.

L'autorisation est, par la présente, accordée à la BIBLIOTHÈQUE NATIONALE DU CANADA de microfilmer cette thèse et de prêter ou de vendre des exemplaires du film.

L'auteur se réserve les autres droits de publication; ni la thèse ni de longs extraits de celle-ci ne doivent être imprimés ou autrement reproduits sans l'autorisation écrite de l'auteur.

Date

August 20, 1984

Signature

V. Varadaraja Sarma

THE UNIVERSITY OF ALBERTA

Corrosion of Steel in Aqueous $H_2O + CO_2$ Systems from 100
to 300°C

by



Varadarajasarma Voruganti

A THESIS

SUBMITTED TO THE FACULTY OF GRADUATE STUDIES AND RESEARCH
IN PARTIAL FULFILMENT OF THE REQUIREMENTS FOR THE DEGREE
OF MASTER OF SCIENCE

IN

METALLURGICAL ENGINEERING

DEPARTMENT OF MINERAL ENGINEERING

EDMONTON, ALBERTA

FALL 1984

THE UNIVERSITY OF ALBERTA

RELEASE FORM

NAME OF AUTHOR Varadarajasarma Voruganti
TITLE OF THESIS Corrosion of a Steel in Aqueous H₂O +
 CO₂ Systems from 100 to 300°C
DEGREE FOR WHICH THESIS WAS PRESENTED MASTER OF SCIENCE
YEAR THIS DEGREE GRANTED FALL 1984

Permission is hereby granted to THE UNIVERSITY OF
ALBERTA LIBRARY to reproduce single copies of this
thesis and to lend or sell such copies for private,
scholarly or scientific research purposes only.

The author reserves other publication rights, and
neither the thesis nor extensive extracts from it may
be printed or otherwise reproduced without the author's
written permission.

(SIGNED) *V. Varadarajasarma*

PERMANENT ADDRESS:

7144-178 Street
Edmonton, Alberta
T5T 3E9

DATED *August 21,* 1984

THE UNIVERSITY OF ALBERTA
FACULTY OF GRADUATE STUDIES AND RESEARCH

The undersigned certify that they have read, and recommend, to the Faculty of Graduate Studies and Research, for acceptance, a thesis entitled Corrosion of a Steel in Aqueous $H_2O + CO_2$ Systems from 100 to 300°C submitted by Varadarajasarma Voruganti in partial fulfilment of the requirements for the degree of Master of Science in Metallurgical Engineering.

Samuel A. Bradford
.....

Supervisor

B. M. Pallett
.....

James A. Plumb
.....

Date..... *August 3, 1984*

Dedication

To my mother, Sam my wife, Sam my friend and Sam my teacher.

Abstract

The injection of steam and CO₂ mixtures at about 300°C and high pressures is likely in the near future for the recovery of viscous-oil deposits. The attendant problems of corrosion of steel from the high temperature condensates are not well known. Work done in the past deals with carbonic acid corrosion up to 120°C only.

In this work the problem was studied for an API pipeline steel X-70 by

1. Weight-loss tests in autoclaves at 200 and 300°C.
2. X-ray diffraction and scanning electron microscopy of the surface films.
3. Potentiodynamic polarization runs from 100-250°C.
4. U-bend stress corrosion cracking tests at 150°C.

The carbonic acid corrosion of the X-70 steel was found to be low, between 5-10 mpy, in the temperature range of 200-300°C, and the presence of ammonium carbonate or bicarbonate lowers the corrosion rates to about 1 mpy. The surface film formed at high temperature and/or high pH was a mixture of magnetite and siderite and was more protective than the low temperature and/or low pH film of hematite and siderite. No immediate danger of stress corrosion cracking was revealed.

Acknowledgements

I would like to express my sincere thanks to my supervisor Dr. S.A. Bradford for his vision, help, encouragement and guidance.

I would also like to thank the technical staff of the Department of Mineral Engineering for their ready help, and amongst them especially :

1. Mrs. Christina Barker
2. Mr. Tom Foreman
3. Mr. Bob Konzuk and
4. Mr. Henry Skrzypek

Also, I would like to extend my thanks to the Alberta Research Council for some of the tests done by their staff as a part of this study.

This work was supported by a grant from the Petroleum Aid to Education trust fund.

Table of Contents

Chapter		Page
1.	Introduction	1
1.1	Enhanced oil recovery operations.	1
1.2	Need for corrosion studies	2
2.	Theory	4
2.1	Electrochemistry	4
2.1.1	Corrosion tendency and electrode potentials	4
2.1.2	Cell potential and EMF series	5
2.1.3	Pourbaix diagrams	7
2.1.4	Electrode kinetics	7
2.1.4.1	Exchange current density	7
2.1.4.2	Polarization	8
2.1.4.3	Activation polarization	8
2.1.4.4	Concentration polarization	9
2.1.4.5	Combined polarization	10
2.1.5	Mixed potential theory	11
2.1.5.1	Mixed electrodes	11
2.1.5.2	1. Pure iron in aqueous solutions with no oxygen or oxidizing agents.	12
2.1.5.3	2. Iron in aqueous solutions in presence of oxidizers or oxygen. ..	13
2.2	Passivity	14
2.3	Effect of high temperatures and pressures	16
2.4	Corrosion rate measurements	18
2.4.1	Weight loss tests	18
2.4.2	Electrochemical methods	19

2.4.2.1	General rate equation	19
2.4.2.2	Rigorous method, known Tafel slopes	20
2.4.2.3	Large potential approximation or Tafel extrapolation	21
2.4.2.4	Small potential approximation	21
2.4.2.5	Rigorous general method or 3 point method	22
2.4.3	Stress corrosion cracking	23
2.4.4	Testing for SCC	27
3.	Literature Survey	29
3.1	Aqueous environments at ordinary temperatures ...	29
3.1.1	Effect of dissolved oxygen	29
3.1.2	Effect of temperature	30
3.1.3	Effect of pH	31
3.1.4	Effect of dissolved carbon dioxide	32
3.2	High temperature water, steam and carbon dioxide	37
3.3	High temperature water and carbon dioxide	38
3.3.1	Effect of dissolved oxygen	39
3.3.2	Presence of carbon dioxide	40
3.3.3	Control of feed water in boilers	41
3.3.3.1	Addition of alkali	42
3.3.3.2	Use of inhibitors	43
3.4	Carbonic acid corrosion in gas condensate wells .	45
3.5	Corrosion characteristics in carbonate and bicarbonate solutions	47
3.6	Summary of literature survey	51
4.	Materials, Equipment, and Experimental Procedure	54

4.1 Steel tested	54
4.2 Chemicals used	55
4.3 Weight loss tests	55
4.4 X-ray diffraction studies	58
4.5 Scanning electron microscopy	59
4.6 Polarization curves	60
4.6.1 Potentiostat unit	60
4.6.2 Corrosion cell arrangement	61
4.7 SCC tests	64
5. Tests, Results and Discussion	66
5.1 Tests and results	66
5.1.1 Coupon weight loss tests in autoclaves	66
5.1.2 X-ray diffraction studies	69
5.1.3 Scanning electron microscope studies	69
5.1.4 Potentiodynamic polarization studies	70
5.1.5 Tests for SCC	73
5.2 Discussion of results	75
5.2.1 Weight loss tests	75
5.2.2 X-ray diffraction studies	77
5.2.3 SEM studies	78
5.2.4 Potentiodynamic polarization curves	79
5.2.5 Tests for SCC	85
5.2.6 Summary of discussion of results	86
6. Conclusions and Recommendations	89
6.1 Conclusions	89
6.2 Recommendations for future work	90
References	155

List of Tables

Table	Page
1. Comparison of Experimental and Calculated Corrosion Rates of Grit-Blasted Samples under Various Conditions (from DeWaard and Milliams ¹⁸)	92
2. Metal Loss, Magnetite Film Thickness and Adherency for Carbon Steel in Water at 310°C (from Gadiyar et al. ²⁴)	93
3. Solubility of Carbon Dioxide in Distilled Water at High Temperatures and High Pressures (from Nesbitt ²⁸)	94
4. Chemical Composition of the X-70 Steel Used for Testing	95
5. Mechanical Properties of the X-70 Steel Used for Testing	96
6. Corrosion Rates from Weight-loss Tests in Autoclaves	97
7. Scale Composition from X-ray ⁹ Diffraction Studies	99
8. Corrosion Characteristics from Polarization Curves	101

List of Figures

Figure		Page
1.	Pourbaix diagram for the system Fe-H ₂ O at 25°C (from West ⁴)	102
2.	Hydrogen-hydrogen ion exchange current densities (from Fontana and Greene ³)	102
3.	Activation polarization curve of a hydrogen electrode (from Fontana and Greene ³)	103
4.	Effect of environmental variables on concentration polarization curve (from Fontana and Greene ³)	103
5.	Combined polarization curve (from Fontana and Greene ³)	104
6.	Electrode kinetic behavior of pure iron in acid solution - schematic (from Fontana and Greene ³)	104
7.	Effect of oxygen on the corrosion of iron in neutral to alkaline solutions	105
8.	Corrosion of metal ^M under diffusion control (from Fontana and Greene ³)	105
9.	Typical anodic dissolution behavior of an active-passive metal (from Fontana and Greene ³)	106
10.	Behavior of an active-passive metal under corrosive conditions (from Fontana and Greene ³)	106
11.	Potential-pH diagrams for Fe-H ₂ O at 250 and 350°C according to Lewis (from Mann ⁷)	107
12.	Corrosion-immunity-passivation diagram for Fe-H ₂ O at 300°C (from Mann ⁷)	107
13.	Schematic relationships showing the effects of environment and alloy additions upon the anodic polarization curve (from Lumsden and Staehle ⁸)	108
14.	Applied-current linear-polarization curve (from Fontana and Greene ³)	108

Figure	Page
15. Effect of oxygen concentration on mild steel in slowly moving distilled water at 25°C in a 48 hour test (from Uhlig ¹⁵)	109
16. Effect of temperature on corrosion of iron in water containing dissolved oxygen (from Uhlig ¹⁵)	109
17. Effect of pH on corrosion of mild steel (from Uhlig ¹⁶)	110
18. Corrosion of mild steel as a function of dissolved CO ₂ and O ₂ concentration (from Uhlig ¹⁶)	110
19. Solubility of CO ₂ in distilled water (from Mungan ²⁷)	111
20. Corrosion of iron in water at 310°C at various values of pH measured at 25°C (from Uhlig ²⁰)	111
21. Potentiostatic anodic polarization curves of iron in deaerated and air saturated solutions of 0.1 M Na ₂ CO ₃ . (from Thomas et al. ³³)	112
22. Potentiostatic anodic polarization curves of iron in deaerated NaHCO ₃ solutions. (from Thomas et al. ³³)	112
23. Cathodic potentiodynamic polarization curves of mild steel in NaHCO ₃ solutions (from Thomas and Davies ³⁴)	113
24. Anodic polarization of Fe in 0.75 M KHCO ₃ + 0.75 M K ₂ CO ₃ (pH 8.8) at a scanning rate of 10 mV/s. (from Davies and Burstein ³⁵)	113
25. Polarization curves and SCC test results for mild steel in 1 N Na ₂ CO ₃ + 1 N NaHCO ₃ at 90°C (from Sutcliffe et al. ³⁶)	114
26. Effect of temperature upon SCC of mild steel in constant strain rate tests at various potentials in 1 N Na ₂ CO ₃ + 1 N NaHCO ₃ (from Sutcliffe et al. ³⁶)	115
27. Microstructure of X-70 steel with 2% nital as the etchant. X500	116

Figure	Page
28. 2000 mL Parr pressure reactor with its heating arrangement and automatic temperature controller	116
29. 2000 mL Parr pressure reactor head assembly and assembled bomb	117
30. Weight-loss test coupons assembled between 2 Teflon discs	117
31. Weight-loss test coupon assembly mounted onto the head of 1000 mL autoclave	118
32. The potentiostat unit along with the corrosion cell	118
33. Corrosion cell assembly	119
34. Salt bridge and its connection to the working electrode autoclave. Schematic.	119
35. Typical U-bend specimens (ASTM G-30)	120
36. U-bend specimens with Teflon sleeves and bolts in position	121
37. U-bend specimens assembled together by welding a rod to the bolt heads	121
38. Surface film in H ₂ O + CO ₂ at 200°C after one week. X560	122
39. Surface film in H ₂ O + CO ₂ at 200°C after one week. X1100	122
40. Surface film in H ₂ O + CO ₂ at 200°C after 7 weeks. X560	123
41. Surface film in H ₂ O + CO ₂ at 200°C after 7 weeks. X1100	123
42. Surface film in H ₂ O + CO ₂ at 200°C after 2 weeks (top side of the sample, freely exposed to the solution). X560	124
43. Surface film in H ₂ O + CO ₂ at 200°C after 2 weeks (top side of the sample, freely exposed to the solution). X1100	124

44.	Surface film in $\text{H}_2\text{O} + \text{CO}_2$ at 200°C after 2 weeks (bottom side of the sample, not freely exposed to the solution). X560	125
45.	Surface film in $\text{H}_2\text{O} + \text{CO}_2$ at 200°C after 2 weeks (bottom side of the sample, not freely exposed to the solution). X1100	125
46.	Surface film in $\text{H}_2\text{O} + \text{CO}_2$ at 300°C after one week. X560	126
47.	Surface film in $\text{H}_2\text{O} + \text{CO}_2$ at 300°C after one week. X1100	126
48.	Surface film in $\text{H}_2\text{O} + \text{CO}_2$ at 300°C after five weeks. X560	127
49.	Surface film in $\text{H}_2\text{O} + \text{CO}_2$ at 300°C after five weeks. X1100	127
50.	Surface film in 1 M $\text{NH}_4\text{HCO}_3 + \text{CO}_2$ at 300°C after one week. X560	128
51.	Surface film in 1 M $\text{NH}_4\text{HCO}_3 + \text{CO}_2$ at 300°C after one week. X1100	128
52.	Surface film in 1 M $\text{NH}_4\text{HCO}_3 + \text{CO}_2$ at 300°C after 3 weeks. X1100	129
53.	Surface film in 1 M $\text{NH}_4\text{HCO}_3 + \text{CO}_2$ at 300°C after 3 weeks. X1800	129
54.	Surface film in 1 M NH_4HCO_3 at 200°C after one week. X560	130
55.	Surface film in 1 M NH_4HCO_3 at 200°C after one week. X1100	130
56.	Surface film in 1 M NH_4HCO_3 at 200°C after 30 days. X560	131
57.	Surface film in 1 M NH_4HCO_3 at 200°C after 30 days. X1100	131
58.	Surface film in 1 M NH_4HCO_3 at 300°C after one week. X560	132
59.	Surface film in 1 M NH_4HCO_3 at 300°C after one week. X1100	132

Figure	Page
60. Surface film in 1 M NH_4HCO_3 at 300°C after 2 weeks. X1100	133
61. Surface film in 1 M NH_4HCO_3 at 300°C after 2 weeks. X1800	133
62. Surface film in 1 M $(\text{NH}_4)_2\text{CO}_3$ at 200°C after 4 weeks. X560	134
63. Surface film in 1 M $(\text{NH}_4)_2\text{CO}_3$ at 200°C after 4 weeks. X1100	134
64. Surface film in 1 M NH_4HCO_3 + 1 M NH_4OH at 200°C after one week. X560	135
65. Surface film in 1 M NH_4HCO_3 + 1 M NH_4OH at 200°C after one week. X1800	135
66. Surface film in 1 M NH_4HCO_3 + 1 M NH_4OH at 200°C after 4 weeks. X560	136
67. Surface film in 1 M NH_4HCO_3 + 1 M NH_4OH at 200°C after 4 weeks. X1100	136
68. Potentiodynamic polarization curve in $\text{H}_2\text{O}^{\text{c}}$ + CO_2 at 100°C.	137
69. Potentiodynamic polarization curve in H_2O + CO_2 at 150°C.	138
70. Potentiodynamic polarization curve in H_2O + CO_2 at 200°C.	139
71. Potentiodynamic polarization curve in H_2O + CO_2 at 250°C.	140
72. Potentiodynamic polarization curve in 1 M NH_4HCO_3 + CO_2 at 100°C.	141
73. Potentiodynamic polarization curve in 1 M NH_4HCO_3 + CO_2 at 150°C.	142
74. Potentiodynamic polarization curve in 1 M NH_4HCO_3 + CO_2 at 200°C.	143
75. Potentiodynamic polarization curve in 1 M NH_4HCO_3 + CO_2 at 250°C.	144
76. Potentiodynamic polarization curve in 1 M NH_4HCO_3 at 100°C.	145

Figure	Page
77. Potentiodynamic polarization curve in 1 M NH_4HCO_3 at 150°C.	146
78. Potentiodynamic polarization curve in 1 M NH_4HCO_3 at 200°C.	147
79. Potentiodynamic polarization curve in 1 M NH_4HCO_3 at 250°C.	148
80. Potentiodynamic polarization curve in 1 M NH_4HCO_3 + 1 M NH_4OH at 100°C.	149
81. Potentiodynamic polarization curve in 1 M NH_4HCO_3 + 1 M NH_4OH at 150°C.	150
82. Potentiodynamic polarization curve in 1 M NH_4HCO_3 + 1 M NH_4OH at 200°C.	151
83. Potentiodynamic polarization curve in 1 M NH_4HCO_3 + 1 M NH_4OH at 250°C.	152
84. Pitting on the sample after polarization run in H_2O + CO_2 at 100°C.	153
85. Corrosion products at 150°C . a. Top: mainly hematite at high potential b. Bottom: mainly magnetite at low potential.	153
86. Pitting on the U-bend SCC sample in H_2O + CO_2 at 150°C after one week.	154

1. Introduction

Steel is extensively used in oil and gas recovery operations. The problems of corrosion and the need for protection in these operations are well recognized. With the development of technology for increased recovery from existing wells and development of new deposits which were once considered not feasible, materials are subjected to more aggressive environments and severe working conditions. Material selection and protection against corrosion is critical for the success of these operations.

1.1 Enhanced oil recovery operations.

It is reported that the average production from a crude oil well is about 34% of the original oil in place'. The importance of enhanced oil recovery (EOR) can be dramatized by the statement that an increase of 1% in recovery in the U.S. would add 4 billion barrels of crude oil, and a 6% increase will make them free from dependence on oil from Middle-East countries'.

Of the various EOR methods currently in practice, thermal recovery using steam injection is the most widely used. Steam injection is a powerful method especially for heavy oil reservoirs, and accounts for well over 500,000 barrels per day (b/d) of heavy oil world wide² (U.S.A. 300,000 b/d, Canada 15,000 b/d). The next most promising method is carbon dioxide flooding. The usual temperature range for CO₂ flooding is 40-70°C.

In view of very viscous oils found in deposits such as tar sands, and other parameters involved, it is expected that there will be many projects in the near future combining the two most powerful EOR techniques. Injection of steam and CO_2 , either together or alternately at temperatures and pressures up to 300°C and 2000 psi respectively, is likely to take place in the near future.

1.2 Need for corrosion studies

Obviously such an aggressive approach for EOR calls for an understanding of the corrosion characteristics of conventional materials in the new operating conditions before deciding to extend their usage or replace with more costly alloys.

Extensive literature is available about corrosion of mild steels in high temperature water and steam in boilers. Here the problem is mainly due to the presence of trace amounts of dissolved oxygen and CO_2 in the feed water. The problem is controlled by efficient deaeration techniques and addition of inhibitors and alkalies to scavenge the remaining traces of oxygen and neutralize the carbonic acid (formed in the condensers below 120°C due to the dissolution of CO_2 in the condensed steam). Also, carbonic acid corrosion in high pressure gas wells is widely recognized and some literature is available on the causes and methods of protection. The literature available on carbonic acid is confined to temperatures below 120°C and lower pressures

which are applicable to gas condensate wells.

As ammonia is likely to be the prime candidate for corrosion prevention, ammonium bicarbonate and carbonate are likely to be present in the condensates formed at high temperatures and pressures. The studies of corrosion and stress corrosion cracking associated with carbonate and bicarbonate environments, available in the literature, are limited to only atmospheric pressures and temperatures up to 90°C.

The present thesis makes a preliminary study of corrosion characteristics of an API pipeline steel X-70 in some of the environments and conditions applicable to the steam and CO₂ injection systems at high temperatures and pressures.

2. Theory

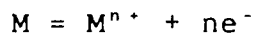
2.1 Electrochemistry

Corrosion is the destructive attack of a metal by chemical or electrochemical reaction with its environment. Corrosion in aqueous solution is usually electrochemical in nature.

2.1.1 Corrosion tendency and electrode potentials

The tendency for any chemical reaction to proceed is measured by the Gibbs free energy change ΔG . The more negative the value of ΔG , the greater is the tendency for the reaction to take place. If ΔG is negative, the reaction rate may be rapid or slow and is governed by the electrode kinetics.

In view of the electrochemical nature of corrosion, the corrosion reaction of a metal M is usually represented as



where n is the number of electrons or chemical equivalents taking part in the reaction.

The tendency to corrode is normally expressed in terms of the electromotive force (emf) of the corrosion cells that are an integral part of a corrosion process. The free energy change (ΔG) in Joules accompanying the corrosion reaction is expressed as

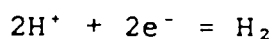
$$\Delta G = -nFE$$

where F is the Faraday constant (96500 Coulombs/eq) and E is

the emf of the cell in volts.

2.1.2 Cell potential and EMF series

The cell potential depends on the concentrations of the reacting ions, temperature and pressure. The standard electrode potentials of different metals at 25°C and at unit activity of the reacting ions are expressed with reference to the hydrogen ion reduction reaction



the emf of which is considered as zero under standard conditions. These values are determined experimentally using half cells consisting of metal/metal ion and hydrogen/hydrogen ion on platinum, and are given in standard books of electrochemistry or corrosion under the title Standard EMF series, as the redox potentials for the reduction reaction of the metal ion. The more noble or positive this value is for a metal, the less is the tendency to corrode.

However, the corrosion reactions that usually take place are rarely at the standard conditions of unit activity and at 25°C. The actual cell potential E for conditions of interest can be calculated using the Nernst equation:

$$E = E^\circ - (2.3 RT/nF)\{\log(a_1/a_2)\}$$

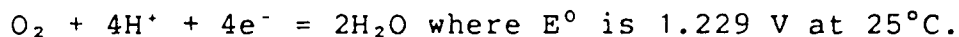
Where E° is the half cell potential under standard conditions, R is the universal gas constant, T is the absolute temperature, n and F were defined earlier, and a_1 and a_2 are the activities of reduced and oxidized species

respectively. From the value of E thus obtained the value of ΔG is calculated.

This forms the basis for the thermodynamic calculations. In most instances, the actual magnitude of the free energy change is unimportant in corrosion applications. The most important is the sign of free energy change for a given reaction, since this indicates whether or not the reaction is spontaneous. The simple rule derived from the free energy calculations can be stated as

In any electrochemical reaction, the most negative or active half cell tends to be oxidized, and the most positive or noble half cell tends to be reduced.

Redox potentials are very useful in predicting corrosion behavior. From the above rule, all metals with reversible potentials more active than hydrogen will undergo anodic dissolution in acids where hydrogen reduction is the main cathode reaction. Likewise, all metals with more noble potentials will not be corroded. However, if there is sufficient oxygen, then the cathodic reaction is the oxygen reduction:



Thus metals like silver and copper with positive potentials at +0.799 V and +0.337 V can undergo corrosion in aerated acids.

The half cell potentials, and the thermodynamic free energy calculations can only be used to state a criterion for corrosion. The actual rate of corrosion is decided by

electrode kinetics.

2.1.3 Pourbaix diagrams

M. Pourbaix devised a compact summary of thermodynamic data in the form of potential-pH diagrams, which relate to the electrochemical and corrosion behavior of metals in water. The main uses of these diagrams are:

1. Predicting the spontaneous direction of the reactions.
2. Estimating the composition of corrosion products.
3. Predicting the environmental changes which will prevent or reduce corrosive attack.

The potential-pH diagram for Fe-H₂O, taken from West⁴ is reproduced in Fig. 1. For a knowledge of corrosion rates the study of electrode kinetics is necessary.

2.1.4 Electrode kinetics

2.1.4.1 Exchange current density

At equilibrium conditions, the rate of oxidation and reduction (r_1 & r_2 respectively) must be equal, and there is no net reaction. The oxidation-reduction rates are conveniently expressed in terms of current density using Faraday's law. These rates in moles per sq.cm. per second are expressed as:

$$r_1 = r_2 = i_0/nF$$

where i_0 is the exchange current density in amperes per cm², n and F having already been defined. The exchange current density is a function of redox reaction, electrode

composition and surface condition, temperature and the ratio of oxidized and reduced species which are present. Fig. 2' gives $H_2 - H^+$ exchange current densities on various metal electrodes. The value of i_0 on platinum is approximately 1 mA/cm² and on mercury is 10^{-12} A/cm².

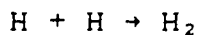
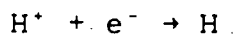
2.1.4.2 Polarization

When corrosion occurs, there is net oxidation occurring at the anode. The electrodes will no longer be at their equilibrium potentials. This deviation from the equilibrium is called polarization. Polarization is defined as the displacement of the electrode potential resulting in a net current. The extent of polarization is usually measured in terms of overvoltage, and is abbreviated as η . The overvoltage or the shift from the equilibrium potential is stated in terms of volts or millivolts. The polarization in corrosion cells is divided into two main types:

1. Activation polarization
2. Concentration polarization.

2.1.4.3 Activation polarization

This refers to electrochemical reactions which are controlled by a slow step in the reaction sequence. For example, the hydrogen evolution takes place according to:



The slow step can be either the electron transfer or formation of hydrogen molecules. The relationship between

the reaction rate and overvoltage for activation polarization is given by the Tafel equation:

$$\eta_a = \pm \beta (\log i/i_0)$$

where i is the oxidation or reduction rate in terms of current density, and β is a constant known as the Tafel constant. The Tafel equation is graphically illustrated in Fig 3', where a logarithmic current scale is used. From the figure it can be seen that electrochemical reactions are very sensitive to small changes in electrode potential. At all potentials more noble than the reversible potential, a net oxidation process occurs and at all potentials more active or negative than the reversible potential, a net reduction occurs.

2.1.4.4. Concentration polarization

This is as a result of depletion of reacting ions near the electrode surface. Again taking the example of hydrogen ion reduction, at low reduction rates, the distribution of H^+ ions in the solution adjacent to the electrode surface is relatively uniform. At very high reduction rates, the region adjacent to the electrode surface will become depleted of H^+ ions. If the reduction rate is increased further, a limiting rate will be reached which is determined by the diffusion rate of H^+ ions to the electrode surface. This limiting rate is the limiting current density i_l , and represents the maximum rate of reduction possible for a given system, and is expressed as:

$$i_l = DnFC/x$$

where D is the diffusion coefficient of reacting ions, C is the concentration of the reacting ions in the bulk solution, and x is the thickness of the diffusion layer. The diffusion layer thickness x is influenced by the shape of the particular electrode, geometry of the system and agitation. i_l is only significant during reduction processes and is usually negligible during metal dissolution.

For an electrode under only concentration polarization, the equation for overvoltage η_c is

$$\eta_c = (2.3RT/nF)[1 - (i/i_l)]$$

Fig. 4³ shows the concentration polarization and the influence of factors (solution velocity, concentration, and temperature) that affect the limiting current densities.

2.1.4.5 Combined polarization

Both types of polarization usually occur at an electrode. At low rates, activation polarization usually controls, while at higher reaction rates concentration polarization becomes controlling. The total polarization is the sum of the two:

$$\eta_t = \eta_a + \eta_c$$

Fig. 5³ shows the combined polarization curve.

During anodic dissolution, η_c is not a factor, and the equation for the kinetics is given by:

$$\eta_{diss} = \beta \log i/i_0$$

this applies to almost all anodic dissolution reactions except for metals which demonstrate active/passive behavior.

During reduction processes, concentration polarization becomes important as the reduction rate approaches the limiting current density. The overall reaction becomes

$$\eta_{red} = -\beta \log(i/i_0) + (2.3RT/nF) \log(1-i/i_l)$$

This applies to all reduction reactions.

Thus, using only three basic parameters β , i_0 and i_l , the kinetics of virtually every corrosion reaction can be described.

2.1.5 Mixed potential theory

This theory is attributed to Wagner and Traud in 1938, and consists of two simple hypotheses:

1. Any electrochemical reaction can be divided into two or more partial oxidation and reduction reactions.
2. There can be no net accumulation of electrical charge during an electrochemical reaction.

From these it follows that during the corrosion of an electrically isolated metal sample, the total rate of oxidation must be equal to the total rate of reduction.

The mixed potential theory, together with the kinetics already discussed, forms the basis of modern electrode kinetics theory.

2.1.5.1 Mixed electrodes

A mixed electrode is an electrode or metal sample which is in contact with two or more oxidation-reduction systems. For a metal undergoing corrosion, the anodic and the cathodic reactions are no longer at their equilibrium

potentials. To illustrate the principles, a simple discussion of corrosion of iron under different conditions is presented below.

2.1.5.2 1. Pure iron in aqueous solutions with no oxygen or oxidizing agents.

Fig. 6¹ qualitatively represents the corrosion of iron in dilute acid solutions where there is no oxygen or oxidizing agents. The two reactions occurring are iron dissolution ($\text{Fe} \rightarrow \text{Fe}^{2+} + 2\text{e}^-$) and hydrogen evolution ($2\text{H}^+ + 2\text{e}^- \rightarrow \text{H}_2$). The electrode cannot remain at either of these reversible potentials, but must lie at some other potential. Since the iron electrode is metallic and is a good conductor, its entire surface must lie at a constant potential. This potential is achieved when the second hypothesis of the mixed potential theory is satisfied; that is, the total rate of oxidation must be equal to the total rate of reduction, and is at the intersection represented by the 'mixed' or corrosion potential E_{cor} . The rate of iron dissolution or hydrogen evolution in terms of current density is represented by i_{cor} .

It is worth noting that the exchange current density i_0 for hydrogen reduction on the metal plays an important role in the high or low corrosion rates observed. A low i_0 for hydrogen shifts the curve to the left, shifting the point of intersection to lower values of i_{cor} or E_{cor} , and a high value of i_0 for hydrogen does the opposite. Though zinc is more active or electronegative than iron (E° for Zn is -0.76 V

and E^0 for Fe is -0.44 V) the corrosion rate in dilute HCl for Zn is much lower than that for Fe, the reason being i_0 for Zn at 10^{-10} A/cm² is much lower than i_0 for Fe which is 10^{-6} A/cm². This shows that, while thermodynamics indicates corrosion for both the metals, the electrode kinetics decides the rate of corrosion.

2.1.5.3 2. Iron in aqueous solutions in presence of oxidizers or oxygen.

The principles illustrated above represent one of the simplest corrosion systems, that is, a metal in contact with a single redox system. Under many actual corrosion conditions, the environments are more complicated. Fig. 7 represents the corrosion behavior of iron in neutral to basic solutions saturated with air or oxygen. The polarization curves for the redox reactions, i.e. metal dissolution, hydrogen reduction and oxygen reduction are indicated. The basic principles of mixed-potential theory are extended to this system. At steady state, the total rate of oxidation must be equal to the total rate of reduction. The total rate of oxidation follows the metal dissolution rate until the reversible hydrogen potential is reached and an increase takes place because of the hydrogen oxidation currents, and a further increase can occur only when the oxygen reduction reversible potential is reached. Similarly, the total rate of reduction is determined by adding the total reduction currents corresponding to oxygen reduction, hydrogen ion reduction and metal reduction. The point at

which the total rate of oxidation equals the total rate of reduction is the mixed or corrosion potential of the system. The graphical construction in this case leads to the condition:

$$i(\text{Fe} \rightarrow \text{Fe}^{2+} + 2\text{e}^-) = i(\text{H}^+ \rightarrow \text{H}_2) + i(\text{O}_2 + 2\text{H}_2\text{O} + 4\text{e}^- \rightarrow 4(\text{OH})^-)$$

It can be noted that the presence of oxygen increases the E_{cor} and i_{cor} , and decreases the hydrogen evolution from $i(\text{H}^+ \rightarrow \text{H}_2)$ to $i'(\text{H}^+ \rightarrow \text{H}_2)$. This phenomenon is often termed depolarization and is a result of shift in the corrosion potential.

The above examples are shown for systems under activation polarization. The same principles can be applied to systems where one or more of the reduction processes are under diffusion control, and will be as shown in Fig. 8'.

2.2 Passivity

Passivity is a phenomenon observed during corrosion of certain metals and alloys. It can be defined as a loss of chemical reactivity under certain environmental conditions, resulting in very low corrosion rates. Passivity is the result of formation of a thin film of corrosion product on the metal surface. This film is only 30 angstroms or less in thickness, and is delicate or strong depending upon the environmental conditions.

Fig. 9³ illustrates the typical behavior of an active-passive metal. The metal initially demonstrates behavior similar to a nonpassive metal. That is, as the

electrode potential is made more positive, the metal follows typical Tafel behavior, and dissolution rate increases exponentially. This is the active region. At more noble potentials, dissolution rate decreases to a very small value and remains essentially independent of potential over a considerable potential region. This is known as the passive region. Finally at very noble potentials dissolution rate again increases with increasing potential in what is known as the transpassive region.

The important characteristic of an active-passive metal is the position of its anodic current density maximum i_c known as the critical anodic current density for passivity and the primary passivation potential E_{pp} for such a current density maximum. Electrode potentials can be crudely equated to the oxidizing power of a medium.

When considering the electrode of an active-passive metal, the peculiar S-shaped anodic polarization curves of these metals leads to interesting results. Fig. 10³ illustrates 3 possible cases which may occur when an active-passive metal is exposed to a corrosive environment such as an acid solution. Reduction processes under activation polarization control are shown by curves 1, 2 and 3. In case 1, there is only one stable intersection point A, which is in the active region and a high corrosion rate is observed. In case 2, there are 3 possible intersection points at which the total rates of oxidation and reduction are equal. These are points B, C and D. Point C is

electrically unstable, and the system can not exist at this point. Points B and D are stable; B is in the active region and corresponds to a high corrosion rate, while D is in the passive region with a low corrosion rate. This system may exist either in the passive or in the active state. In case 3 there is only one stable point in the passive region at point E. For such a system the metal or alloy will spontaneously passivate and remain passive. This system can not be made active and always demonstrates a very low corrosion rate.

From a practical viewpoint, case 3 is most desirable. Case 2 is most undesirable since an unexpected transition from a passive to active state as a result of surface damage or other factors could lead to a rapid attack.

From Fig.10 it can be seen that the current maximum or nose of the anodic polarization curve is important. A spontaneous passivation process only occurs if the cathodic reduction process clears the tip of the nose of the anodic dissolution curve as shown in case 3.

2.3 Effect of high temperatures and pressures

For any chemical reaction at a given temperature and pressure, the equilibrium constant K , the standard free energy change ΔG° , the standard enthalpy change ΔH° and the standard entropy change ΔS° are related:

$$\Delta H^\circ - T\Delta S^\circ = \Delta G^\circ = - RT \ln K \quad (1)$$

The temperature dependence of enthalpy and entropy is given

by the change in the heat capacity at constant pressure, ΔC_p°

$$(\partial \Delta H^\circ / \partial T)_p = \Delta C_p^\circ; (\partial \Delta S^\circ / \partial T)_p = \Delta C_p^\circ / T \quad (2)$$

The following relations result from the integration of (2) between a reference temperature θ , and the given temperature T , represented by subscripts. The usual reference temperature is 298.5 K. or 25°C.

$$\Delta G_T^\circ = \Delta H_\theta^\circ + \int_\theta^T \Delta C_p^\circ dT - T(\Delta S_\theta^\circ + \int_\theta^T \Delta C_p^\circ d \ln T) \quad (3)$$

$$\Delta G_T^\circ = \Delta G_\theta^\circ - (T-\theta)\Delta S_\theta^\circ + \int_\theta^T \Delta C_p^\circ dT - T \int_\theta^T \Delta C_p^\circ d \ln T \quad (4)$$

The corresponding equation for equilibrium constant is

$$\text{Rln} K_T = \text{Rln} K_\theta - (1/T - 1/\theta)\Delta H_\theta^\circ - 1/T \int_\theta^T \Delta C_p^\circ dT + \int_\theta^T \Delta C_p^\circ d \ln T \quad (5)$$

The values of ΔG_θ° , ΔH_θ° and ΔS_θ° are known from the computations in standard publications. Values of heat capacities are measured experimentally, and various empirical correlations are adopted to describe these values.

The effect of changing pressures on the solvent over the range of temperatures is also considered. The basic thermodynamic relation to determine the effect of pressure is

$$(\partial \Delta G / \partial P)_T = \Delta V \quad (6)$$

where ΔV is the volume change for the reaction.

From the above considerations and using different empirical relationships and approximations, the potential-pH diagrams are extrapolated for higher temperatures.

Two such diagrams by Lewis⁶ for iron in water, reproduced in a paper by Mann⁷, are shown in Fig. 11. Passivation is assumed to be possible with Fe_3O_4 or $\alpha\text{-Fe}_2\text{O}_3$, and the diagram of immunity-passivation is constructed for a

temperature of 300°C and shown in Fig. 12. In neutral and dilute alkaline solutions, Fe_3O_4 is the stable oxide formed by the overall reaction



In the pH range 7-12 (measured at room temperature), the oxide forms a thin film over the metal surface and observed corrosion rates are low. This pH range compares with the passive region between 7 and 9.5 measured at 300°C. The traditional boiler water treatment of deoxygenation and alkalization leads to operation in this region of the Pourbaix diagram.

Briefly, the main factors that affect the kinetics of corrosion reactions at high temperatures and pressures are as follows:

1. Higher reaction rates at elevated temperatures.
2. Changes of pH due to increase in the ionization constants of water and acids.
3. Decrease in solubility of gases like oxygen, carbon dioxide, etc., with temperature, and an increase in their solubility with pressure.

Fig. 13* briefly depicts the effects of various factors.

2.4 Corrosion rate measurements

2.4.1 Weight loss tests

The weight loss test is a gravimetric method for measuring the corrosion rates. This method is useful only to study the

uniform and average rates of corrosion, and loses its applicability when the study is specific for pitting, loss of a particular component of the alloy, etc.

In this method, a number of weighed coupons are exposed to corrosive environments, and the coupons are withdrawn in succession at regular intervals. The corrosion products are cleaned thoroughly from each sample by either one or a combination of mechanical, chemical or electrochemical methods. The cleaned samples are weighed and the weight loss in each case is noted. From the weight loss thus obtained and the known values of surface area and time of exposure for the coupon, the corrosion rate is calculated.

2.4.2 Electrochemical methods

The electrochemical methods of corrosion rate measurements are based on the mixed potential theory.

2.4.2.1 General rate equation

A corroding system may be under the influence of two or more anodic and cathodic reactions. Out of these only one of the anodic reactions, usually the metal dissolution, and only one of the cathodic reactions are dominating. The currents induced by the remaining systems are almost negligible.

Let E^* and I^* be the equilibrium or corrosion potential and current respectively. I_a' and I_c' are the anodic and cathodic currents at a potential E . Since there is no net current at E^*

$$\text{at } E^* : I^* = I_a = I_c \quad (1)$$

In a polarized condition at a potential E , the net current I is the difference of anodic and cathodic currents I_a & I_c .

$$\text{at } E : I = \pm(I'_a - I'_c) \quad (2)$$

Current I at potential E is given by the Tafel equation

$$(E - E^*) = \beta_a \log I'_a / I_a \quad (3)$$

$$\text{or } I'_a / I_a = \exp 2.3(E - E^*) / \beta_a \quad (4)$$

The cathodic currents will be

$$I'_c / I_c = \exp 2.3(E - E^*) / \beta_c \quad (5)$$

β_c is negative whereas β_a is positive.

Substituting these in equation (2) we get

$$I / I^* = \pm [\exp\{2.3(E - E^*) / \beta_a\} - \exp\{2.3(E - E^*) / \beta_c\}] \quad (6)$$

which is the dimensionless general rate equation developed by Wagner and Traud'. When the cathodic reaction is diffusion controlled $\beta_c = \text{infinity}$ and the equation simplifies to

$$I / I^* = \pm [\exp\{2.3(E - E^*) / \beta_a\} - 1]$$

From the general rate equation a number of different methods have been developed to determine the corrosion rates.

2.4.2.2 Rigorous method, known Tafel slopes

The situation arises often that the anodic and cathodic slopes are known to remain constant over the set of conditions under investigation. In such cases the Tafel slopes may be determined once, and thereafter, the determination of corrosion rate requires just a single current measurement at any value E . Simple substitution of the measured values of I and E and E^* into the equation (6)

yields the value of corrosion current.

2.4.2.3 Large potential approximation or Tafel extrapolation

The rate equation described above contains two exponential terms on the right-hand side, one of which has a positive exponent and the other a negative exponent. The negative term becomes negligible for large values of $(E - E^*)$, and the polarization curves are then given by

$$\text{Anodic: } I/I^* = \exp \{2.3(E - E^*)/\beta_a\}$$

$$\text{Cathodic: } I/I^* = \exp \{2.3(E - E^*)/\beta_c\}$$

These are also the values for partial current Tafel lines. In other words, at large potentials, usually about 50 mV from E^* , the polarization curve coincides with the partial current curves.

Thus, the anodic Tafel slope is determined as the slope of a linear semilogarithmic plot of large potential I and E measurements. Extrapolation of this line to $E = E^*$ yields the corrosion current.

This method has a disadvantage for passivating metals. On the anodic side at large potentials passivation may set in, and the above discussion no longer holds. However, the method is valid on the cathodic side if there is no concentration polarization at large potentials.

2.4.2.4 Small potential approximation

This method is called the linear polarization method and is also known as the polarization resistance method. This was developed by Wagner and Traud in 1938. It is based

on the fact that equation (6) gives a direct proportionality between the meter current and overvoltage ΔE as the latter becomes very small.

Taking the derivative dI/dE as E approaches E^* , it is found that

$$dI/dE = (2.3/\beta_a + 2.3/\beta_c) I^*$$

Within 10 mV more noble or more active than the corrosion potential, it is observed that the applied current density is a linear function of the electrode potential as illustrated in Fig. 14³. From the slope of the curve thus obtained and knowing the values of β_a and β_c , the corrosion current can be calculated.

2.4.2.5 Rigorous general method or 3 point method

The 3 point method was developed by Barnartt in 1970¹⁰ making use of the general rate equation. Here the currents are measured at selected potentials of ΔE , $2\Delta E$ and $-2\Delta E$. The ratios r_1 and r_2 are defined as

$$r_1 = (I \text{ at } 2\Delta E)/(I \text{ at } -2\Delta E)$$

$$r_2 = (I \text{ at } 2\Delta E)/(I \text{ at } \Delta E)$$

It was shown that these ratios are interrelated through the quadratic equation.

$$U^2 - r_2U + \sqrt{r_1} = 0$$

The two roots of which are

$$\text{+ve root } U_1 = \exp(2.3\Delta E/\beta_a)$$

$$\text{-ve root } U_2 = \exp(2.3\Delta E/\beta_c)$$

The first root gives the value of β_a and the second root gives β_c . When the Tafel slopes are known, any one of the I

and E data points is substituted into the general rate equation to obtain the corrosion current.

2.4.3 Stress corrosion cracking

The ASTM (American Society for Testing and Materials) definition for stress corrosion cracking (SCC) is "A cracking process requiring the simultaneous action of a corrodent and sustained tensile stress."

Many investigators, however, have classified all cracking failures occurring in corrosive mediums as SCC, including failures due to hydrogen induced cracking. These two types of cracking respond differently to environmental variables. For example, cathodic protection is an effective method for preventing SCC whereas it rapidly accelerates hydrogen cracking. Hence it is suggested by many that these two processes should be treated separately.

SCC often occurs in innocuous and mild environments in which the metal or alloy is virtually unattacked or rapidly passivated over most of its surface, while fine cracks, either intergranular or transgranular or both, propagate through the metal under the action of stress. There are very slight or no corrosion products. High strength materials are more susceptible to SCC than low strength materials. As the list of environments that cause SCC for any alloy is extending, the hypothesis that only particular or specific ions cause SCC is much debated and perhaps not valid anymore. It is suggested that for any combination of alloy

and environment that can cause SCC, there is a threshold stress below which no cracking can occur. This threshold stress is between 5-90% of the yield stress. Such stresses are usually present in the designed stress levels or from residual stresses resulting from welding, heat treatment, etc.

The field of SCC is noted for controversies, arguments and many hypotheses. There are many theories presented and contested, and no single theory is all-encompassing to account for the SCC observed in various metals/environments. In a recent paper on SCC, Ford¹ gives an excellent summary of the subject of SCC. The various models of SCC can be broadly classified as

1. Dissolution models

In these models crack extension is mainly by corrosion and assisted by stress.

2. Mechanical models

In these models crack extension is mainly by mechanical failure and assisted by corrosion.

3. Hydrogen embrittlement models

From the numerous models proposed in the above three categories, only the two most popular and widely accepted models are discussed here.

Film rupture model:

This is a dissolution model and Logan^{1,2}, incorporating many people's ideas, first fully explained the model.

Briefly, the film rupture model states that initially there is a passive film which under the action of stress breaks at microscopic or submicroscopic spots. Pre-existing paths for corrosion may or may not be present. This localized rupture leads to a situation of small anodes of fresh metal and large cathode of remaining film-covered metal. Intensive corrosion takes place at these small anodes. This process repeats, leading to cracking. The fact that cracking can be stopped by cathodic protection and proceeds in steps gives more support to this mechanism.

Hydrogen decohesion model:

This is one of the hydrogen embrittlement models and was proposed by Troiano¹³.

There is considerable hydrogen charging of the metals either during the thermal treatments or in the corrosion reactions. The atomic hydrogen formed is quickly adsorbed on the surface of the metal and is highly mobile. This hydrogen is transported either by diffusion or by dislocation motion to various sites in the metal and these sites are : lattice, grain boundaries, incoherent or coherent precipitates, dislocation tangles, voids or pores, etc. Thompson and Bernstein¹⁴ represent in a simple yet comprehensive diagram the various steps or the reaction paths for hydrogen from its generation to the fracture of the metal.

Briefly, the decohesion theory states that hydrogen reduces the cohesive strength between the atoms. Under the action of stress the atomic hydrogen quickly moves to points

of triaxial stress just ahead of the crack tip. A critical combination of stress and hydrogen concentration is reached. This results in rupture of the atomic bonds and extension of the crack tip. This process is repeated and agrees well with the discontinuous nature of crack propagation observed.

Whatever the mechanism, it is important to note that both corrosion and tensile stress play important roles in the cracking. Stress results in rupturing the protective films which could be tarnish films, thin oxide films, layers richer in the more noble component or other passive films. The repassivation kinetics plays an important role, which depends upon the passivation characteristics of the metal and aggressiveness of the environment. If the repassivation rate is very high, only pit formation may occur. If it is too low only general corrosion may occur. It is the critical combination of repassivation kinetics and the strain rate that causes SCC.

In view of the general passivation of the metal including the cracked surfaces and localized corrosion at the crack tip, the usual range of potential in which cracking takes place is where an active/passive or passive/active transition takes place.

The susceptibility to SCC is affected by the chemical composition and the metallurgical structure of the metal, i.e. preferential orientation of grains, composition and distribution of precipitates, dislocation interactions, etc.

These factors interact with the environment composition and stress to affect time to cracking, etc. As is the case with most chemical reactions SCC is usually accelerated by increasing temperature, but sometimes temperature may increase the repassivation rates and help in reducing the SCC susceptibility.

2.4.4 Testing for SCC

The laboratory testing for SCC can be broadly classified as :

1. Constant total strain tests.
2. Constant load tests.
3. Constant strain rate tests.
4. Fracture mechanics tests.

Without going into the merits of different types of testing, it is sufficient to say that the method selected depends upon the purpose, results required, and the equipment available. Often, these tests are complementary.

In the present work, the constant total strain type with a U-bend specimen was chosen as recommended in ASTM G-30-79. The significance and use of U-bend specimens as mentioned in the standard are reproduced:

- a). The U-bend specimen may be used for any metal alloy sufficiently ductile to be formed into the U shape without mechanically cracking. The specimen is most easily made from strip or sheet but can be machined from plate, bar, castings or weldments.

b). Since the U-bend usually contains large amounts of elastic and plastic strains, it provides one of the most severe tests available for smooth (as opposed to notched or precracked) stress corrosion test specimens. The stress conditions are not usually known and a wide range of stresses can exist in a single stressed specimen. The specimen is therefore unsuitable for studying the effects of different applied stresses on SCC or for studying variables which have only a minor effect on cracking. The advantage of the U-bend specimen is that it is simple and economical to make and use. It is most useful for detecting large differences between SCC resistance of 1) different metals in the same environment 2) one metal in different metallurgical conditions in the same environment, or 3) one metal in several environments.

3. Literature Survey

3.1 Aqueous environments at ordinary temperatures

3.1.1 Effect of dissolved oxygen

At ordinary temperatures in neutral or near neutral water, dissolved oxygen is necessary for appreciable corrosion of iron. Fig. 15¹³ shows typical data of corrosion of mild steel as a function of oxygen concentration. In the absence of dissolved oxygen,⁴ the corrosion rate at room temperature is negligible, for both pure iron and steel.

Although increase in oxygen concentration at first accelerates corrosion, it is found that beyond a critical concentration the corrosion rate drops again to a very low value. This occurs sooner in distilled water than when Cl^- ions are present. In distilled water the maximum corrosion occurs at 12 ml O_2 /liter. This value increases with dissolved salts and with temperature, and decreases with increase in velocity and pH.

As explained in the section on mixed potential theory, oxygen is a depolarizer, and the main cathodic reaction taking place is oxygen reduction. As the oxygen concentration is increased, the cathodic reaction increases and the anodic dissolution increases. Above the critical concentration, the cathodic reduction curve clears the anodic peak, and the point of intersection of the anodic and cathodic curves will be such that metal will be passivating

and the corrosion rate will be very low.

Because passivity requires higher oxygen concentrations, in the event of local breakdown of passive film, active-passive cells are established (e.g. near crevices). Such a breakdown is accompanied by severe pitting, particularly at higher temperatures, in the presence of halide ions, etc. This behavior limits the practical use of higher oxygen concentrations as a means of reducing corrosion of steel.

3.1.2 Effect of temperature

When corrosion is controlled by diffusion of oxygen, the corrosion rate at a given oxygen concentration approximately doubles for every 30°C rise in temperature. In an open vessel, allowing dissolved oxygen to escape, the rate increases with temperature to about 80°C and then falls to a very low value at the boiling point as shown in Fig. 16'. The falling off of corrosion above 80°C is related to a marked decrease of oxygen solubility in water as the temperature is raised, and this effect eventually overshadows the accelerating effect of temperature alone. In a closed system oxygen cannot escape and the corrosion rate continues to increase with temperature until all oxygen is consumed.

When corrosion is attended by hydrogen evolution the rate is more than doubled for every 30°C rise. The rate for iron corroding in HCl, for example, approximately doubles

for every 10°C rise.

3.1.3 Effect of pH

The effect of pH on corrosion of iron in aerated water at room temperature is shown in Fig. 17'. Sodium hydroxide and hydrochloric acid were used to adjust pH in the alkaline and acid ranges.

Within the range of pH 4-10 corrosion rate is independent of pH and depends only on how rapidly oxygen diffuses to the metal surface. The major diffusion barrier of the film, hydrous ferrous oxide, is continuously renewed by the corrosion process. Regardless of pH of water within this range, the surface of iron is always in contact with an alkaline solution of saturated hydrous ferrous oxide.

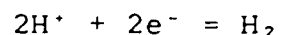
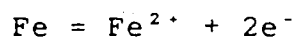
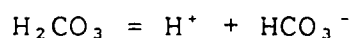
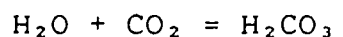
Within the acid region (pH less than 4), the ferrous oxide film is dissolved, the surface pH falls and the metal is more or less in direct contact with the aqueous environment. The increased rate of reaction is then the sum of both an appreciable rate of hydrogen evolution and oxygen depolarization.

Above pH 10, increase in alkalinity of the environment raises the pH at the iron surface. The corrosion rate correspondingly decreases because iron becomes increasingly passive in the presence of alkalis and dissolved oxygen. The potential of iron in water of pH less than 10 changes from an active value of -0.4 or -0.5 V to a noble value of 0.1 V in 1N NaOH, with an accompanying decrease in corrosion

rate. If the alkalinity is markedly increased, for example, to 16 N NaOH, passivity is disrupted and the potential achieves a very active value of -0.9 V. The corrosion rate correspondingly increases to about 0.0001 to 0.004 ipy (0.05-2.0 mdd), but that is still a relatively low rate. In this region, iron corrodes with the formation of soluble sodium ferrite (NaFeO_2). In the absence of dissolved oxygen, the reaction proceeds with the evolution of hydrogen, forming sodium hypoferrite (Na_2FeO_2).

3.1.4 Effect of dissolved carbon dioxide

Carbon dioxide in appreciable concentration accelerates the corrosion of iron. Dissolved carbon dioxide, or carbonic acid, is similar to any acid that reacts with iron evolving hydrogen.



This fact is of practical importance in the corrosion of steam return lines, where carbon dioxide expelled from boiler water dissolves in the condensate to form carbonic acid above room temperature. This is also important in oil and gas recovery operations where carbon dioxide is either present in the well or deliberately injected for enhanced recovery.

The corrosion rates of mild steel (0.15% C) in various concentrations of dissolved carbon dioxide or carbon dioxide plus oxygen at 60 and 90°C are given in Fig. 18''. Carbon dioxide is not as corrosive as oxygen in equal concentrations. At 60°C, for example, 4 mL of oxygen per liter produces seven times more corrosion in a given time than a solution containing the same concentration of carbon dioxide. At gas concentrations of 20 mL/L at the same temperature, oxygen is ten times more corrosive than carbon dioxide.

The work of Heuyn and Bauer, mentioned by Speller'', found that, compared with the rate of corrosion in water saturated with air, the addition of 15% carbon dioxide doubled the rate, while water saturated with carbon dioxide (without air) was only one third as corrosive. Bauer also found that water saturated with oxygen-free carbon dioxide is less corrosive than water saturated with air. According to Speller, these results were confirmed by distilled water immersion tests at 70°C in the National Tube Company research laboratory. Where the water was saturated with carbon dioxide, the loss of wrought iron or steel pipes of various commercial grades was 20% lower, and where saturated with air and 12% carbon dioxide the loss was 24% higher than when saturated with air alone. The composition of iron was not a factor in the air saturated water, but in carbonic acid waters with or without air, wrought iron and copper-bearing steel gave better results.

C. Dewaard and D.E. Milliams ' ' reported the results of carbonic acid corrosion on an X-52 steel at different partial pressures of carbon dioxide up to one bar, and gave the corrosion rates obtained by the linear polarization technique as shown in Table 1. They found that above 80°C all specimens became passive in a matter of hours, and proposed a relation between pH and temperature, in the range of 5- 80°C as follows:

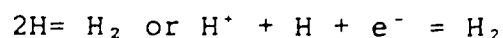
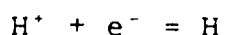
$$\text{pH}(\text{CO}_2, \text{ partial pressure}=1) = 4.17 \times 10^{-3}t + 3.71$$

where t is the temperature in degrees C.

They proposed that the corrosion rate of steel in carbonic acid obeys the relation

$$\log i = -1.3 \text{ pH} + B$$

In the usual corrosion of steel in an acid without air, the rate determining step is the hydrogen reduction reaction

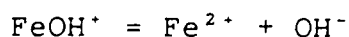
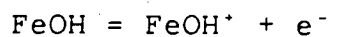
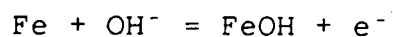


The relation between the corrosion current i and pH is shown to be of the form

$$\log i = -A.\text{pH} + B$$

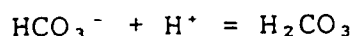
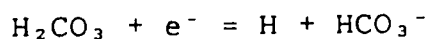
and when it is assumed that the anodic dissolution reaction does not depend on pH, the value of A = 1.

However, Bockris et al. obtained evidence of a pH dependent mechanism



With this mechanism, the anodic dissolution rate at any constant potential is inversely proportional to H^+ ion concentration which leads to a less marked dependence of corrosion rate on pH, A being about 0.5.

The experimental value obtained by DeWaard et al. is 1.3 which does not agree with the value of 0.5. They propose a correlation of corrosion rates with the concentration of undissociated acid rather than that of dissociated acid (pH). They suggest the cathodic reactions



After an initial adsorption on the metal surface, an undissociated carbonic acid molecule is directly reduced. The subsequent combination of H atoms to form H_2 molecules is probably much faster, and hence will not be rate determining. This also holds for the recombination of bicarbonate ion, with H^+ diffusing from bulk of the electrolyte towards the metal as shown above. Only when there is a cathodic shift in potential, the diffusion of hydrogen ions cannot keep up with the amount of HCO_3^- formed and the second reaction will be rate determining, and is equivalent to $H^+ + e^- = H$

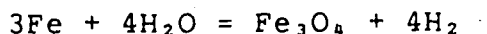
With the above hypothesis, Deeward et al. arrived at a value of $A = 1.25$ which was in close agreement with the experimental value of 1.3. The effect of temperature on corrosion rate at a constant pH was described with an activation energy of 10.7 kcal/mole. Finally it was stated

that quantitative predictions of corrosion rates as a function of the CO_2 partial pressure and the temperature are possible provided passivation does not occur.

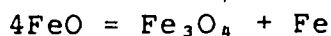
V.P. Kuznetsov¹ investigated the characteristics of carbonic acid corrosion of steel 45 at a CO_2 pressure of 5 kgf/cm^2 and temperatures up to 120°C in distilled water similar to a particular gas well condensate. These tests were conducted in autoclaves and the corrosion rates at 8, 20, 40, 60, 80, 100, and 120°C without mixing were 1.8, 1.9, 3.1, 5.3, 6.8, and 3.9 mm/year respectively; with mixing they were 2.5, 4.7, 8.7, 15.8, 20.4, 18.5, and 14.2 mm/year respectively. Up to 60°C the corrosion products form a very noncohesive permeable film of a black substance with magnetic properties. X-ray structural analysis showed that it had an amorphous structure. With an increase in temperature to 80°C pale gray iron carbonate (siderite) was observed in the corrosion products and the amount formed was greater without mixing. Its crystals filled the pores in the previously formed noncohesive film, making it more compact, stronger, and less permeable. With a subsequent increase in temperature, Kuznetsov observed an increase in the alkalization of the layer in the vicinity of the electrode and the amount of siderite deposited, and the permeability of the oxide film decreased.

3.2 High temperature water, steam and carbon dioxide

Steam attacks iron resulting in a protective film of magnetite (Fe_3O_4) as follows



The mechanism of this reaction, so far as it is understood²⁰, indicates that Fe_3O_4 is formed below about 570°C and that above this temperature FeO forms instead. The latter then decomposes on cooling to a mixture of magnetite and iron according to the equation



Around 300°C , which is the point of our interest, the corrosion of steel by steam is practically negligible and harmless. Even at 595°C from the tests conducted on various steels²¹ the corrosion rates were found to be less than 2 mm/year.

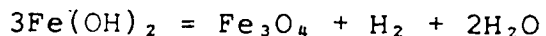
Evans²², while discussing problems in nuclear power plants mentioned the paper by Catchpole²³. Catchpole states that in CO_2 atmospheres at $350\text{--}450^\circ\text{C}$ mild steel is oxidized to Fe_3O_4 , which gradually thickens and breaks away. Preliminary investigations suggested that the effects were likely to be small and should cause no appreciable weakening due to metal loss. However, after a broken bolt was found at a power station, a more searching investigation was carried out. This confirmed the original expectations as regards free surfaces, but at trapped surfaces between nuts and bolts, the increase in volume due to oxidation was found to be capable of leading to failure. By limiting temperatures

to 360°C, with only an occasional operation at 380°C, the situation was brought under control. G.B. Gibbs et al.,²⁴ discussing the same problem in 1982, mentioned that the problem was due to the presence of traces of condensed steam and carbon monoxide. They recommend the use of mild steels only up to 300°C, and 9% Cr steels in the 300-500°C range.

Summing up, so long as H₂O is in the steam phase both H₂O and CO₂ form a protective magnetite layer and do not pose any problems. But carbon dioxide atmospheres above 350°C can lead to problems of breakaway oxidation if traces of condensed steam and carbon monoxide are present, especially at trapped surfaces.

3.3 High temperature water and carbon dioxide

At lower temperatures²⁰ (e.g. room temperature to about 100°C and probably at higher temperatures) before a relatively thick surface film develops, experiments show that Fe(OH)₂ is the initial reaction product and not Fe₃O₄. The Fe(OH)₂ formed eventually decomposes into magnetite according to the Schikorr reaction



Any factors that disturb the protective magnetite layer on steel, either chemically or mechanically, induce a higher rate of reaction, usually in a localized region, causing pitting or sometimes grooving.

H.S. Gadiyar et al.²⁵ in their study of corrosion and magnetite growth on C-steels at 310°C in water confirmed the

above mechanism. Their results are given in Table 2.

3.3.1 Effect of dissolved oxygen

Oxygen in aqueous solutions acts as a depolariser and increases the corrosion rate. As the oxygen concentration increases beyond a particular level the cathodic reaction clears the critical current density required for passivation and iron will passivate. The manner in which the oxygen content of water affects the amount and distribution of corrosion was brought out by Ruther and Hart²⁴ who studied a range from below 0.1 up to 540 ppm with temperatures between 50-315°C. At 260°C a low oxygen (less than 0.1 ppm) concentration gave a uniform brown-black coating on the metal, and after an initial period, the corrosion became low, to a rate of 0.4-0.5 mg/cm² in a 30 day test. At intermediate concentrations of oxygen of about 50 ppm, there was severe pitting and much higher metal loss. At a higher oxygen concentration of 540 ppm, a thin protective film was formed so that the corrosion rate was only about 0.25-0.3 mg/cm², which was actually lower than when very little oxygen was present. The protective film formed at high oxygen concentrations consisted of α -Fe₂O₃, and at lower concentrations the film was magnetite. This might seem to suggest that the proper way to protect is not to remove oxygen, but to keep at the highest possible concentration. Methods of avoiding corrosion based on high oxygen concentrations are difficult and indeed might be dangerous.

Any small area screened from oxygen would likely to suffer corrosion, and the large cathode-anode ratio could easily lead to intense pitting attack.

Uhlig²⁰, in connection with boilers, recommends the following maximum limits for oxygen:

Cold water	0.3 ppm
Hot water	0.1 ppm
Low pressure boilers	0.03 ppm
High pressure boilers	0.005 ppm

The above results are achieved by deaeration both by mechanical and chemical methods.

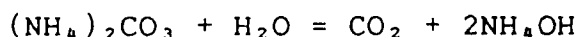
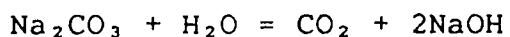
3.3.2 Presence of carbon dioxide

In all the literature reviewed, the problem of corrosion due to CO_2 was mostly up to 90°C and some to 120°C . In boilers, the problem of corrosion is felt only in the condensers where the temperatures are below 120°C .

The problem of CO_2 is only with the dissolution of CO_2 in the condensed steam, forming carbonic acid. The solubility of CO_2 in water decreases with increase in temperature, but increases with increase in pressure. The data of solubility of CO_2 in water up to 120°C and 700 atmospheres from Dodds et al. is reproduced in Fig. 19²¹. In the usual range of interest of pressure and temperature in enhanced oil recovery operations of 100-200 atmospheres and 120°C the solubility is a maximum of about 5 kg of CO_2 /100 kg of H_2O . However at higher operating temperatures

between 120-300°C this is expected to be much lower. The results given by Nesbitt²⁴ for 100 atmospheres pressure at 200, 250 and 300°C are given in Table 3.

In boiler applications the dissolved CO₂ in high temperature waters is fixed as carbonates with alkali additions. The carbonates are unstable and dissociate into CO₂ and the hydroxides. For example,



As the boilers operate at pressures ranging from 200 psi to about 2000 psi, the problem of CO₂ corrosion seems to be at temperatures below 120°C.

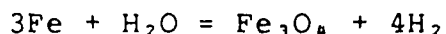
Except for the papers already discussed and literature from boiler applications, no information is found above 120°C.

3.3.3 Control of feed water in boilers

In boiler applications, the addition of alkali to feed water limits any corrosion caused by CO₂ to the boiler itself, by converting dissolved CO₂ to carbonates. At the prevailing boiler temperatures, the carbonates dissociate as mentioned above, bringing hot carbonic acid into contact with condenser and return line systems. Steel return line systems suffer serious corrosion if the CO₂ content of the boiler water is high. Soluble FeCO₃ is formed which returns to the boiler, where it decomposes, the CO₂ being again available for further corrosion.

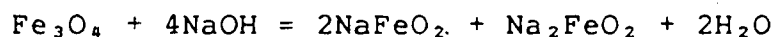
3.3.3.1 Addition of alkali

Addition of NaOH to water reduces the rate of the reaction

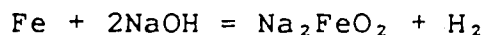


Feed water for a high pressure boiler is treated to a pH (measured at room temperature) of about 10.5 to 11.0. In low pressure boilers (less than 250 psi) this value is commonly 11-11.5. In some high pressure boilers, particularly in Germany, NH_3 is used instead of NaOH at correspondingly lower pH values (8.5-9).

Fig 20²⁰ gives the corrosion behavior of iron at 310°C at various values of pH measured at 25°C. It is apparent from the figure that excess alkali can be damaging to a boiler in that the corrosion rate increases rapidly as pH is increased above 13. Excess of alkali may slowly dissolve the magnetite film in accord with



forming sodium hypoferrite or ferroate Na_2FeO_2 and sodium ferrite NaFeO_2 , both of which are soluble in hot concentrated NaOH. In addition, concentrated alkali reacts directly and more rapidly with iron to form hydrogen and sodium ferroate



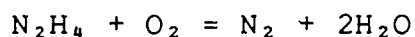
Reactions of this kind account in part for pitting and grooving of boiler tubes and are those that account for excessive corrosion rate of iron at high values of pH. Along these lines Potter and Mann²¹ found that at 340°C, for

example, thickness of the final magnetite layer formed in a given time increased as NaOH concentration increased from 5 to 20%. These data suggest that high concentrations of OH^- ions, by some unknown mechanisms directly stimulate the $\text{Fe-H}_2\text{O}$ reaction in the presence of an intervening layer of magnetite. There is also the possibility, however, that OH^- ions favour formation of sodium ferroate or ferrite which later hydrolyzes on cooling to magnetite and NaOH.

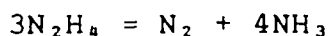
The uniform corrosion due to high initial pH is not so dangerous as the accidental concentration of an alkali in the boiler water at a crevice, such as is formed between rivetted plates or in a cracked oxide scale or at a hot spot on the tube surface, which may lead to caustic cracking of steels. For this reason it has been held advisable to add buffer ions such as PO_4^{3-} (Na_3PO_4) which limit the increase in pH a water can achieve no matter how much the alkali gets concentrated. The minimum amount of PO_4^{3-} recommended for this purpose varies from 30 ppm at a pH of 10.5 to 90 ppm at pH of 11.

3.3.3.2 Use of inhibitors

Hydrazine (N_2H_4) is usually injected³⁰ into feed water as soon after the deaerator as possible, and has been in use for some years for the principal purpose of removing residual dissolved oxygen from feed water, generally replacing sodium sulfite for this purpose. Hydrazine reacts with dissolved oxygen according to:



At ordinary temperatures this reaction is slow. At elevated temperatures, i.e. above 175°C, hydrazine decomposes according to the equation



In view of the slow rate of reaction of hydrazine with very small concentrations of dissolved oxygen, the results probably do not come only from its reducing properties, but also from the alkalizing effect of ammonia which is the decomposition product of excess hydrazine. Also hydrazine reduces Fe_2O_3 to Fe_3O_4 which is considered more protective at higher temperatures.

The amount of ammonia produced depends on two main factors: a) the treatment rate in excess of the dissolved oxygen equivalence and b) the quantity of ferric oxide in the system. It is customary to treat with hydrazine at a rate 100% greater than the dissolved oxygen concentration in the feed water system.

It is suggested that a significant part of the benefits of hydrazine treatment is due to the ammonia produced; then it is cheaper and more logical to reduce the hydrazine dosage and inject ammonia as part of the treatment. Such treatments have been found satisfactory in medium pressure boilers(600-900 psi) and ammonia concentrations up to 1.0 ppm are used. However, in boilers, an excess of ammonia is harmful in view of Cu-bearing alloys used in the condensers. A disadvantage of ammonia, where steam condenses under pressure, is that the distribution of ammonia between vapour

and condensate is unfavourable in that the condensate is depleted of ammonia. The substitution for ammonia by cyclohexylamine or morpholine has been advocated because they have lower distribution ratios than ammonia and therefore confer a higher pH to the condensate.

However at high pressures, particularly for supercritical boilers, the number of acceptable reagents for feed water treatment becomes very limited. Morpholine and cyclohexylamine are probably not sufficiently stable; other amines of similar complexity are likely to be no better in this respect, and non-volatile reagents like NaOH must be obviously excluded from supercritical boilers in view of dangers of SCC. This leads to but one choice for feed water conditioning, namely ammonia.

The dissolved oxygen level must be very low, not more than 0.005 ppm after deaeration, and whether hydrazine treatment will be of value as an oxygen scavenger is doubtful, although both hydrazine and ammonia are used in the American supercritical stations.

3.4 Carbonic acid corrosion in gas condensate wells

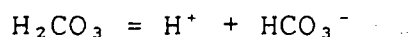
The problem of carbonic acid in high pressure gas condensate wells was first brought out publicly by Bacon and Brown²¹ in April 1943. They first noted corrosion in the Opelika, Texas field in September 1942. Since then the petroleum industry has recognized the wide-spread existence of corrosion in high pressure gas condensate wells. The

problem was originally contained by the use of soda ash (Na_2CO_3) water (1/2 lb/gallon of water, 2 gallons per 1,000,000 cu.ft.of gas produced). Before the soda ash was used, the dissolved iron in the distillate water was 200-1000 ppm, the pH of the water was 5.0-6.0, and CO_2 was 1% by volume. After the use of soda ash pH was 7.0-8.0, and the dissolved iron 5- 30 ppm.

A further report by H.A. Carlson³² highlighted the problem and gave a summary of the work being done to understand and combat the problem. He emphasized the fact that the corrosion was mainly due to dissolved CO_2 (as the wells were sweet wells) and that the actual pH of the solution at 40-400 psi was 3.4-3.3 which was highly corrosive.

H.E. Greenwell et al.³³ discuss the use of ammonia to prevent casing corrosion problems in gas condensate wells. In that paper they gave the theoretical background for calculating the ammonia required to counter the problems caused by H_2S and CO_2 .

From an estimation of partial pressures of H_2S and CO_2 , their concentrations per liter of the condensate were calculated. Using the relevant dissociation constants (in the article there is no mention of temperature, and the values used seem to be quite close to the values at room temperature), the pH of the condensate was calculated from:



For a partial pressure of 4.08 atmospheres in wells having

100 psi casing pressure, the equivalent concentration of H_2CO_3 is 14.09×10^{-2} mol/liter, and the ionization constant is

$$(\text{H}^+) (\text{HCO}_3^-) / \text{H}_2\text{CO}_3 = 3.5 \times 10^{-7}$$

$$(\text{H}^+) (\text{HCO}_3^-) = 3.5 \times 14.09 \times 10^{-9}$$

$$= 5.21 \times 10^{-8}$$

$$(\text{H}^+) = 2.28 \times 10^{-8}$$

$$\text{pH} = 3.6$$

If pH is to be maintained at 8, the HCO_3^- will be

$$(\text{H}^+) = 1 \times 10^{-8}$$

$$(\text{HCO}_3^-) = 5.21 \times 10^{-8} / 1 \times 10^{-8} = 5.21 \text{ mol/liter}$$

Thus, an equivalent amount of (NH_4^+) must be present, which will be 5.21 mol/liter. Greenwell et al. further described various trials taken, methods of monitoring the effectiveness, and the favourable results obtained.

Nowadays, the problem of carbonic acid corrosion in gas condensate wells is well recognized and being countered with the use of inhibitors, many of them being acid neutralizers.

3.5 Corrosion characteristics in carbonate and bicarbonate solutions

The aqueous bicarbonate and carbonate solutions are neutral to alkaline depending on their concentrations. Passivation of steels in these solutions, products of corrosion, and their solubility at ordinary temperatures have been studied in detail.

Thomas et al.³⁴ studied the anodic passivation of iron in carbonate and bicarbonate solutions at room temperature. The polarization curves obtained by them using 0.1 M and 1 M NaHCO_3 and 0.1 M Na_2CO_3 are reproduced in Figs. 21 and 22.

They concluded that passivation in carbonate solutions occurs in two stages. In the first stage, the iron surface becomes passivated in the same way as in solutions of other inhibitive ions, by formation of an oxide film which is mainly magnetite. At the same time a film containing ferrous carbonate forms on the surface. In the second stage of passivation at higher potentials, the ferrous carbonate in the film is oxidized to hydrated ferric oxide. This accounts for the anomalous second oxidation peak of iron in carbonate solutions. As the carbonate concentration in the solution is increased, the amount of carbonate film on the surface also increases.

In the NaHCO_3 solutions, the first stage of passivation is similar to that in carbonate solutions. The second stage of passivation occurs to a much smaller extent, as shown by the poorly defined second oxidation peak.

Dissolved oxygen in the solution does not react directly with the iron surface in these solutions to form the passivating films. The effect of oxygen is rather that its reduction at the iron surface enables an equivalent anodic current to flow.

Thomas and Davies³⁵ discussed the stability of Fe_2O_3 and Fe_3O_4 films as a function of NaHCO_3 concentrations in a

series of cathodic polarization curves at 25°C as shown in Fig. 23. They concluded that two distinct passivating films can exist on iron in near-neutral solutions. The film stable at more positive potentials consists essentially of ferric oxide. The film stable at more negative potentials is a lower oxide, probably magnetite. In air-saturated solutions at 25°C, increasing the anion concentrations up to 10^{-2} M makes the passivating Fe_2O_3 less stable by displacing the Flade potential to more positive values. Further increase in anion concentration from 10^{-2} M to 10^{-1} M makes the Fe_2O_3 more stable by displacing the Flade potentials to more negative values. At concentrations above 10^{-1} M, no Flade potential of Fe_2O_3 is observed and its potential range of stability overlaps that of the Fe_3O_4 film so that inhibition of corrosion can occur. Increasing the concentration of NaHCO_3 makes the Fe_3O_4 film less stable at its Flade potential.

Davies and Burstein³⁴ also made similar studies with KHCO_3 solutions at a pH of 8.8. They reported that in the anodic polarization curves, before the first peak as reported by Thomas et al.³⁴, there was also a shoulder in the curve as shown in Fig. 24. They proposed that from the rest potential to the shoulder, essentially $\text{Fe}(\text{OH})_2$ was forming independent of the anion concentrations. Only after the shoulder, was there formation of FeCO_3 , which was present in the form of soluble $\text{Fe}(\text{CO}_3)_2^{2-}$ up to the first peak, and iron dissolution during this period increased with

the anion concentration.

J.M. Sutcliffe et al.³⁷ reported on the intergranular SCC of carbon steels in carbonate and bicarbonate environments. The potent solutions contained CO_3^{2-} and HCO_3^- together with a suitable cation such as NH_4^+ , Na^+ , or K^+ , in proportions such that the initial pH was in the approximate range of 8-10.5, and the solution concentrations down to 0.25 N. For a given pH, the intergranular cracking was confined to a relatively narrow range of electrode potentials corresponding to that region of the polarization curve where the anodic peak gave way, at its more positive side, to the region of rapid passivation. Their results on a low carbon steel (C, 0.08; Si, 0.01; Mn, 0.35; S, 0.03; P, 0.02; and N, 0.002) at 90°C in a 1 N Na_2CO_3 + 1 N NaHCO_3 are reproduced in Fig. 25. They also indicated that in a temperature range of 22-90°C tested by them, the severity of cracking and the range of potential in which cracking takes place, increase with temperature as shown in Fig. 26. There was no mention by them about temperatures beyond 90°C, and higher pressures.

Berry and Payer³⁸ reported SCC by aqueous solutions of CO and CO_2 . They mentioned that pipeline steels are susceptible to SCC at partial pressures of CO and CO_2 as low as 1 psi (6.9 kPa). For SCC to occur, CO, CO_2 and H_2O as water must be simultaneously present. For preventing SCC they recommended adequate dehydration of the gas prior to injection into the pipe line and keeping the temperature

above the dew point. Though this paper is not directly relevant to steam injection systems using CO_2 along with steam, there is some need for concern as CO_2 used may contain sufficient CO to warrant protective measures. They also indicated that oxygen in the gas mixture greatly increases the severity of SCC and should be avoided..

3.6 Summary of literature survey

Briefly summing up the literature survey, the following points, relevant to steam injection systems using steam and CO_2 at higher pressures and temperatures, are important.

1. Dry steam along with CO_2 up to about 300°C are not considered harmful to mild steels. They form a protective layer of magnetite and the corrosion rates are extremely low. However, above 350°C , if steam is wet and in the presence of traces of CO, there can be breakaway oxidation leading to severe corrosion and sometimes failure of trapped surfaces like bolt heads, nuts, etc..
2. In boilers, where CO_2 is only a trace impurity and usually fixed in the feed water as a carbonate/bicarbonate by the addition of alkalies, it is never a problem. Failure to fix the CO_2 in feed water leads to severe corrosion and pitting in the condenser lines where the steam condenses, usually

below 120°C. In view of the caustic SCC problem when non-volatile alkalies like NaOH are used, the present trend for high pressure boilers is to use ammonia, or inhibitors like hydrazine which decompose at high temperatures giving ammonia to fix the CO₂ when condensation takes place.

3. Oxygen causes severe pitting and must be avoided in the system. In high pressure boilers operating at pressures up to 2000 psi, it is recommended that the oxygen levels be kept below 0.005 ppm. In addition, the remaining oxygen is fixed by the use of inhibitors like hydrazine.
4. The carbonic acid corrosion problem is well recognized in the condensates of gas and oil wells. The usual preventive measures include the use of inhibitors to neutralize the acid. In one instance successful trials were reported for the use of ammonia.
5. Extensive literature is not available about carbonic acid corrosion. In the literature surveyed, the problem is dealt with at low temperatures (below 120°C) and low pressures, as the problem starts only when water is present in the liquid phase and CO₂ dissolves forming the acid. The solubility at any given pressure falls with increasing temperature, and increases with

pressure. At high partial pressures of CO_2 and when it is one of the main constituents of the mixture being injected, the problem has not been studied.

6. The passivation characteristics of steels in carbonate/bicarbonate environments have been studied in considerable detail. The anodic polarization curves have two current peaks. The passivation at lower potentials is due to the formation of magnetite and at higher potentials due to hematite. At high temperatures magnetite is considered more protective.

7. SCC of mild steels in carbonate/bicarbonate environments with solution concentrations down to 0.25 N has been recognized. The susceptibility and severity increases with temperature in the temperature range of 22-90°C studied. No studies are reported at higher temperatures and pressures.

4. Materials, Equipment, and Experimental Procedure

4.1 Steel tested

Samples cut from a pipe section of an API X-70 pipeline steel supplied by Battell Columbus Laboratories for an earlier work done in the Department of Mineral Engineering at the University, were used for various tests in this work. The chemical composition and mechanical properties of the steel are given in Tables 4 and 5 respectively. This steel is a pipeline steel according to API (American Petroleum Institute) specifications and has its strength level between API steels J-55 and N-80 which are finding frequent use in steam injection systems.

The samples were cut from a 0.72 inch (18 mm) thick mill fabricated pipe section. The microstructure of this steel at X500 with 2% nital as the etchant is shown in Fig. 27. This is a typical ferrite-pearlite microstructure, with grains oriented in the rolling direction. Pearlite appears in thin bands with the fine grained ferrite in the interband spacing. The steel derives its strength mainly from the fine grain size of ferrite which is obtained from the grain refining action of microalloying elements Nb and V. Cu is added to improve the corrosion resistance of the steel.

4.2 Chemicals used

Corrosive test solutions were prepared from certified ACS grade chemicals and distilled water. The distilled water with a resistance of 18 megohms was obtained from a Millipore water treatment unit located in the Department of Zoology on the University's campus. The CO₂ and nitrogen gases used in this work were of the ordinary commercial prepurified grade (N₂-99.995% and CO₂-99.95%) from the gas cylinders supplied by Liquid Carbonic Canada Ltd.

4.3 Weight loss tests

The two autoclaves used for the weight loss tests were as follows:

1. 2000 mL bench mounted pressure reactor from Parr Instrument Co..
Catalogue # 4522
Maximum working pressure: 1900 psi (13.4 MPa)
Maximum temperature: 350°C.
Cylinder diameter inside: 4.00 inches (10.2 cm)
Cylinder depth inside: 10.50 inches (26.7 cm)
Bomb material: 316 stainless steel

The autoclave is shown in Figs. 28 and 29, both taken from the manufacturer's manual. Fig. 28 indicates the complete assembled reactor along with automatic temperature controller by its side. Fig. 29 indicates the bomb head assembly and the assembled bomb.

The autoclave is equipped with an internal agitator and fittings for treating liquids and gases under pressure, for measuring their temperature, for withdrawing gas or liquid samples, and for releasing any unexpected overpressure.

2. 1000 mL autoclave from Autoclave Engineers Inc.

Manufacturer's serial #: LC 4660

Inside diameter: 3.00 inches (7.6 cm)

Depth of the vessel: 9.50 inches (24.1 cm)

Rated working pressure: 5000 psi (34.5 MPa)

Material of construction: 316 stainless steel

As is the case with the Parr reactor, this autoclave is equipped with similar accessories except for automatic temperature controller. A separate temperature controller, with an iron-constantan thermocouple inserted into the thermowell was used.

The weight loss coupons, closely conforming in the total surface area to the NACE Standard RP-07-75 were made by first cutting the samples from the main pipe sample, and reducing to the required thickness by surface grinding. The samples were next numbered with number punches, and the dimensions measured by a vernier caliper to 0.01 mm accuracy. The samples were then sand-blasted, washed clean with distilled water, degreased, and weighed to a tenth of a milligram.

The required number of samples was then assembled between two Teflon discs of convenient size as shown in Fig. 30. This sample assembly was next mounted on the centrally

located agitator shaft running through the autoclave head (in the present work no agitation was used). The sample assembly mounted onto the head of the 1000 mL autoclave is shown in Fig. 31. An almost identical arrangement was used for the 2000 mL autoclave also. The samples were again cleaned with acetone and dried before introduction into the autoclave filled with the test solution. Small samples (for study of corrosion products under the scanning electron microscope) of about 1×0.5 cm, sandblasted and cleaned like the coupons, were placed on the top Teflon disc before finally sealing the autoclave.

In all the tests where CO_2 was not used, nitrogen was passed through the solution for 15-20 min. to deaerate the solution. The valves were then closed and the autoclave was heated and controlled at the test temperature with the help of the controller unit. In the tests using CO_2 , the same gas was passed through the solution for about 15-20 min., pressurized to the desired levels, all the valves were closed and the system was heated as mentioned above. The details of various tests are mentioned in Chapter 5.

Coupons were withdrawn from the test at the desired periods and the remaining coupons were placed back in the test solutions and similar deaeration and heating procedures were followed.

The coupons withdrawn from the test solution were first rinsed clean of the test solution with gently flowing distilled water and acetone. They were then mounted on the

X-ray diffractometer to take the diffraction pattern. After this, coupons were descaled in concentrated 6 M HCl inhibited by 3.5 g/l of hexamethylene tetramine. The coupons were first immersed for about 1 min. in the acid at 30-45°C, removed from the acid, neutralized in saturated NaHCO₃ solution, washed with distilled water and acetone, dried and weighed. The same process was repeated for 1/2 min. intervals until the surface appeared clean of all corrosion products. Whenever necessary some scrubbing with a nylon brush was done to clean the corrosion products during washing. The weight loss due to corrosion products was recorded. Attempts to measure the weight gain was given up in view of an unknown part of the corrosion products going into the test solution with no consistency. With the sample area known from the dimensions measured, the corrosion rates were calculated as discussed in Chapter 5.

4.4 X-ray diffraction studies

The diffractometer consisted of the following units:

1. X-ray generator unit

Manufactured by Rigaku-Denki Co. Ltd.

Rating: 60 KV

In these studies Cu-K alpha radiation was used at 35 KV and 15 mA.

2. Goniometer unit

Horizontal Goniometer made by Phillips Scientific Equipment.

Model # 1380

The samples were scanned at $1^\circ 20$ per min.

3. X-ray focussing monochromator.

by AMRAY INC. Model # E 3-202 GVW 7189.

4. Proportional detector probe

Made by Phillips Scientific Equipment.

Model # PW 1965/20/30.

5. Step scan control unit

Made by Phillips Scientific Equipment

Model # PW 1374/00

6. Flat bed recorder

Made by Phillips Scientific Equipment

Model # 8000/06/07

A range of 4×10^2 cps and a time constant of 1 second were found to give good diffraction patterns with the background reduced to a minimum.

4.5 Scanning electron microscopy

The scanning electron microscope used for the studies was an ISI-60 manufactured by International Scientific Instruments Inc.

Main features of the instrument are:

Resolution 60 A (at a working distance of 8 mm and an accelerating voltage of 30 KV)

Magnification: X10 to X600000

Accelerating voltage: 25 KV, 5 KV, 10 KV, 15 KV, 30 KV.

Electron lens: three stage, electromagnetic.

Electron gun: Hairpin tungsten filament

Pictures were taken with Polaroid camera fittings with the SEM at one or more magnifications of 560, 1100 and 1800.

4.6 Polarization curves

4.6.1 Potentiostat unit

The potentiostat unit along with the corrosion cell for the polarization runs is shown in Fig. 32 and consisted of the following:

1. ECO Model 551 Potentiostat-Galvanostat.

Output voltage: ± 33 V at full load

Output current: ± 1 A.

The potentiostat gives a fast response, and is capable of measuring the rest potential of the cell when no potential is applied. Both the cathodic and anodic currents can be measured in the ranges of 0-100 μ A, 0-1 mA, 0-10 mA, 0-100 mA, and 0-1 A.

2. ECO Model 567 Digital Function Generator.

This is designed to be used as a drive for the potentiostat. It supplies the necessary waveforms to carry out all the modern electrochemical corrosion work. With the preset potential reading on the potentiostat as zero, the function generator can scan in either direction to a desired level set on it, and then automatically return the scan to zero.

3. ECO Model 560/Log Linear/Logarithmic interface

This instrument is capable of interfacing with the ECO potentiostat, and provides 23 linear ranges from 0.5 uA to 10 uA, and 4 logarithmic ranges of 4 decades each with the thresholds fixed at 0.1, 1, 10, and 100 uA.

4. Hewlett-Packard Model 7044A X-Y Recorder

This recorder was used to plot the logarithmic current on the X-axis and the potential in mV on the Y-axis. This also has a provision to adjust the scales.

4.6.2 Corrosion cell arrangement

The corrosion cell used for the high temperature and high pressure polarization work was designed and assembled by a Russian scientist Dr.D. Nadezhdin in the year 1979 while he was at the University of Alberta as a research associate. The cell assembly is shown in Fig. 33 and consists of the following 3 units.

1. a working electrode of X-70 steel enclosed in an autoclave (referred to as AE1 hereafter).
2. a counter electrode of Pt wire enclosed in a similar autoclave (referred to as AE2 hereafter).
3. an external reference electrode system using a standard calomel reference electrode at room temperature.

Both AE1 and AE2 are of 316 stainless steel (ss), with 1.5 in. (3.8 cm) internal dia. and 8 in. (20.3 cm) depth. They were manufactured by Autoclave Engineers Inc., and rated for 10000 psi (69 MPa) working pressure. The three units of the cell mentioned above are described as follows:

1. The working electrode system

The working electrode of X-70 steel was made from a small 10 mm dia. cylindrical specimen mounted into a 3/4 in. (1.9 cm) Teflon rod of about 2 in. (5 cm) length. The mounting was done by first drilling an undersized hole into the curved surface of the Teflon block, and heating it with an air gun to about 200°C. The specimen was tapered at one end and fitted into the Teflon block. Thus only a 10 mm dia. surface was exposed outside and the remainder of the specimen was sealed inside the block. The electrical connection to the specimen was provided by a 1/8 in. (3.2 mm) dia. ss rod fitting into an undersized hole made into the specimen from one end of the Teflon block. This assembly was finally mounted onto the head of AE1 with the ss rod running through a hole in the AE1 head. Teflon sleeves and tape were used to insulate the ss rod from the autoclave head and the test solution. At the top of the head nylon Swagelock fittings were used as pressure seals. The autoclave head with the working electrode was then screwed into the autoclave body when required.

The AE1 body was connected on one side to the AE2 body by a 1/4 in. (6.4 mm) ss tube and pressure fittings. On the opposite side, the AE1 body was connected to the reference electrode salt bridge system by an ironwood plug through pressure fittings. The working electrode, the reference electrode and the ironwood plug were all maintained at the

same horizontal level. Just below this level The AE1 body has an iron-constantan thermocouple close to the working electrode through a pressure fitting. Finally, under all the connections mentioned, the AE1 body has a heating system made of resistance heating wire mounted on ceramic insulators and wrapped around the AE1 body. A mica sheet was used to electrically insulate the heating wire from the AE1 body. A simple manually operated voltage regulator was used for heating control.

2. Counter electrode system:

A piece of coiled Pt wire was connected to a ss rod and mounted through the head of AE2 using Teflon sleeves for insulation and nylon Swagelok fittings in a similar way as the working electrode. The AE2 body was connected on one side to the working electrode unit as mentioned above. On the opposite side the AE2 body was connected to a ss tube and a valve for introducing gases and for pressure control. At the bottom the AE2 body was connected to a pressure gauge.

3. Reference electrode system:

The reference electrode system consisted of a standard calomel reference electrode by Fisher Scientific Co. in a saturated KCl solution salt bridge. The ironwood plug, connecting the salt bridge to the test solution near the working electrode, is enclosed in a water-cooled jacket. This water cooling maintains the reference electrode at room temperature. The ironwood plug can be kept tightly

pressed into the pressure fitting by a threaded rod running through the container of the salt bridge solution. A sketch of salt bridge and the connection by the ironwood plug to the working electrode autoclave is shown in Fig. 34.

This external reference electrode system is similar to that used by Gerasimov¹¹ and has the advantage over the other methods using porous silica plugs, in that the ironwood plug maintains ionic conductivity without serious pressure loss in the autoclave.

For every polarization run, the working electrode was polished to 600 grit, rinsed with ethanol, and the electrical contact with the ss rod ensured.

The actual test solutions, temperatures and other details are mentioned in Chapter 5.

4.7 SCC tests

The SCC tests were conducted according to ASTM recommended practice G 30-79.

The samples were prepared to closely conform to example 1 given in Fig. 2 of the specifications, reproduced in Fig. 35. The two legs of the U-bend specimen were held together by a connecting bolt, properly insulated from the specimen with Teflon sleeves and washers. Fig. 36 shows a U-bend specimen with the bolt in position. Fig 37 shows a number of specimens mounted on a rod by welding to the bolt heads of the specimens. For each test solution, one such attachment

having 4 samples was mounted onto the centrally located agitator shaft of the 1000 mL or 2000 mL autoclaves. The rest of the procedure for deaerating, heating the solutions, withdrawal of samples etc., was similar to the weight loss tests. The actual details of solutions used along with the other necessary information are given in Chapter 5.

5. Tests, Results and Discussion

5.1 Tests and results

5.1.1 Coupon weight loss tests in autoclaves

Tests were conducted in different mediums at 200 and 300°C in 1000 and 2000 mL autoclaves. Also, some tests were conducted at the Alberta Research Council (ARC) in 300 and 100 mL autoclaves, and these tests are marked with a superscript of * in the presentation of the results.

The details of various tests conducted at the University of Alberta are as follows:

1. $\text{H}_2\text{O} + \text{CO}_2$ at 200° in 2000 mL autoclave.

Test periods: 1, 2, 3, 4, 5, 6 and 7 weeks.

Initial volume of H_2O : 1565 mL.

Pressurized at room temperature with CO_2 to about 750-800 psi (5.2-5.5 MPa). At 200°C, pressure controlled at 1450-1550 psi (10-10.7 MPa).

Solution was renewed whenever a sample was removed.

2. $\text{H}_2\text{O} + \text{CO}_2$ at 300°C in 1000 mL autoclave.

Test periods: 1, 2, 3, 4 and 5 weeks.

Initial volume of H_2O : 520 mL.

Pressurized at room temperature with CO_2 to 450-500 psi (3.1-3.4 MP). At 300°C, pressures controlled at 1450-1550 psi (10-10.7 MPa).

Solution was renewed whenever a sample was removed.

3. 1 M $\text{NH}_4\text{HCO}_3 + \text{CO}_2$ at 300°C in 1000 mL autoclave.

Test periods: 1, 2 and 3 weeks.

Initial volume of H_2O : 520 mL.

Pressurized at room temperature with CO_2 to about 400-450 psi (2.8-3.1 MPa). Pressures reached at 300°C: 2400-2500 psi (16.5-17.2 MPa) and remained stable. No regulation of pressure was done.

Solution was renewed whenever a sample was removed.

4. 1 M NH_4HCO_3 at 300°C in 2000 mL autoclave.

Test periods: 1 and 2 weeks.

Initial solution volume: 1150 mL.

Pressures at 300°C regulated at 1450-1550 psi (10-10.7 MPa).

Solution was renewed whenever a sample was removed.

Small strip of platinum wire was attached to one of the 2-week samples to study the effect of galvanic corrosion.

5. 1 M NH_4HCO_3 + 1 M NH_4OH at 200°C in 2000 mL autoclave.

Test periods: 1, 2 and 4 weeks.

Initial solution volume: 1550 mL.

Pressures reached: 950-975 psi (6.5-6.7 MPa). Due to leakages and solution losses final pressures dropped to 600 psi (4.1 MPa).

Solution was not renewed during the test.

Small strip of platinum was attached to one of the 4-week samples to study the effects of galvanic corrosion.

6. 1 M $(NH_4)_2CO_3$ at 200°C in 1000 mL autoclave.

Test periods: 1, 2 and 4 weeks.

Initial solution volume: 800 mL.

Pressures reached at 200°C: 1250-1300 psi (8.6-9.0 MPa).

Due to leakages, and solution losses, final pressures dropped to 600 psi (4.1 MPa).

Solution was not renewed during the test.

For the tests at ARC, only machining of samples and exposure in corrosive media in the autoclaves were done at ARC. All the other necessary jobs were done at the University. These tests were as follows:

- a. At 300°C in 100 mL autoclaves in solutions of $\text{H}_2\text{O} + \text{CO}_2$, 1 M $\text{NH}_4\text{CO}_3 + \text{CO}_2$, and 1 M NH_4HCO_3 .
- b. At 200°C in 300 mL autoclaves in solutions of $\text{H}_2\text{O} + \text{CO}_2$ and 1 M NH_4HCO_3 .

The results of all the tests are given in Table 6, and the tests done at ARC are identified with a superscript of *. The corrosion rates are given both in the units of mils per year (mpy) and milligrams per square decimeter per day (mdd). The corrosion rates are calculated using the formulae as follows:

$$\text{mpy} = 100 W / A \cdot d$$

$$\text{mdd} = 534 (2.54)^2 W / DAT \text{ where } W \text{ is the weight lost in milligrams due to corrosion, } A \text{ is the area of the specimen in cm}^2, d \text{ and } T \text{ are the test duration in days and hours respectively, and } D \text{ is the density of the specimen in g/cm}^3$$

Observations of the surface film behavior during descaling operations, such as flake formation, adherence to the surface, etc., are given in the remarks column.

5.1.2 X-ray diffraction studies

X-ray diffraction studies were conducted on the weight loss coupons prior to descaling operations. After removal from the autoclaves, the samples were first rinsed clean of the solution with gently running distilled water and acetone and dried. Then the samples were mounted on the diffractometer and the diffraction patterns were taken with Cu-K alpha radiation. The corrosion products were identified with the help of standard tables and the results are presented in Table 7.

5.1.3 Scanning electron microscope studies

Small samples up to a size of 1-1.5 cm long and 0.5-1 cm wide were introduced along with weight loss test coupons into the autoclaves for a study of the surface film under the scanning electron microscope (SEM). These samples were withdrawn at regular intervals along with weight loss coupons, rinsed clean of the solution in the same way as for coupons and mounted in the SEM. Pictures were taken at one or more convenient magnifications of 560, and 1100 and 1800. For ammonium carbonate solution, which was the first test, as no samples for SEM were introduced, only one sample cut from one of the coupons after 30 days exposure was studied.

As there were too many pictures taken, only the pictures for the first and last week specimens, and those where specific features or changes are revealed, are reproduced in Fig. 38 to Fig. 67.

5.1.4 Potentiodynamic polarization studies

A series of polarization curves was run potentiodynamically to study the passivation characteristics of the X-70 steel.

The polarization runs were made at temperatures of 100, 150, 200, and 250°C. Testing above 250°C was not attempted in view of equipment limitations (Teflon blocks and nylon pressure seals). The details of various tests are as follows:

1. $\text{H}_2\text{O} + \text{CO}_2$

Water was initially saturated at room temperature with CO_2 to a pressure of 100-120 psi (0.7-0.8 MPa) and then the pressures were further regulated at 500 psi (3.4 MPa) with CO_2 at 100, 150, and 200°C. At 250°C the pressure was regulated at 900 psi (6.2 MPa).

2. 1 M $\text{NH}_4\text{HCO}_3 + \text{CO}_2$.

The solutions were saturated and pressurized to the same pressures as above.

3. 1 M NH_4HCO_3 . The pressures reached at 100, 150, 200, and 250°C were 80-100, 180-220, 300-350, and 450-550 psi respectively (0.55-0.7, 1.24-1.92, 2.1-2.41, 3.1-3.8 MPa respectively).

4. 1 M $\text{NH}_4\text{HCO}_3 + 1 \text{ M } \text{NH}_4\text{OH}$.

The pressures reached were nearly the same as in the case of NH_4HCO_3 solutions.

In each case the solution was deaerated with nitrogen for about 45 min.-1 hour before the autoclave was sealed off

with the sample. The solutions were rapidly heated in about 30-45 min. to the desired temperatures and then heating was controlled to stabilize the temperatures. About 45 min.-1 hr were allowed for stabilization at test temperatures.

Originally, attempts were made to allow the samples to remain in the solutions at test temperatures for longer durations so as to allow the formation of stable passive film and then start the polarization run from the rest potential. As the rest potentials wander or change with the progress of film formation and require a very long time for stabilization and during this period the pressure in the autoclave was dropping due to leakages, there was very poor reproducibility. This procedure was given up, and the runs were started only after the temperature stabilization of 45 min.-1 hour mentioned above. First, the samples were polarized in the negative direction to potentials of -1200 to -1500 mV from the rest potential and then from this level polarization runs were made in the positive direction to about 2000-2500 mV at a scan rate of 10 mV per minute. After reaching the transpassive region and then traversing to potentials where the currents are nearly an order of magnitude higher, the scans were reversed to study the tendency and extent of hysteresis loop formation which is considered as an indication of pitting susceptibility.

It must be mentioned that the polarization run part of this study was the most troublesome and frustrating for the following reasons:

1. Rectangular and cylindrical samples mounted in heat-setting bakelite or cold setting plastic moulds were resulting in solution leakages to the unexposed parts of the sample due to cracking of the mounts at the sample edges. Only after many attempts, reasonably satisfactory samples could be made in Teflon cylindrical blocks.
2. Problem of insulation of stainless steel electrode lead rods from the solution and from the autoclave body. This could be overcome only after fabricating tight-fitting Teflon sleeves and jamming the rods with Teflon tape.
3. Pressure leakages from various points in the autoclave. This problem was gradually overcome, though not fully, to a level where polarization runs could be made with a maximum of 15-25% drop in pressure in the 5-6 hours required for the run.
4. Large electrical disturbances leading to wild fluctuations in the current recordings during the week days. The recordings were comparatively noise-free on weekends, especially on Sundays.

All the above factors resulted in the abandoning of many runs either midway through after 3-4 hours of work, or after the full run. Many of the runs were repeated and majority of them were done on weekends. After ensuring reasonable reproducibility, the best of them were redrawn after some smoothing (but still maintaining the essential features). These are reproduced in Figs. 68 to 83.

After the polarization run, the samples were examined under a microscope at a magnification up to X100 for any pit formation. Pitting was observed in the case of $H_2O + CO_2$ at $100^\circ C$ and is reproduced in Fig. 84.

The transformation of corrosion products from $FeCO_3$ to Fe_3O_4 or Fe_2O_3 was studied in 1M NH_4HCO_3 solution at $150^\circ C$. Specimens were held for about 2 hours at potentials immediately after the first and second current peaks in polarization runs, then the potentiostat was switched off. Solution was immediately drained by opening the valve, and the sample was allowed to cool. X-ray diffraction was done on these samples and color pictures were taken. A color photograph along with the scale composition are reported in Fig. 85.

From the polarization curves obtained, the corrosion rates in microamperes per sq.cm. and in mpy, and values of Tafel slopes are calculated by Barnartt's 3 point method. These results along with other relevant information are reported in Table 8.

5.1.5 Tests for SCC

In view of the reported susceptibility of mild steel to SCC in carbonate/bicarbonate solutions with increasing severity at higher temperatures, in the range of $25-90^\circ C$, and the susceptibility of pipeline steels in $CO_2 + H_2O$ (in the liquid phase) with traces of CO , it was thought necessary to conduct a preliminary investigation at $150^\circ C$ to get a quick

indication of the trend at higher temperatures. The following tests were conducted:

1. $\text{H}_2\text{O} + \text{CO}_2$
2. 1 M $\text{NH}_4\text{HCO}_3 + \text{CO}_2$
3. 1 M NH_4HCO_3

At this point of time both the autoclaves had developed leakages and the spares necessary to fix these leakages were not readily available. Due to time constraints work was not continued.

For the tests conducted, the U-bend samples were withdrawn at regular intervals of 1, 2 or 3, and 4 weeks. The samples were first checked for the amount of relaxation as soon as the stressing bolt was removed. It was observed to be uniform at about 2.5 mm for all samples and was the same as that for an unexposed sample. This was one preliminary indication of absence of any cracking. The samples were washed free of solutions and observed at various magnifications up to X500 for the presence of any cracks. Severe pitting was observed on the samples exposed to $\text{H}_2\text{O} + \text{CO}_2$ medium right from the first week. A picture taken at about X5 indicating the pitting is reproduced in Fig. 86.

The samples were then sliced into 4 sections at the bend of the U with a diamond cutting saw, mounted in bakelite, polished, etched and observed under the microscope up to X500 for the presence of any cracks. The appearance under the microscope in each case was compared with that of

the unexposed sample as a reference.

5.2 Discussion of results

5.2.1 Weight loss tests

The results of weight loss tests done at ARC are considered to be less significant in view of the smaller size of the samples used due to restrictions in size of the autoclaves, and thus are not discussed. However, none of these tests show corrosion rates in excess of those obtained in large autoclaves, and hence, do not indicate any alarming situation.

For all the media tested, the highest corrosion rate in the first week was around 14 mpy in H_2 and CO_2 at $200^\circ C$. This had evened out subsequently, and stood around 5-6 mpy after 6 weeks.

The second highest initial corrosion rate, around 5 mpy, was for the same medium at $300^\circ C$ which more or less remained constant for the first 4 weeks. There was a sudden increase to about 9.5 mpy in the fifth week.

Though corrosion products in the above two cases appeared quite adherent, needing 3-4 min for descaling, the observation of corrosion products in the test solution after each period is a matter of concern. This can be due to either a poorly passivating film, or due to the dissolution of corrosion products in the test solution at high temperatures and precipitation on cooling.

The corrosion rates in all the other tests were initially between 2-3 mpy, which, subsequently evened out to about 1 mpy.

In 1 M NH_4HCO_3 + CO_2 the corrosion products are adherent, needing 3-4 min for descaling in HCl at 40-45°C with slight flake formation.

In the case of 1 M NH_4HCO_3 (a pH of 7.9 at room temperature) there was no flake formation during descaling, and corrosion products looked adherent, needing about 1-3 min in HCl at 30-35°C for complete removal. In 1 M $(\text{NH}_4)_2\text{CO}_3$ (pH 8.5 at room temperature), the corrosion products appeared most adherent and needed 3-4 min in HCl at 40-45°C for cleaning with no flake formation. In the case of 1 M NH_4HCO_3 + 1 M NH_4OH solution (pH at room temperature was 9.6-9.7), the corrosion products fell off as heavy flakes during cleaning, taking 2-3 min in HCl at 30-35°C. This is probably an indication of internal stresses on the surface film which may result in erosion corrosion problems if there are fluid flows.

In both the tests with platinum wire no excessive corrosion rates were observed.

A very rough rule for checking results with respect to minimum test time is suggested in ASTM G 4-68 as :

hours (duration) = 2000/mils per year.

which means that for solutions other than H_2O + CO_2 , where corrosion rates are 1 mpy or less, the testing period should be roughly 12 weeks and above. For H_2O + CO_2 medium, where

the rates are above 5 mpy, the minimum test period should be 400 hours or about 2.4 weeks.

In spite of the insufficient test durations in some cases, the above results indicate that in the range of 200-300°C the X-70 steel quickly passivates and the corrosion rates are about 1 mpy or less in all the solutions except $\text{H}_2\text{O} + \text{CO}_2$. In the case of $\text{H}_2\text{O} + \text{CO}_2$ the corrosion rates are between 5-10 mpy with considerable transfer of corrosion products to the solution. However, it may be noted that no particular attention was paid to the oxygen content in the solutions except for passing CO_2 or nitrogen through the solution for a period of 20-30 min. Also, these tests were done under static conditions with no fluid flows.

5.2.2 X-ray diffraction studies

The scale compositions from X-ray diffraction studies show that there are 3 possible corrosion products: FeCO_3 (siderite), Fe_3O_4 (magnetite), and Fe_2O_3 (hematite).

The results indicate that in bicarbonate and carbonate solutions at a high initial starting pH (above roughly 8.5) the corrosion product is mainly FeCO_3 , which remains reasonably stable. This may get converted to Fe_3O_4 over long periods, the process probably getting accelerated in the presence of oxygen.

At intermediate pH levels (less than 8), as in 1 M NH_4HCO_3 with or without CO_2 , some of the FeCO_3 initially formed gets quickly converted to Fe_3O_4 and both are present

together.

At lower pH values (less than about 6 at room temperatures), as is expected with H_2O saturated with CO_2 , most of the FeCO_3 initially formed quickly transforms into Fe_2O_3 at lower temperatures, i.e. around 200°C , and the two exist together. At higher temperatures, i.e. around 300°C , the transformation is to Fe_3O_4 . This probably shows higher oxidizing characteristics of the solution at lower temperatures due to greater solubility of CO_2 .

Also it is evident from the weight loss tests that FeCO_3 by itself or together with Fe_3O_4 is a better passivating film than when Fe_2O_3 is present. However, observation of flake formation at high initial pH values indicates that FeCO_3 is subject to erosion corrosion.

5.2.3 SEM studies

From these studies, it is hard to make any definite correlations or draw conclusions except for the following observations in conjunction with X-ray diffraction studies.

1. FeCO_3 appears as regularly shaped crystals of uniform size as shown in Figs. 63 and 67, whereas Fe_3O_4 and Fe_2O_3 have a semicrystalline or amorphous appearance with small particle size and are often present in clusters as shown in Figs. 39 and 47.
2. Scale formed in solutions with higher initial pH shows more crystalline appearance but some cracks are visible indicating stressed structure.

3. Scales formed in lower pH solutions appeared less crystalline and more porous as can be seen from Figs. 38 and 46.

4. The unexposed portion of the small sample (which was resting on the Teflon disc) showed more crystalline FeCO_3 , whereas the free exposed surface showed more Fe_3O_4 and Fe_2O_3 as shown in Figs. 42 to 45.

Except in the $(\text{NH}_4)_2\text{CO}_3$ solution, samples in almost all the solutions showed the presence of either cracks or a porous structure indicating dangers of erosion corrosion under dynamic conditions of fluid flows.

5.2.4 Potentiodynamic polarization curves

The use of an external reference electrode (at room temperature and pressure) to measure the potentials of working electrodes in high temperature and high pressure aqueous solutions overcomes the main problem of instability associated with internal reference electrodes (near the working electrode at the same conditions of pressure and temperature). But there are some parasitic thermal emfs generated needing corrections when converting to the standard hydrogen scale. The main contributions for such a correction, as discussed by Bogearls and van Haute⁴⁰ in their very recent paper, are:

1. Temperature influence on electrochemical half-cell potentials of the reference electrodes (assuming the presence of an internal reference electrode).

2. Thermal liquid junction potential due to the cooled salt bridge employed.

In view of the difficulties involved with high temperatures and pressures, no precise method is yet available to determine the correction to be applied. Bogearls and van Haute propose a simple linear correction, and, if it gains acceptance, will make the computations easy.

The precise values of potentials are mainly needed for establishing the thermodynamic E-pH equilibrium diagrams. Since the present thesis is only concerned with a preliminary study of kinetics of corrosion and passivation characteristics, no attempt is made either to apply the corrections or to discuss the thermodynamic equilibria.

It is difficult to establish any meaningful correlations from the values of corrosion potentials obtained due to the following:

1. The free corroding or rest potential was changing with time depending upon the nature and extent of film formation. This can be seen from the difference in values obtained at 100°C in 1 M NH_4HCO_3 solution under two different conditions. When the metal was allowed to remain for a period of 2.5 hours in the solution at 100°C without any external polarization, the corrosion potential was at -692 mV. But, when the metal was allowed only about 45 min for stabilization, polarized to -1400 mV, and then the sweep started in the positive direction,

a value of -1347 mV was obtained as corrosion potential. The corrosion potential is also a function of the oxygen content of the solution which was not measured.

2. In the case of a polarization sweep from the negative to positive direction, the corrosion potential was a function of the cleanliness of the surface, which in turn depended upon the extent of initial polarization before starting the sweep and the time of holding at the starting potential. The scanning rate also had an influence on the values of corrosion potentials obtained.

No systematic study was made on the above-mentioned factors, and hence, no comments are made on the various effects.

Barnartt's 3-point method was used to calculate the corrosion rates and Tafel constants. It must be mentioned that the extrapolations from the polarization curves involved considerable approximations and judgement. This was due to the quick passivation in certain cases, fluctuations involved, questionable accuracy in getting the values for small potentials of 15 to 100 mV from curves with a total sweep of about 2500 mV and the logarithmic current scale.

In spite of the difficulties of experimentation and extrapolation mentioned above, the corrosion rates obtained agree reasonably well in the case of $H_2O + CO_2$ with those from weight loss tests (between 5-10 mpy). Also, there is a general trend of lower corrosion rates at higher temperatures which agrees well with the findings of others,

considered to be as a result of decreasing solubility of CO_2 with increasing temperatures. It may be noted that the test at 250°C was at about 900 psi (6.2 MPa) as compared to 500 psi (3.4 MPa) for the other 3 temperatures and there is no drastic increase in corrosion rate. This indicates that the temperature effects are much greater than the pressure effects. This agrees well with the predominant effect of temperature on solubility of CO_2 in water.

The corrosion rates obtained in 1 M $\text{NH}_4\text{HCO}_3 + \text{CO}_2$ also show a progressive decrease with temperature and the values are around 1 mpy or less at 200°C and above. This also agrees well with the values obtained in the weight loss tests.

In the case of 1 M NH_4HCO_3 , no calculations could be made for 100°C as the polarization run was started from the rest potential. Both at 150 and 200° the rates are about 1.3 mpy which agree well with the values obtained at 200°C . For 250°C the value came to 5.5 mpy which is quite in excess of trend indicated at both 200 and 300°C . This may be due to error arising out of extrapolation as mentioned before. However, even this value is indicative of lower corrosion rates at higher temperatures.

In 1 M $\text{NH}_4\text{HCO}_3 + 1 \text{ M } \text{NH}_4\text{OH}$ the corrosion rate at 100°C was comparatively quite high at about 22 mpy. The rate decreased with rising temperature and is around 3-4 mpy at $200\text{--}250^\circ\text{C}$. Though this value is higher than that obtained in weight-loss tests, it can be said that the agreement is

quite good.

Other comments that can be made on the appearance of the curves are:

1. In $\text{H}_2\text{O} + \text{CO}_2$ the curves do not exhibit any passivation up to 200°C , but there is a gradual decrease in current with rising temperature. At 250°C there is a distinct passivation and the currents are less by nearly an order of magnitude. The sample after polarization at 100°C exhibited considerable localized corrosion as shown in Fig. 84. The polarization curve at 250°C showed a hysteresis loop in the reverse scan. Though this is an indication of pitting tendency, the sample did not show any pitting.
2. In $1 \text{ M } \text{NH}_4\text{HCO}_3 + \text{CO}_2$ there is a progressive shifting of the curves to high currents up to 200°C and then at 250°C there is a sudden reversal, with the currents reduced by about 2 orders of magnitude. At 100°C there is a distinct first current peak and the presence of a second peak, though much less distinct, cannot be ruled out. At 150°C and 200°C two current peaks are evident. At 250°C no distinct current peak or passivation is observed, but the highest current values obtained are 2-3 orders of magnitude less than the other 3 cases, indicating a drastically reduced corrosion activity. No pitting was observed in any case.
3. In $1 \text{ M } \text{NH}_4\text{HCO}_3$ two distinct current peaks are present at all the 4 temperatures. Brief passivation can be observed

after the first peak at 150°C. The appearance of a small shoulder can also be noted at both 150 and 200°C before the first peak. No systematic pattern is observed in the values of current peaks or the passive currents.

A study by X-ray diffraction of the corrosion products of the samples held for about 2 hours just above the first and second current peaks shows the same pattern as observed by workers at low temperatures. The products after the first peak, i.e. at a lower potential, showed predominantly Fe_3O_4 and some FeCO_3 , and were greyish black in color. The products at a higher potential, i.e. after the second peak, were mainly Fe_2O_3 with some FeCO_3 and were reddish brown in color. A color photograph of both the samples together is shown in Fig. 85.

4. In 1M NH_4HCO_3 + 1M NH_4OH no clear pattern can be observed except that an extremely high first current peak is noted at 100°C. There are a number of peaks present and there is a general trend for the curves to shift to lower currents with rising temperature.

From the foregoing discussion it can be concluded that with increasing temperatures, especially above 200°C, there is a general downward trend in the corrosion rates to generally acceptable levels, i.e. 1-5 mpy. Presence of oxygen or any oxidizing agents cannot be considered benevolent as this might raise the potentials to those ranges where intense general or localized corrosion takes place. This observation agrees well with

the precautions taken in boiler applications to scavenge the last traces of oxygen. Fe_3O_4 along with some FeCO_3 is the product of corrosion at lower potentials in bicarbonate solutions and is more protective than Fe_2O_3 formed at higher potentials.

In $\text{H}_2\text{O} + \text{CO}_2$ the effects of rising temperature in lowering the corrosion rates are much more than the opposing effects of increasing pressure. The presence of ammonium carbonate is very beneficial in reducing the corrosion rates, which agrees with boiler experience.

5.2.5 Tests for SCC

None of the samples showed the presence of any cracks. However, in $\text{H}_2\text{O} + \text{CO}_2$ all the samples showed severe localized corrosion which is alarming. This can be clearly seen from Fig. 86.

The results do not show any immediate danger of SCC. The results of Sutcliffe et al. indicate increased tendency of SCC in the bicarbonate and/or carbonate solutions for the mild steel they tested up to 90°C . The same tendency is not revealed here. The difference can be attributed to the following:

1. Susceptibility to SCC is dependent on the individual characteristics of the steel such as chemical composition, microstructure, method of fabrication, heat treatments given, etc.
2. SCC is highly dependent on the potential, and the present

work is carried out at free corroding potentials almost in the absence of any oxygen.

3. The testing by Sutcliffe et al. was done by the slow strain rate method which is bound to lead to the breaking of the specimen and hence crack initiation in the short test period is not a problem. Tests of the present work are in a way handicapped in the sense that the testing time may not be sufficient for crack initiation.

The above points are brought out only to indicate that though there is no immediate and obvious danger of SCC at 150°C, the susceptibility to SCC must be viewed with caution until further testing is done taking all the possible variables into consideration.

In $H_2O + CO_2$ the results can be viewed with more confidence as the time factor for crack initiation is not a consideration in view of severe localized corrosion.

All that can be said about SCC is that no imminent or impending danger of SCC exists at 150°C in the environments tested.

5.2.6 Summary of discussion of results

The entire discussion of results can be briefly summed up as follows:

1. Weight loss tests indicate that in the temperature range of 200-300°C the X-70 steel quickly passivates in all the solutions tested. The corrosion rates settle down to 1 mpy or less in 1M NH_4HCO_3 , 1M $NH_4HCO_3 + CO_2$, 1M $(NH_4)_2CO_3$

and 1M NH_4HCO_3 + 1M NH_4OH solutions. In H_2O + CO_2 solutions the corrosion is initially higher at 200°C, around 14 mpy, as compared to about 5-6 mpy at 300°C, and in both the cases it settles down to 5-6 mpy after the first 3-4 weeks (except for a sudden increase to about 9 mpy shown at 300°C in the fifth week).

2. X-ray diffraction and SEM studies indicate that at pH values above 8.5 (as in 1M $(\text{NH}_4)_2\text{CO}_3$ and 1M NH_4HCO_3 + 1M NH_4OH) the product of corrosion is siderite. At intermediate pH levels below 8 (as in 1M NH_4HCO_3 and 1M NH_4HCO_3 + CO_2) the initial corrosion product is siderite, part of which quickly gets converted to magnetite and both coexist. At low pH values say, below 6 (as is expected in H_2O saturated with CO_2), the main product of corrosion at lower temperatures, i.e. 200°C, is hematite which is less protective than the film of magnetite formed at 300°C.

The SEM photographs indicate cracked or a porous film in all the cases except in $(\text{NH}_4)_2\text{CO}_3$, suggesting dangers of erosion corrosion where fluid flows are involved and this possibility needs further assessment.

3. The results of polarization curves agree reasonably well with that of weight-loss tests indicating much reduced corrosion activity at 200°C and above. Presence of oxygen or oxidizing agents is definitely harmful since this may raise the potentials to those levels where active corrosion or severe localized corrosion may take place.

Though severe localized corrosion was observed on the sample at 100°C in $\text{H}_2\text{O} + \text{CO}_2$ only, and not at higher temperatures or in other solutions, the presence of a hysteresis loop at 250°C in $\text{H}_2\text{O} + \text{CO}_2$ must be viewed with caution to avoid arising of such high potentials. The presence of severe localized corrosion on the samples of SCC in $\text{H}_2\text{O} + \text{CO}_2$ at 150°C is yet another pointer for the need of such a caution.

4. There is no apparent or immediate or increased susceptibility to SCC at 150°C. However, the long term susceptibility should be evaluated.

6. Conclusions and Recommendations

6.1 Conclusions

The following conclusions can be drawn about the corrosion of X-70 steel in aqueous CO_2 solutions in the temperature range of 100-300°C:

- 1a. In the temperature range of 200-300°C, the corrosion rate in $\text{H}_2\text{O} + \text{CO}_2$ is between 5-10 mpy. The presence of NH_4HCO_3 lowers the corrosion to about 1 mpy.
- 1b. In $(\text{NH}_4)_2\text{CO}_3$ and NH_4HCO_3 (pH about 8 and above at room temp.) the corrosion was 1 mpy or less.

This shows that the carbonic acid corrosion of X-70 steel is low in the temperature range of 200-300°C (rates below 10 mpy are generally considered acceptable) and there is a promising possibility of using ammonium carbonate, bicarbonate or ammonia for further reducing the corrosion.

2. In the 200-300°C range, at high temperatures and/or high starting pH values, the surface film is a mixture of siderite and magnetite which is more protective than a mixture of hematite and siderite formed at low temperature and/or low pH values.

The presence of cracks revealed in the SEM studies and the separation in heavy flakes of the scale formed at a high starting pH (9.5) during descaling indicate a stressed film which might give erosion corrosion problems.

3. The polarization curves did not show stable low current passive regions.

This indicates that presence of oxygen is harmful as this might raise the potentials to regions of active or intense localized corrosion.

4. There was no indication of any immediate or increased susceptibility to SCC at 150°C.

This is a deviation from the trend of increased susceptibility with temperature reported by Sutcliffe et al.³⁷ in their work up to 90°C for a low carbon steel.

5. Severe localized corrosion was observed at 100 and 150°C in $H_2O + CO_2$.

This indicates that, though the corrosion rates are low at high temperatures, an inhibitor or neutralizer like ammonia must always be used.

The above observations, based on the study, agree very well with boiler practice where ammonia along with oxygen scavengers like hydrazine are used in super-critical boilers, as mentioned by Fortune³⁸. The results also agree with the use of ammonia to control gas condensate well corrosion by Greenwell et al.³³ at a pH of 8.

6.2 Recommendations for future work

1. The present work was done under static conditions with no fluid flows. An assessment of corrosion rates in dynamic conditions of gas and fluid flows is necessary for a knowledge of erosion corrosion problems that might arise. Such a study is all the more necessary in view of cracks in the surface film revealed in SEM.

studies.

2. Except for purging the solutions with N_2 or CO_2 for 15-20 min., the present work did not measure the oxygen levels in the solutions. A study to find the effects of varying levels of oxygen would be useful.
3. A more dependable corrosion cell arrangement which can ensure good reproducibility with minimum noise should be constructed to determine precise corrosion potentials and the effects of different variables like CO_2 partial pressures, etc.
4. Further investigation of susceptibility to SCC at different potentials, temperatures, and solution combinations and concentrations is desirable.
5. Work should be done to determine the exact changes in solubility of CO_2 and pH values at high temperatures and pressures, and the effects of these changes on corrosion.

Table 1. Comparison of Experimental and Calculated Corrosion Rates of Grit-Blasted Samples Under Various Conditions

(from DeWaard et al.¹⁰)

Temperature (°C)	Partial CO ₂ pressure (bar)	Calculated corrosion rate (mm/y)	Experimental corrosion rate (mm/y)
5.5	1	0.40	0.40
12	1	0.56	0.60
15	1	0.66	0.70
15	0.52	0.43	0.40
15	0.37	0.35	0.30
15	0.21	0.24	0.20
22	2	1.51	1.60
22	1	0.95	0.90
30	1	1.32	1.30
40	0.92	1.99	1.70
50	0.88	2.89	2.30
60	0.80	3.94	3.90
70	0.69	5.02	4.30
80	0.53	5.79	5.70

Table 2. Metal Loss, Magnetite Film Thickness and Adherency
for Carbon Steel in Water at 310°C

(Saturation Pressure, 1440 psi)

(from Gadliyar et al.²⁵)

Exposure time (h)	Metal Loss (mm/y)	Adherent oxide, (um)	% Adherency
----------------------	----------------------	-------------------------	-------------

1. pH 7, oxygen less than 0.05 ppm:

140	0.048	1.20	73
530	0.02	1.90	75.6

2. pH 7, oxygen 3.5 ppm:

140	0.06	1.52	74
530	0.034	3.24	75.8

3. pH 10, oxygen less than 0.05 ppm:

140	0.038	1.02	78.3
530	0.018	1.80	79.6

4. pH 10.5, oxygen 3.5 ppm:

140	0.055	1.43	75.8
530	0.031	3.20	82.2
1460	0.015	4.12	78.8
3050	0.008	4.50	77.5
5060	0.005	4.71	78.1
6650	0.004	5.10	80.6

Table 3. Solubility of CO₂ in Water at at High Temp. andPressures(from Nesbitt²⁸)

T°C	Pressure (atm)	Mole fractions		Mole fractions	
		in gas		in liquid	
		x(CO ₂ ,g)	x(H ₂ O,g)	x(CO ₂ ,l)	x(H ₂ O,l)
200	100	0.789	0.211	0.012	0.988
250	100	0.465	0.535	0.011	0.989
300	100	0.110	0.890	0.004	0.996

Table 4. Chemical Composition of the X-70 Steel Used for
Testing

The chemical composition of the X-70 steel in weight percent is as follows:

Element	Ladle analysis	Check analysis
Carbon	0.10	0.09
Silicon	0.25	0.25
Manganese	1.48	1.48
Phosphorus	0.014	0.012
Sulphur	0.002	0.002
Niobium	0.05	0.04
Aluminum	0.033	0.035
Vanadium	0.10	0.10
Copper	0.31	0.33
Nickel	0.32	0.31
Carbon Equivalent		0.40

Table 5. Mechanical Properties of the X-70 Steel Used for
Testing

The mechanical properties of the X-70 steel are as follows:

Yield strength, psi	74,100 (511 MPa)
Tensile strength, psi	89,700 (618.5 MPa)
Elongation, percent	43
Yield ratio, percent	84
CV-100, ft-lb	88 (119.2 J)

+ CV-100 is defined as the energy level of the lowest temperature Charpy specimen exhibiting 100% shear area.

Table 6. Corrosion Rates from Weight-loss
(Tests done at Alberta Research Council are marked with a superscript *)

Solution and temperature	Period (days)	Area (cm ²)	Weight loss (mg)	Corrosion loss mpy	Corrosion rate mdd	Remarks
A. H ₂ O + CO ₂						
Test # 1. 200°C	7	43.42	232.1	14.3	78.1	After each period, test solution was found to have corrosion products. No flake formation during descaling which took 3-4 min in HCl at 40-45°C
	14	42.51	287.1	8.81	48.2	
	21	41.95	314.3	6.52	35.6	
	28	42.83	384.9	5.86	31.7	
	35	42.85	521.8	6.35	34.8	
	42	43.25	500.1	5.02	27.5	
	49	43.78	621.1	5.28	28.9	
Test # 2. * 200°C						
	7	17.51	14.4	2.14	8.5	
	14	17.48	15.6	1.16	6.4	
	30	17.48	44.4	1.54	8.5	
Test # 3. 300°C						
	7	43.51	88.2	5.29	29.1	Quite adherent film. Took 3-4 min for descaling in HCl at 40-45°C. Much less corrosion products in the test solution.
	14	43.79	132.4	3.94	21.6	
	21	43.25	289.6	5.83	31.9	
	28	43.75	384.7	5.74	31.4	
	35	43.53	788.5	9.45	51.7	
Test # 4* 300°C						
	8	11.16	18.9	4.42	21.1	
	15	11.15	25.4	2.77	15.3	
	30	11.15	23.9	1.30	7.2	
B. 1 M NH ₄ HCO ₃ + CO ₂						
Test # 5* at 300°C	7	11.16	0.4	0.09	0.5	
	14	11.15	3.7	0.43	2.4	
	28	11.15	7.0	0.40	2.2	

(Contd)

Table 6 continued.

Solution and temperature	Period (days)	Area (cm ²)	Weight loss (mg)	Corrosion rate (mpy)	Corrosion rate (mdd)	Remarks
B. 1 M NH ₄ HCO ₃ + CO ₂ Test # 6 at 300°C	7	42.97	35.2	2.2	12.0	Required 3-4 min in 45°C HCl. Slight flake formation observed.
	14	42.94	47.6	1.45	7.9	
	21	42.90	48.9	0.99	5.4	
	21	42.97	52.5	0.94	5.1	
C. 1 M NH ₄ HCO ₃ Test # 7 * at 200°C	7	17.45	6.3	0.94	5.1	
	14	17.45	9.0	0.67	3.7	
	30	17.49	12.0	0.42	2.3	
Test # 8 * at 300°C	8	11.14	13.2	2.70	14.8	
	14	11.17	14.3	1.66	9.1	
	28	11.16	16.3	0.95	5.2	
Test # 9 at 300°C (with Platinum wire)	7	43.00	33.8	2.05	11.1	No flake formation while cleaning. Required 1-3 min. in 30-35°C HCl.
	14	42.92	52.2	1.59	8.6	
	14	42.95	49.8	1.51	8.3	
	14	43.00	39.6	1.20	6.6	
D. 1 M NH ₄ HCO ₃ + 1 M NH ₄ OH Test # 10 at 200°C	7	46.68	52.5	2.93	16.1	Heavy flake formation while cleaning. Required 2-3 min. in 30-35°C HCl.
	15	47.90	84.5	2.14	11.7	
	30	47.48	86.2	1.11	6.1	
	30	47.11	78.8	1.02	5.6	
E. 1 M (NH ₄) ₂ CO ₃ Test # 11 at 200°C	7	44.95	46.1	2.68	14.6	No flaking. Adherent film. Required 3-4 min. in 40-45°C HCl.
	15	42.68	52.0	1.59	8.1	
	30	43.42	72.7	1.09	5.6	

(Conversion factor for corrosion rate: 1 mpy = 0.0254 mm/y)

Table 7. Scale Composition from X-ray Diffraction Studies.

(Results from ARC are marked with a superscript*)

Solution	Temperature (°C)	Time (weeks)	Composition
1a. H ₂ O + CO ₂	200	1	FeCO ₃ and slight Fe ₂ O ₃
		2	FeCO ₃ and Fe ₂ O ₃
		3	FeCO ₃ and Fe ₂ O ₃
		4	FeCO ₃ and Fe ₂ O ₃
		5	FeCO ₃ and Fe ₂ O ₃
		6	FeCO ₃ and Fe ₂ O ₃
		7	FeCO ₃ and Fe ₂ O ₃
1b. H ₂ O + CO ₂ [*]	200	1	FeCO ₃
		2	FeCO ₃
		3	Fe ₂ O ₃
2a. H ₂ O + CO ₂	300	1	Fe ₃ O ₄ and very slight FeCO ₃
		2	Fe ₃ O ₄ and very slight FeCO ₃
		3	Fe ₃ O ₄ and FeCO ₃
		4	Fe ₃ O ₄ and FeCO ₃
		5	Fe ₃ O ₄ and FeCO ₃
2b. H ₂ O + CO ₂ [*]	300	1	FeCO ₃
		2	FeCO ₃ and slight Fe ₃ O ₄
		4	FeCO ₃
3a. 1 M NH ₄ HCO ₃ + CO ₂	300	1	FeCO ₃
		2	FeCO ₃
		3	Fe ₃ O ₄ and very slight FeCO ₃
3b. 1 M NH ₄ HCO ₃ [*] + CO ₂	300	1	FeCO ₃ and slight Fe ₃ O ₄
		2	FeCO ₃ and slight Fe ₃ O ₄
		4	FeCO ₃ and slight Fe ₃ O ₄

Table 7 contd.

Solution	Temperature (°C)	Time (weeks)	Composition
4a. 1 M $\text{NH}_4\text{HCO}_3^*$	200	1	Fe_3O_4
		2	Fe_3O_4 and slight
			FeCO_3
		4	Fe_3O_4
4b. 1 M $\text{NH}_4\text{HCO}_3^*$	300	1	Fe_3O_4
		2	Fe_3O_4 and FeCO_3
		4	Fe_3O_4 and FeCO_3
4b. 1 M NH_4HCO_3	300	1	Fe_3O_4 and slight
			FeCO_3
		2	Fe_3O_4
5. 1 M $(\text{NH}_4)_2\text{CO}_3$	200	1	FeCO_3
		2	FeCO_3
		4	FeCO_3
6. 1 M NH_4HCO_3 + 1 M NH_4OH	200	1	FeCO_3
		2	FeCO_3 and slight
			Fe_3O_4
		4	Fe_3O_4

Table 8. Corrosion Characteristics from Polarization Curves
 (Corrosion rates by Barnartt's 3 point method)

Solution and temperature	E(corr) (mV)	i(corr) $\mu\text{A}/\text{cm}^2$	Corrosion rate mpy	β_a	β_c
<u>A. $\text{H}_2\text{O} + \text{CO}_2$:</u>					
100°C	-1200	25.2	11.6	0.22	-0.23
150°C	-935	22.8	10.5	0.11	-0.09
200°C	-960	14.1	6.5	0.21	-0.24
250°C	-1060	15.7	7.2	0.24	-0.18
<u>B. 1 M $\text{NH}_4\text{HCO}_3 + \text{CO}_2$:</u>					
100°C	-550	9.53	4.4	0.22	-0.08
150°C	-740	8.38	3.9	0.04	-0.07
200°C	-860	2.67	1.2	0.05	-0.05
250°C	-805	0.08	0.04	0.27	-0.15
<u>C. 1 M NH_4HCO_3:</u>					
100°C \$					
150°C	-1040	2.75	1.3	0.08	-0.04
200°C	-960	2.74	1.3	0.15	-0.06
250°C	-820	11.9	5.5	0.09	-0.08
<u>D. 1 M $\text{NH}_4\text{HCO}_3 + 1 \text{ M } \text{NH}_4\text{OH}$:</u>					
100°C	-1100	47.1	21.6	0.08	-0.05
150°C	-1140	16.2	7.4	0.04	-0.03
200°C	-800	4.6	3.2	0.18	-0.17
250°C	-766	8.40	3.9	0.15	-0.11

\$ 3 point method could not be applied in this case as the polarization run was started from the rest potential.

(Conversion factor for corrosion rate: 1 mpy = 0.0254 mm/y)

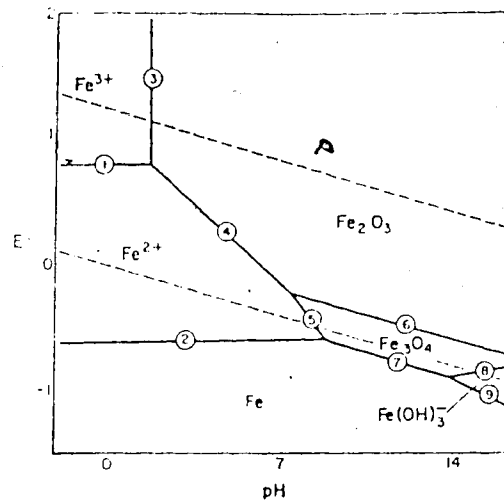


Fig. 1. Pourbaix diagram for the system Fe-H₂O at 25°C (from West⁴)

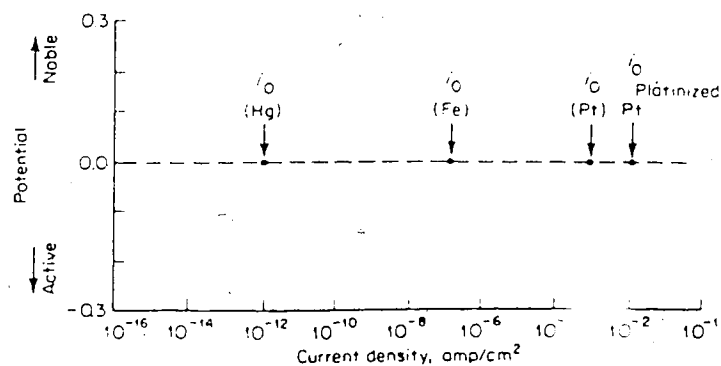


Fig. 2. Hydrogen-hydrogen ion exchange current densities (from Fontana and Greene³)

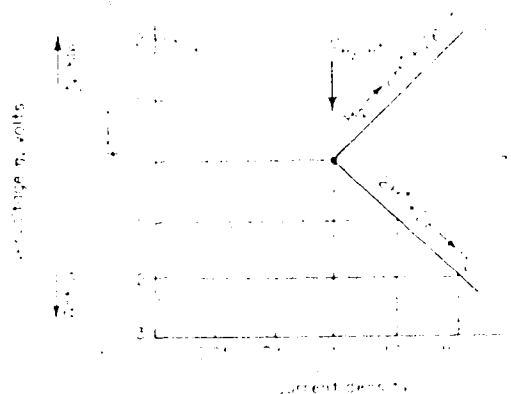


Fig. 3. Activation polarization curve of a hydrogen electrode (from Fontana and Greene³)

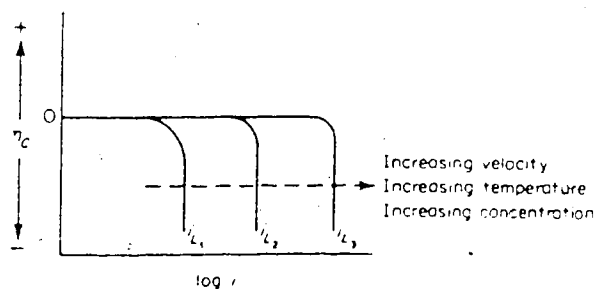


Fig. 4. Effect of environmental variables on concentration polarization curve (from Fontana and Greene³)

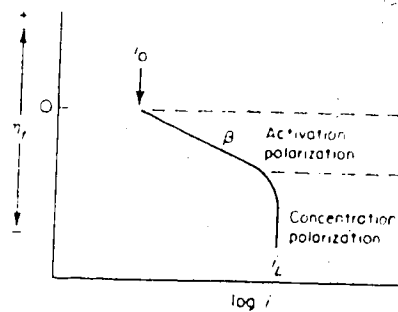


Fig. 5. Combined polarization curve (from Fontana and Greene³)

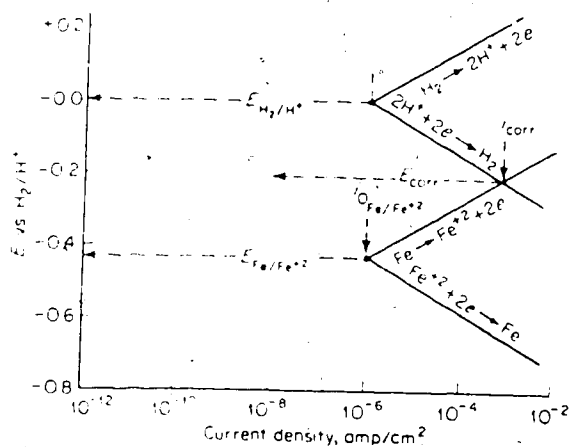


Fig. 6. Electrode kinetic behavior of pure iron in acid solution - schematic (from Fontana and Greene³)

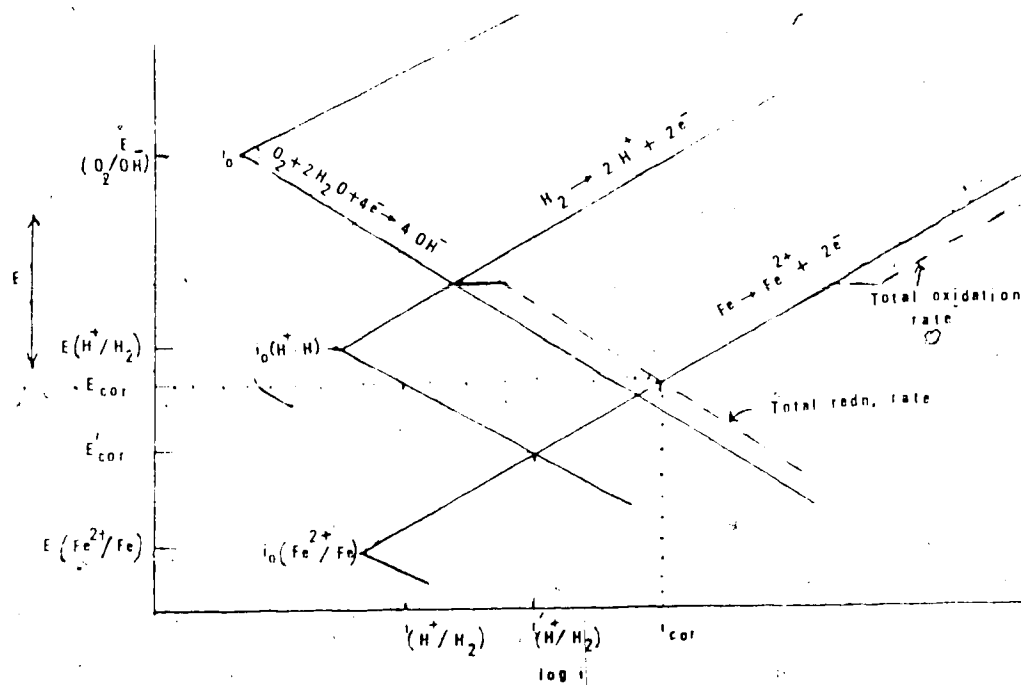


Fig. 7. Effect of oxygen on the corrosion of iron in neutral to alkaline solutions

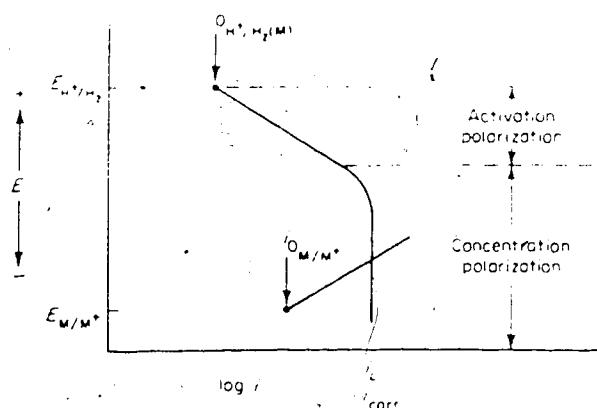


Fig. 8. Corrosion of metal M under diffusion control (from Fontana and Greene³)

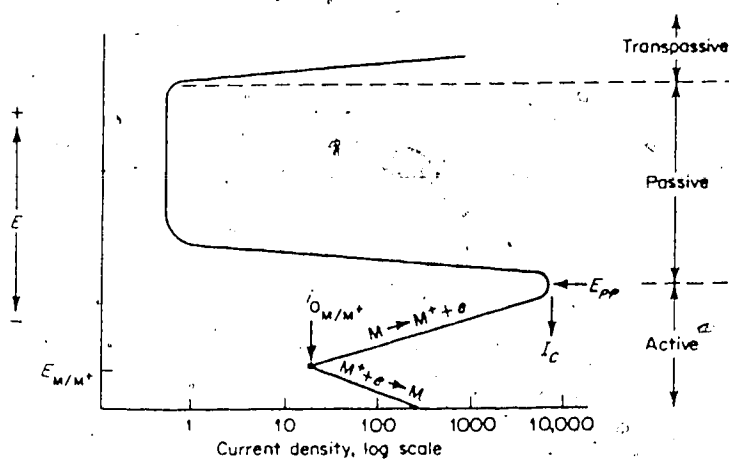


Fig. 9. Typical anodic dissolution behavior of an active-pass metal (from Fontana and Greene³)

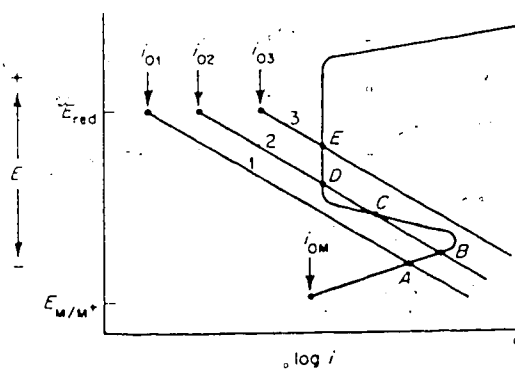


Fig. 10. Behavior of an active-passive metal under corrosive conditions (from Fontana and Greene³)

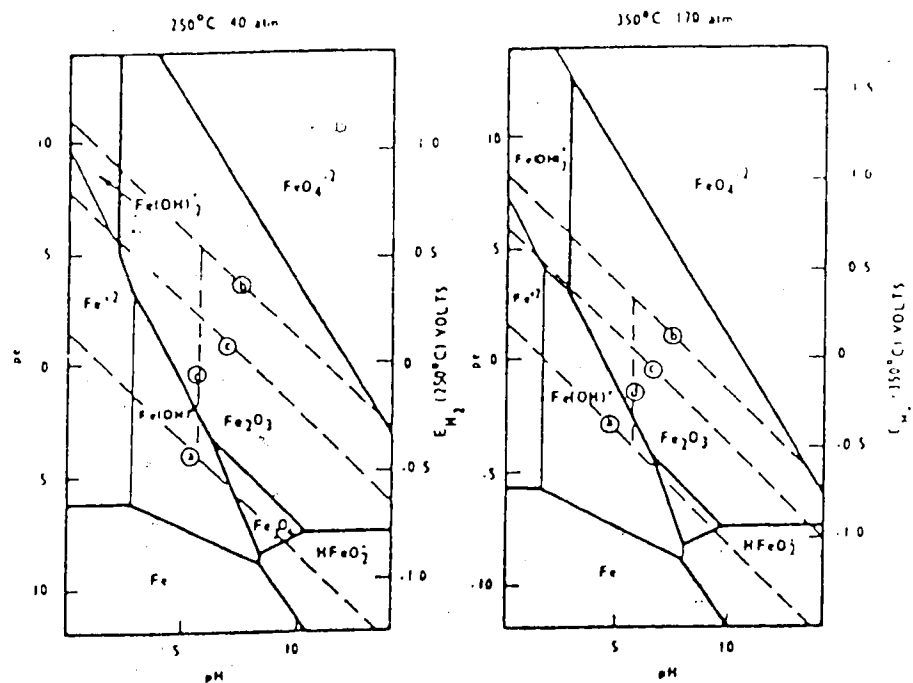


Fig. 11. Potential-pH diagrams for Fe-H₂O at 250 and 350°C according to Lewis (from Mann⁷)

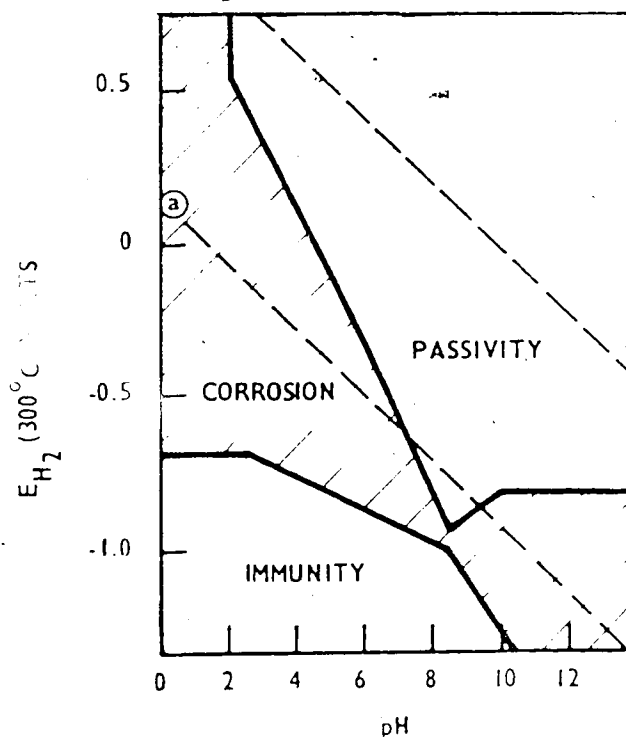


Fig. 12. Corrosion-immunity-passivation diagram for Fe-H₂O at 300°C (from Mann⁷)

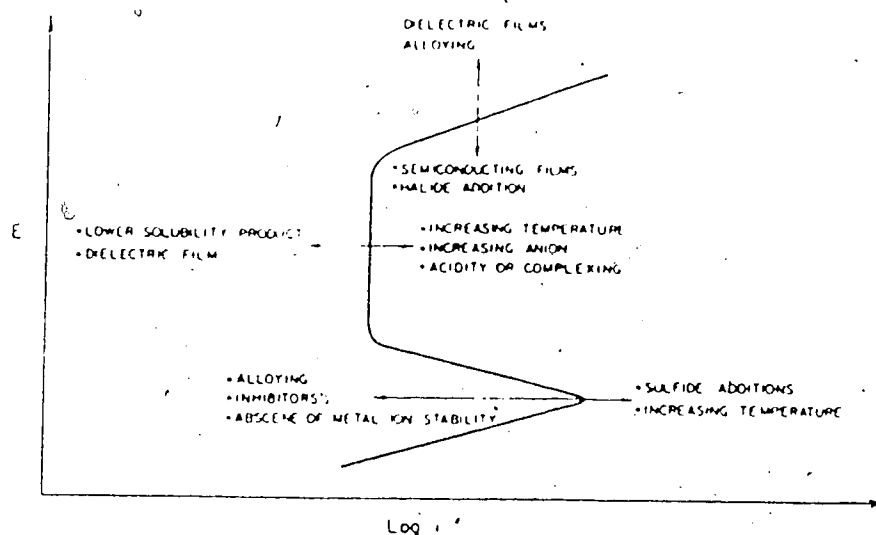


Fig. 13. Schematic relationships showing the effects of environment and alloy additions upon the anodic polarization curve (from Lumsden and Staehle⁴)

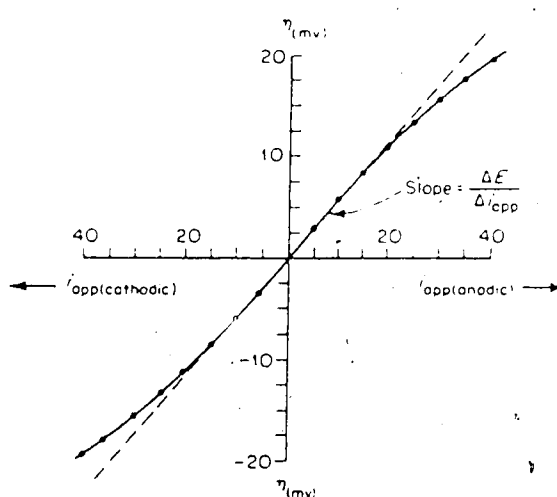


Fig. 14. Applied-current linear-polarization curve (from Fontana and Greene⁵)

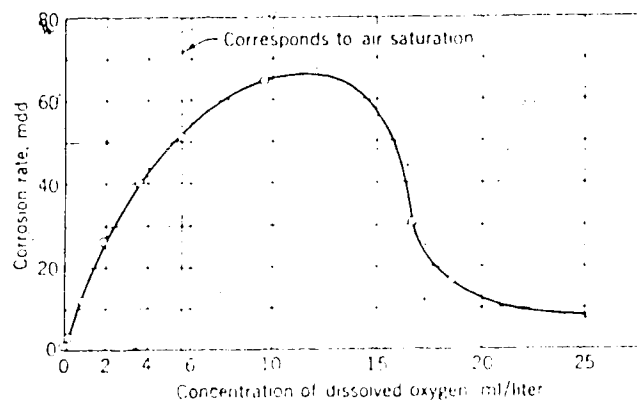


Fig. 15. Effect of oxygen concentration on mild steel in slowly moving distilled water at 25°C in a 48 hour test (from Uhlig¹⁵)

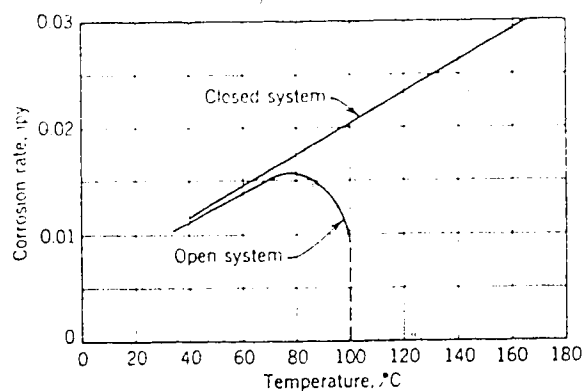


Fig. 16. Effect of temperature on corrosion of iron in water containing dissolved oxygen (from Uhlig¹⁵)

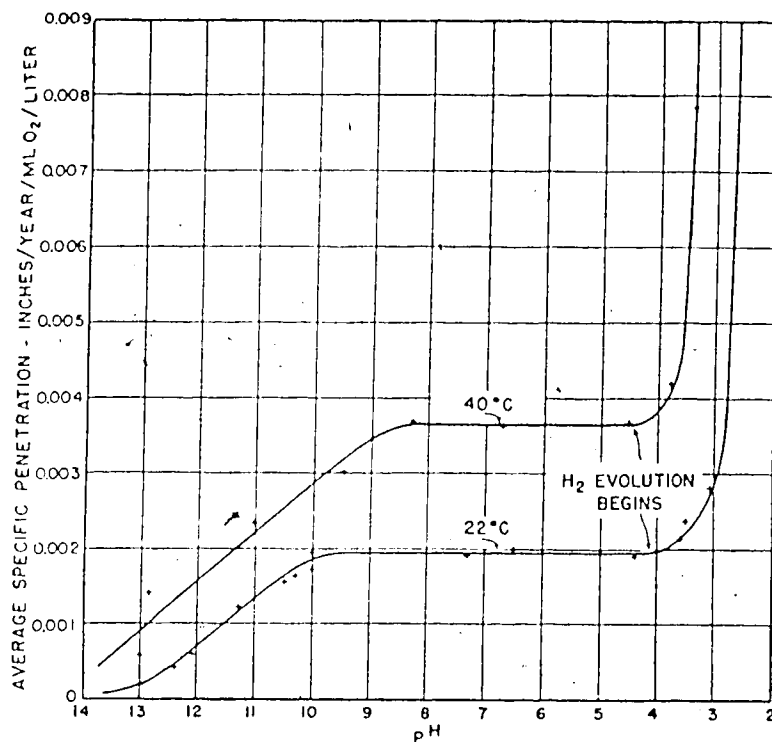


Fig. 17. Effect of pH on corrosion of mild steel (from Uhlig¹⁶)

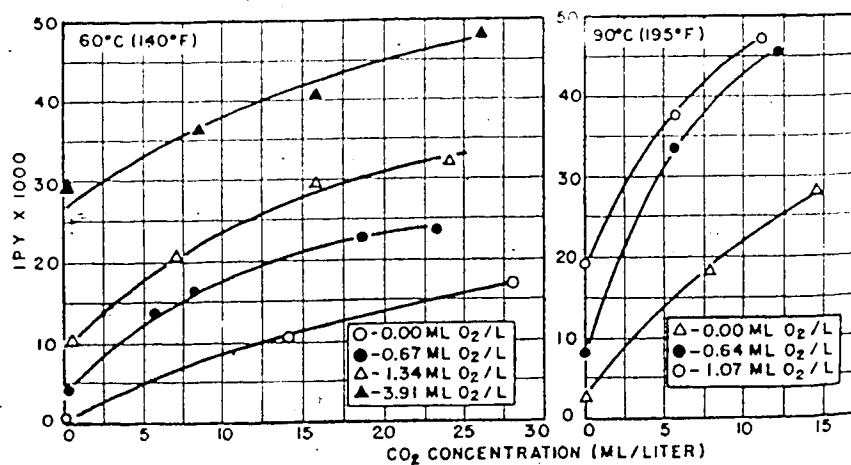


Fig. 18. Corrosion of mild steel as a function of dissolved CO₂ and O₂ concentration (from Uhlig¹⁶)

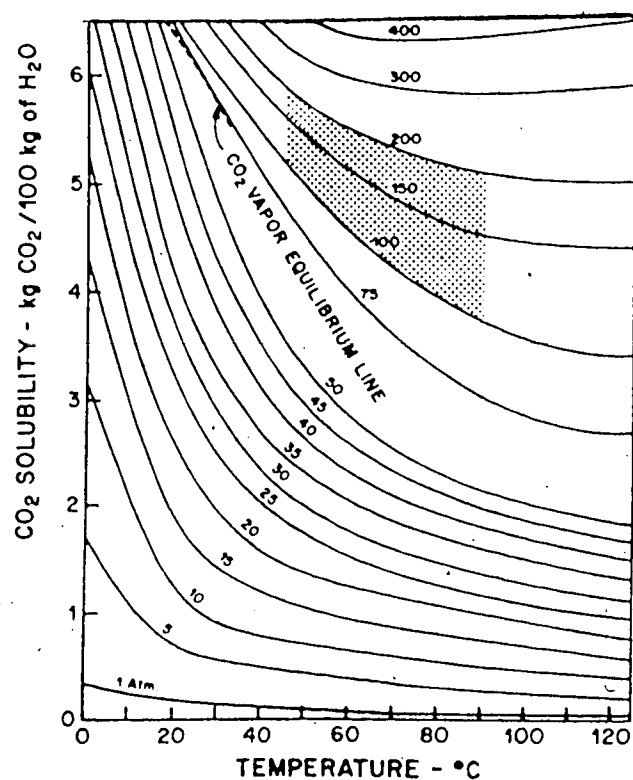


Fig. 19. Solubility of CO₂ in distilled water (from Mungan²⁷)

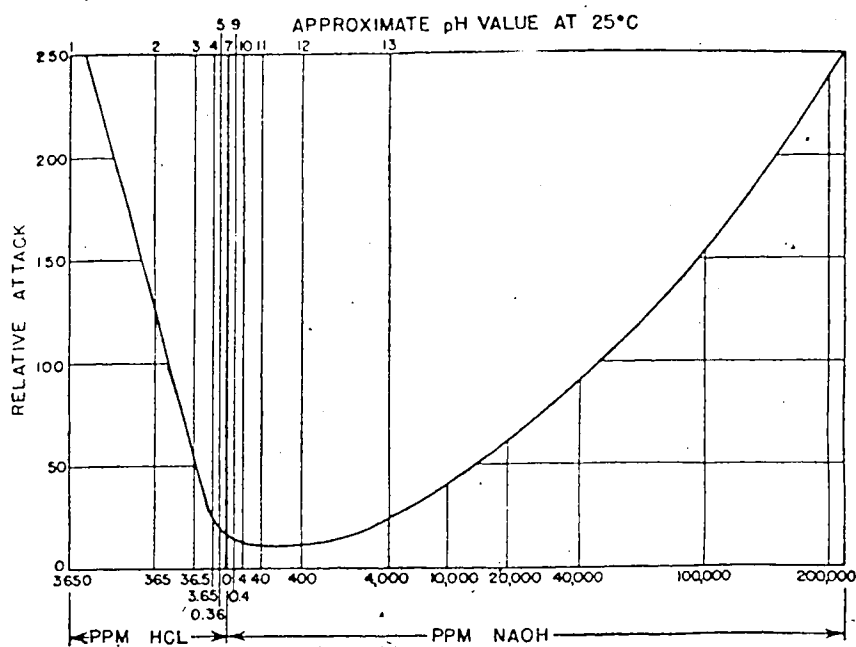


Fig. 20. Corrosion of iron in water at 310°C at various values of pH measured at 25°C (from Uhlig²⁰)

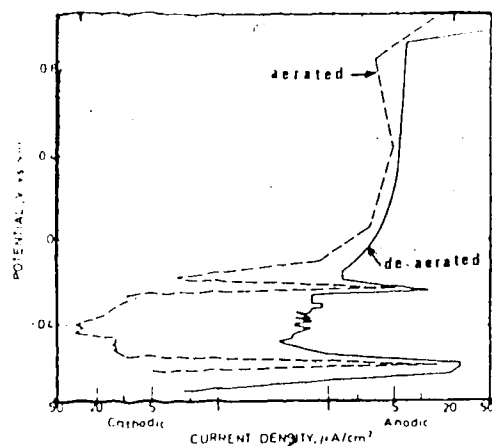


Fig. 21. Potentiostatic anodic polarization curves of iron in deaerated and air saturated solns. of 0.1 M Na_2CO_3 . (from Thomas et al.³³)

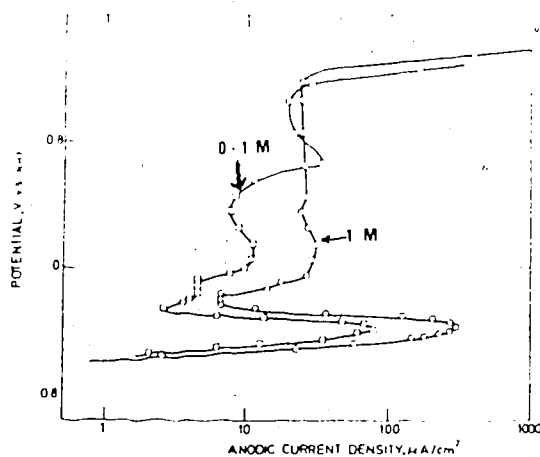


Fig. 22. Potentiostatic anodic polarization curves of iron in deaerated NaHCO_3 solns. (from Thomas et al.³³)

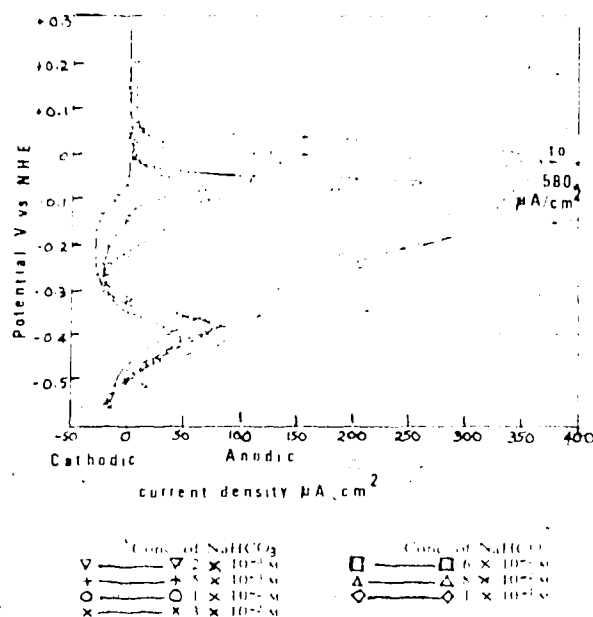
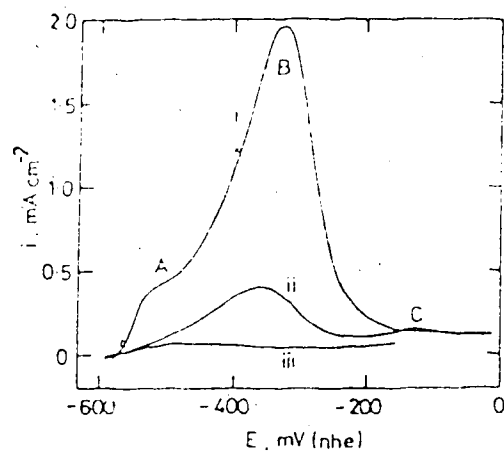


Fig. 23. Cathodic potentiokinetic polarization curves of mild steel in NaHCO_3 solutions (from Thomas and Davies³⁴)



Anodic polarization of Fe in 0.75M KHCO_3 , $0.75\text{M K}_2\text{CO}_3$, pH 8.8, $dE/dt = 10\text{ mV s}^{-1}$ from -650 mV (NHE) . (i) $\omega = 58.3\text{ Hz}$; (ii) $\omega = 0$; (iii) $\omega = 58.3\text{ Hz}$, solution saturated with $\text{Fe(III)} 4.4 \times 10^{-3}\text{ M}$.

Fig. 24. Anodic polarization of Fe in $0.75\text{ M KHCO}_3 + 0.75\text{ M K}_2\text{CO}_3$ (pH 8.8) at a scanning rate of 10 mV/s (from Davies and Burstein³⁵)

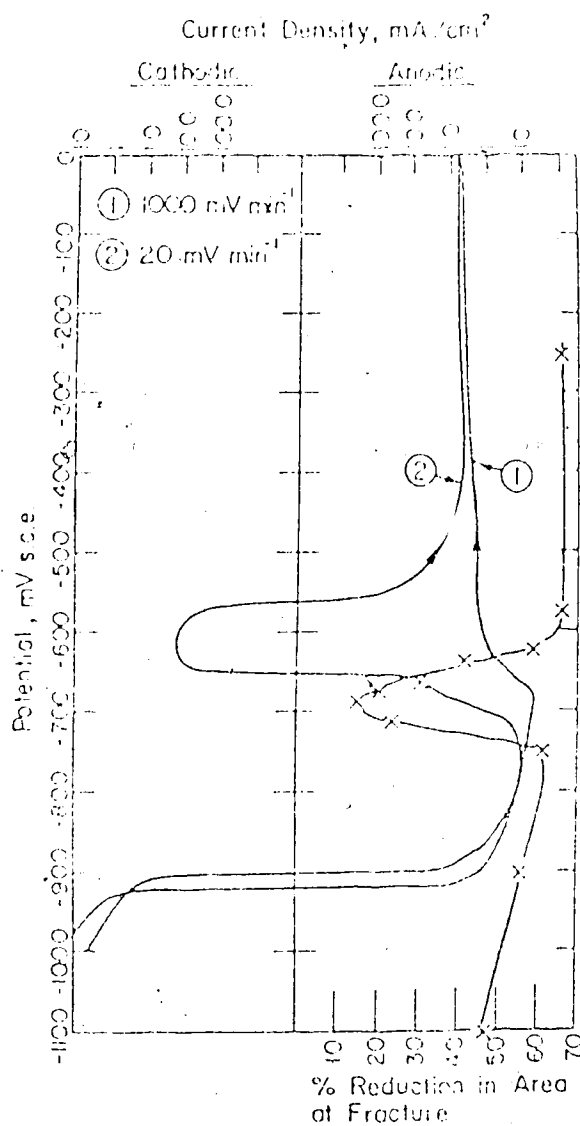


Fig. 25. Polarization curves and SCC test results for mild steel in 1 N Na_2CO_3 + 1 N NaHCO_3 at 90°C (from Sutcliffe et al.³⁶)

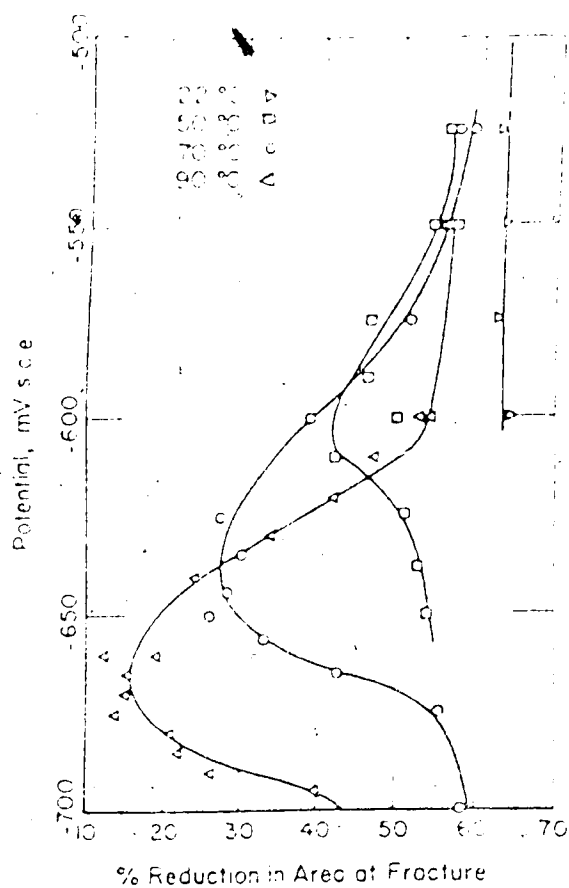


Fig. 26. Effect of temperature upon SCC of mild steel in constant strain rate tests at various potentials in 1 N $\text{Na}_2\text{CO}_3 + 1 \text{ N NaHCO}_3$ (from Sutcliffe et al.³⁶)

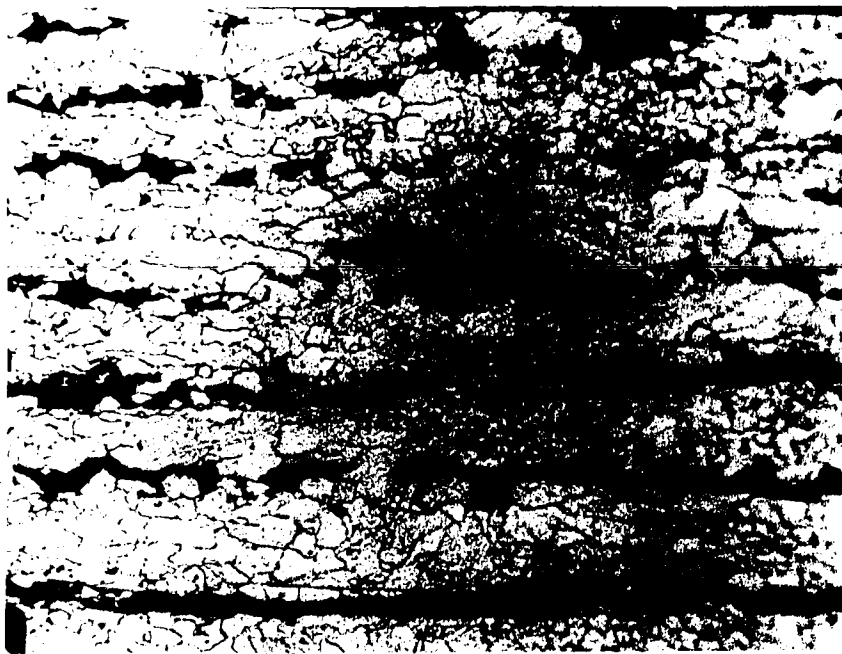


Fig. 27. Microstructure of X-70 steel with 2% nital as the etchant. X500

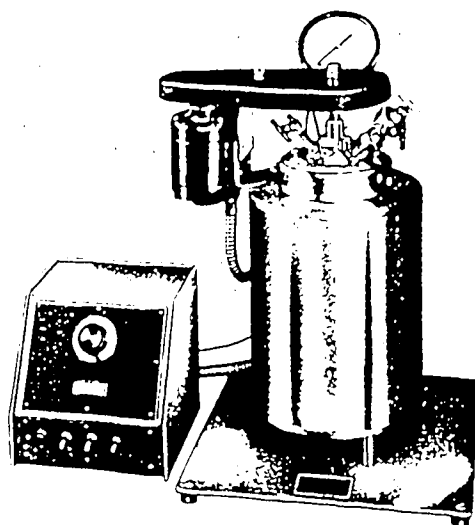


Fig. 28. 2000 mL Parr pressure reactor with its heating arrangement and automatic temperature controller

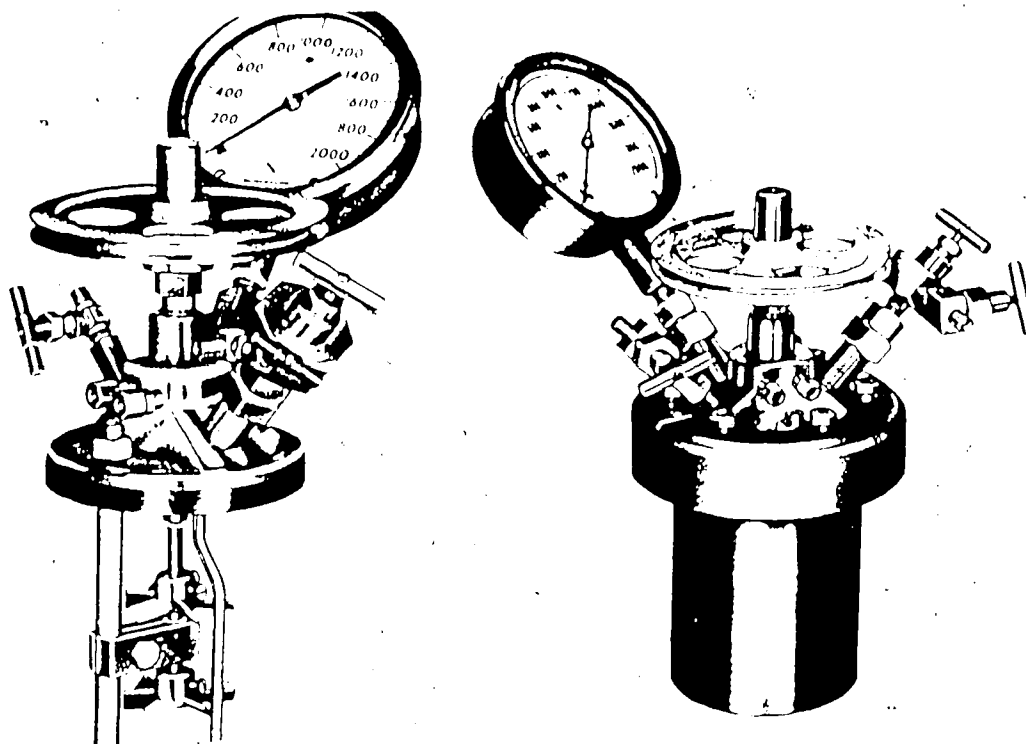


Fig. 29. 2000 mL Parr pressure reactor head assembly and
assembled bomb

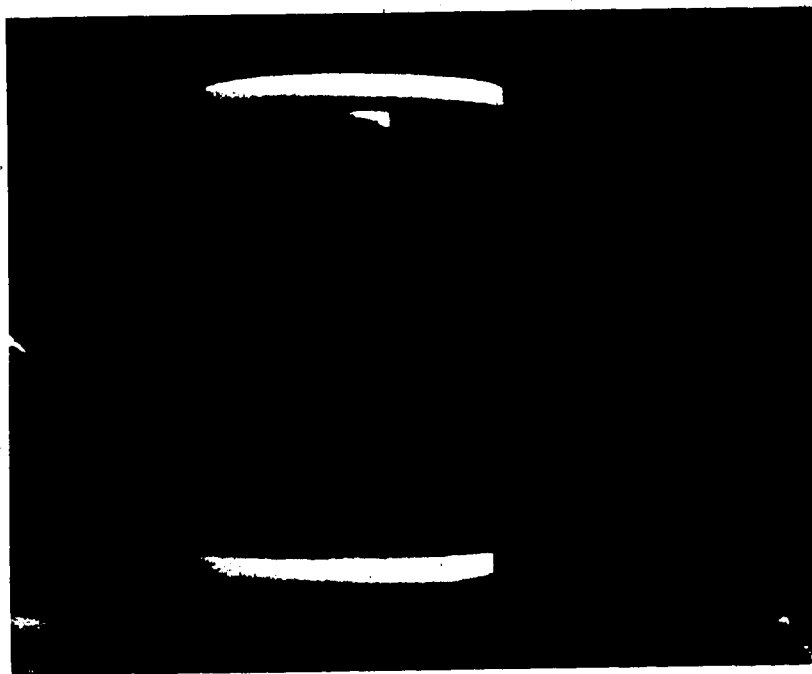


Fig. 30. Weight-loss test coupons assembled between 2 Teflon
discs

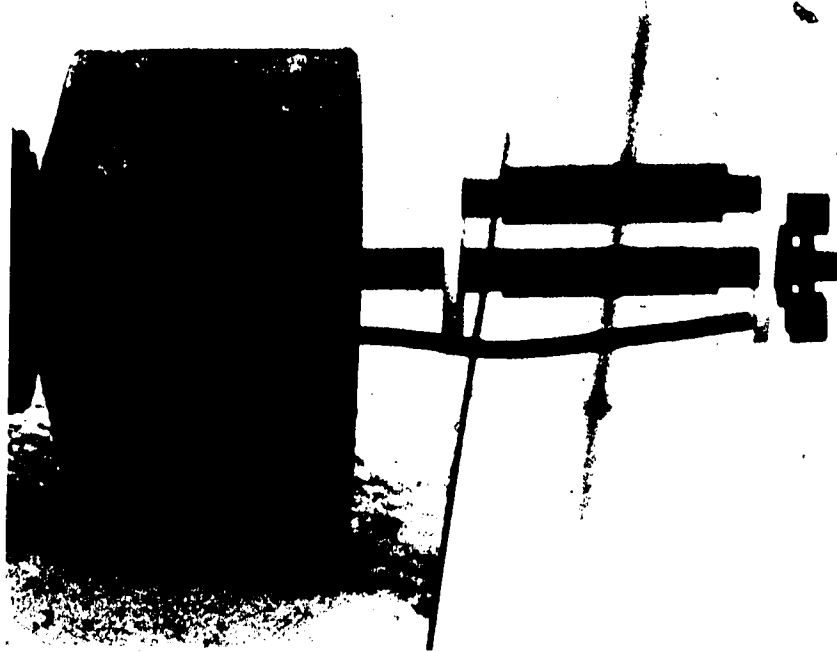


Fig. 31. Weight-loss test coupon assembly mounted onto the head of 1000 mL autoclave

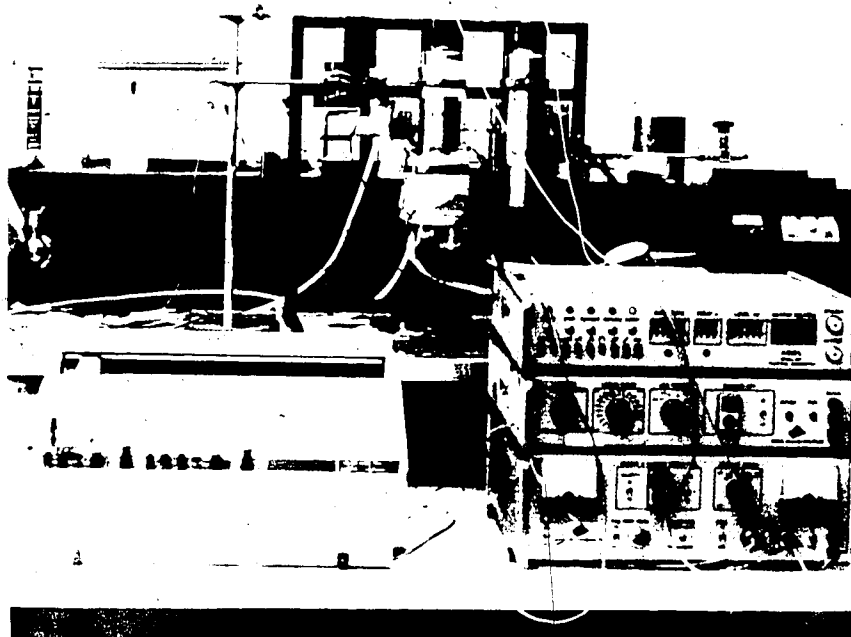


Fig. 32. The potentiostat unit along with the corrosion cell



Fig. 33. Corrosion cell assembly

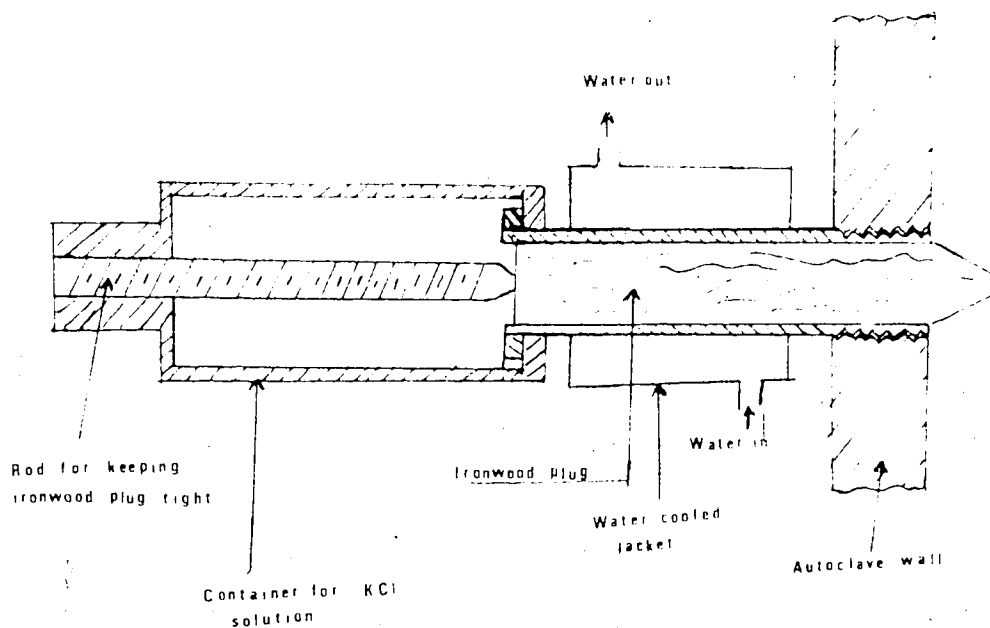
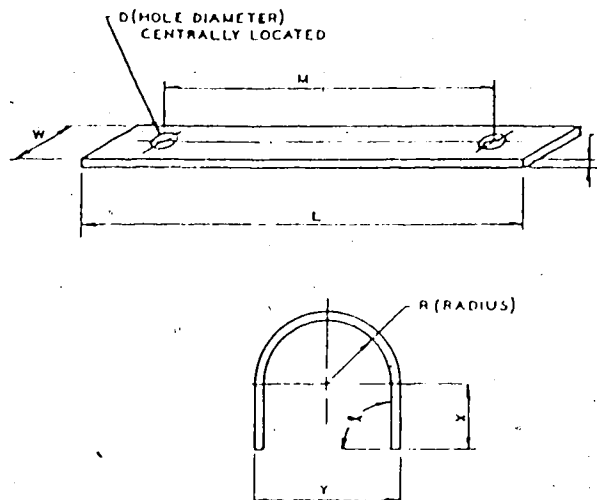


Fig. 34. Salt bridge and its connection to the working electrode autoclave. Schema c.

ASTM G 30



Typical Dimensions (SI Units)

Example	L, mm	M, mm	W, mm	T, mm	D, mm	X, mm	Y, mm	R, mm	α , rad
1	80	50	20	2.5	10	32	14	5	1.57
2	100	90	9	3.0	7	25	38	16	1.57
3	120	90	20	1.5	8	35	35	16	1.57
4	130	100	15	3.0	6	45	32	13	1.57
5	150	140	15	0.8	3	61	20	9	1.57
6	310	250	25	13.0	13	105	90	32	1.57
7	510	460	25	6.5	13	136	165	76	1.57

Fig. 35. Typical U-bend specimens (ASTM G-30)

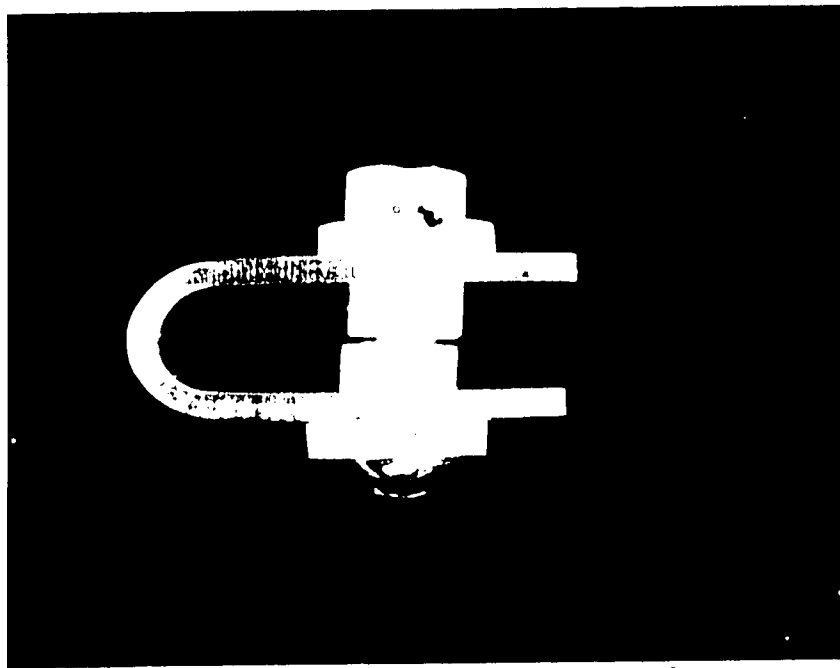


Fig. 36. U-bend specimens with Teflon sleeves and bolts in position

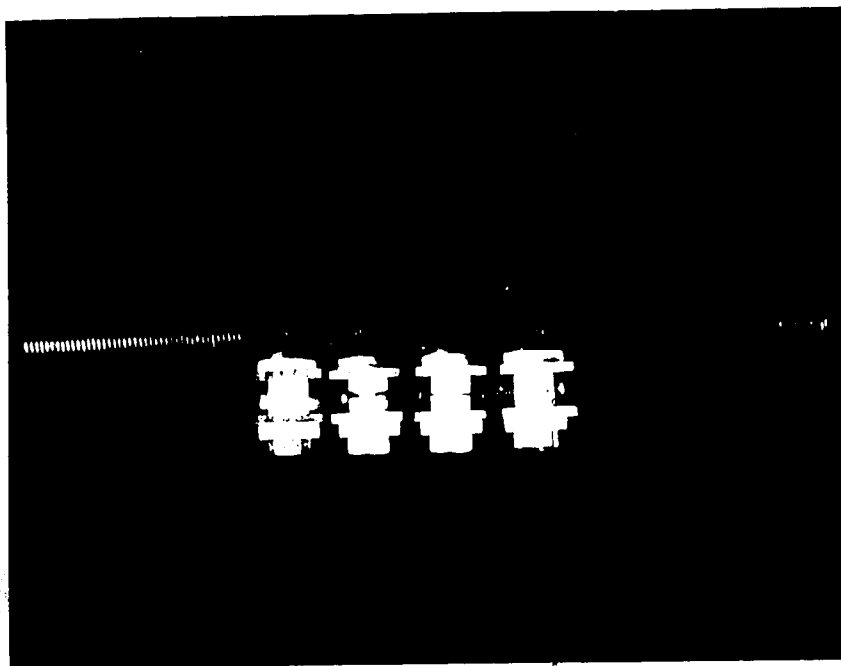


Fig. 37. U-bend specimens assembled together by welding a rod to the bolt heads

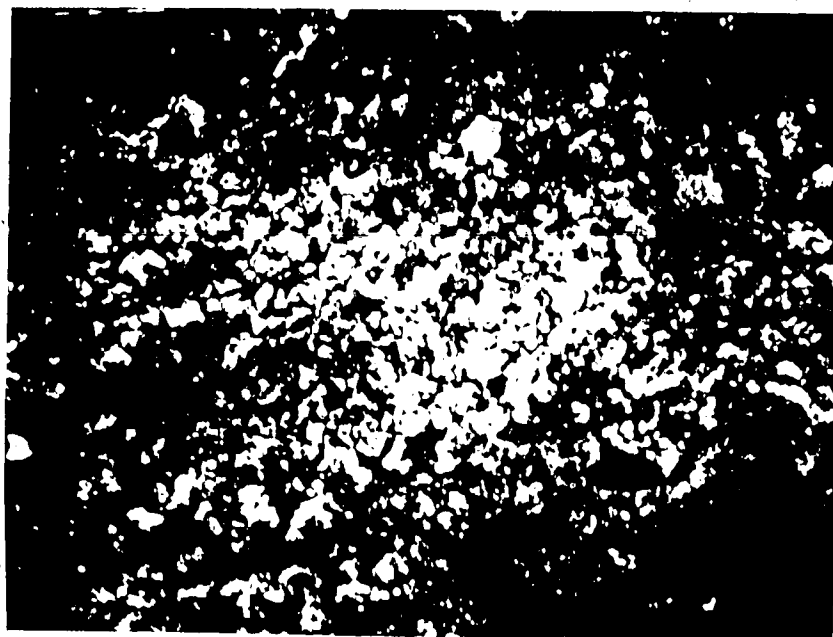


Fig. 38. Surface film in $\text{H}_2\text{O} + \text{CO}_2$ at 200°C after one week.

X560

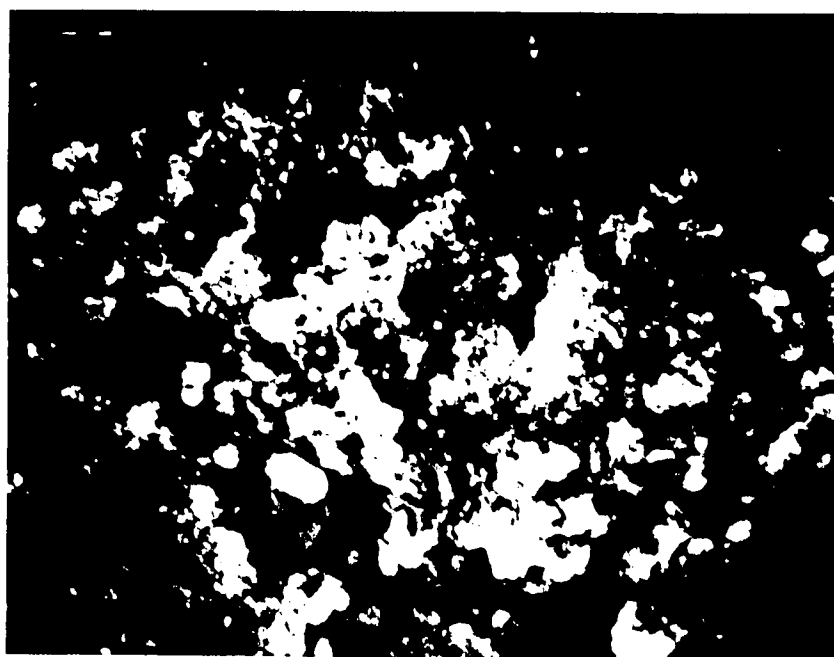


Fig. 39. Surface film in $\text{H}_2\text{O} + \text{CO}_2$ at 200°C after one week.

X1100



Fig. 40. Surface film in $\text{H}_2\text{O} + \text{CO}_2$ at 200°C after 7 weeks.

X560

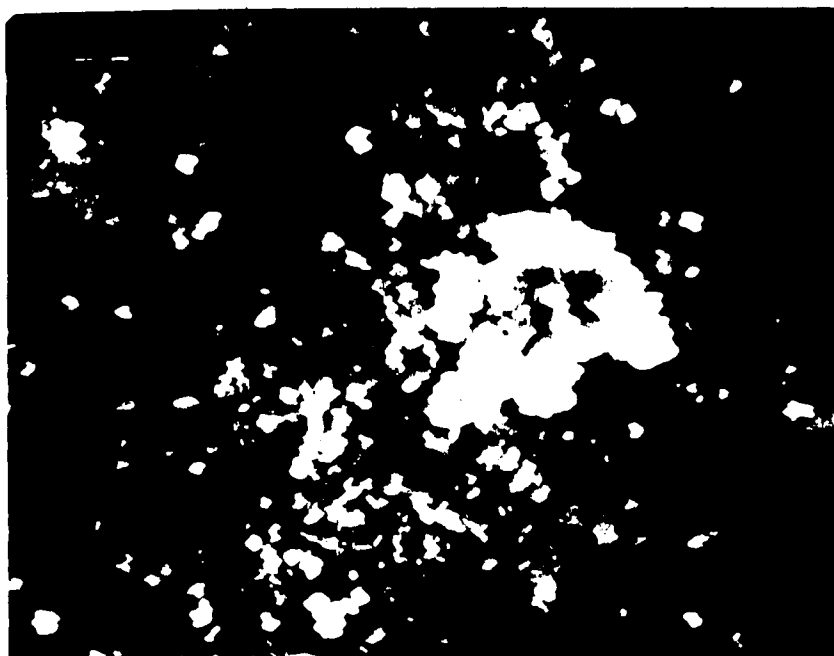


Fig. 41. Surface film in $\text{H}_2\text{O} + \text{CO}_2$ at 200°C after 7 weeks.

X1100

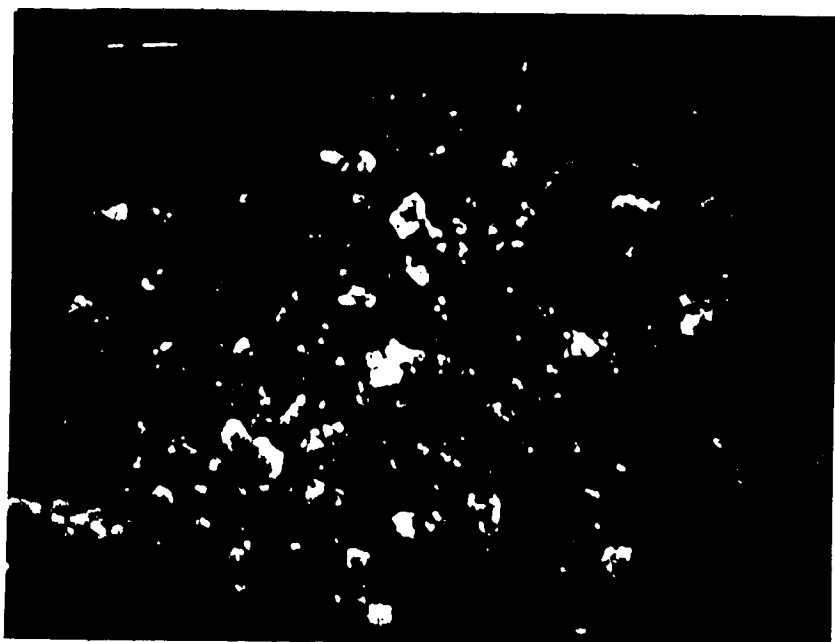


Fig. 42. Surface film in $\text{H}_2\text{O} + \text{CO}_2$ at 200°C after 2 weeks
(top side of the sample, freely exposed to the solution).

X560

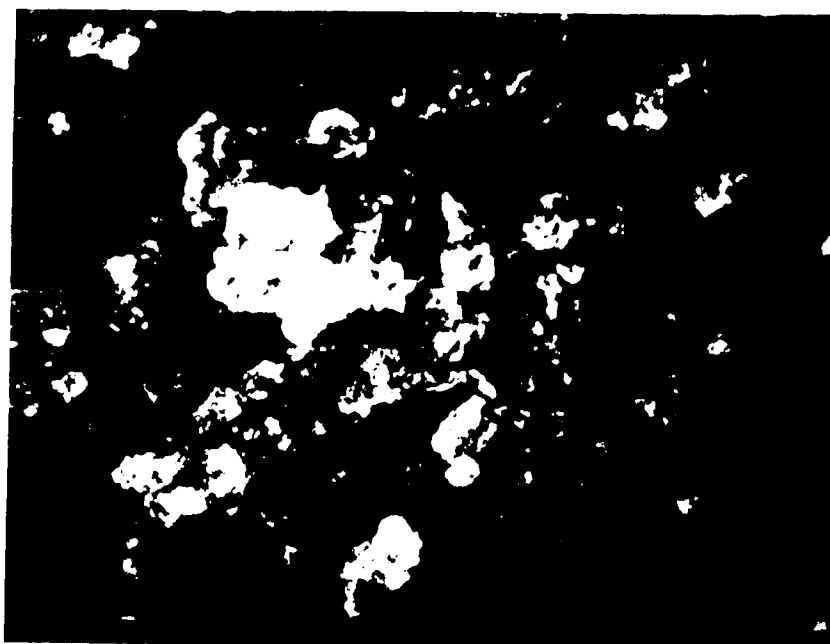


Fig. 43. Surface film in $\text{H}_2\text{O} + \text{CO}_2$ at 200°C after 2 weeks
(top side of the sample, freely exposed to the solution).

X1100

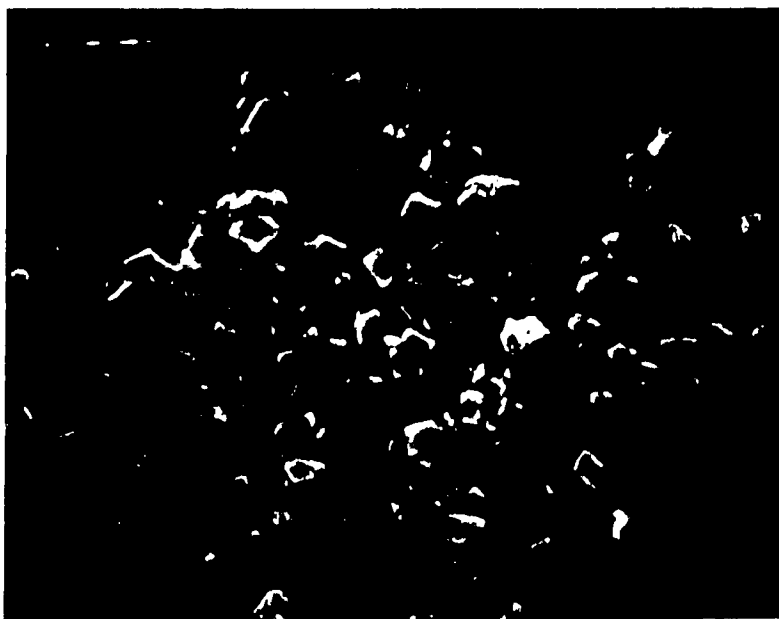


Fig. 44. Surface film in $\text{H}_2\text{O} + \text{CO}_2$ at 200°C after 2 weeks
(bottom side of the sample, not freely exposed to the
solution). X560



Fig. 45. Surface film in $\text{H}_2\text{O} + \text{CO}_2$ at 200°C after 2 weeks
(bottom side of the sample, not freely exposed to the
solution). X1100

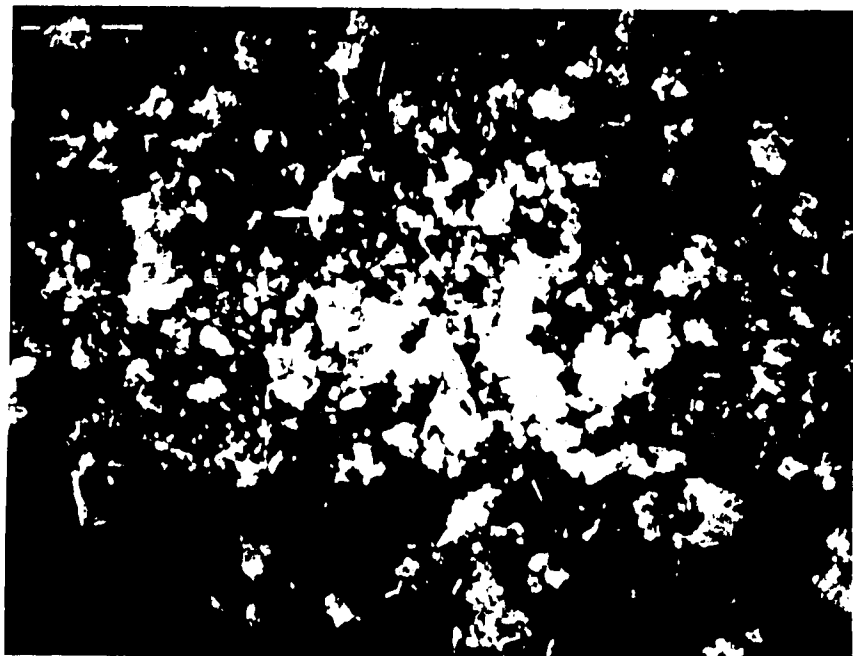


Fig. 46. Surface film in $\text{H}_2\text{O} + \text{CO}_2$ at 300°C after one week.

X560

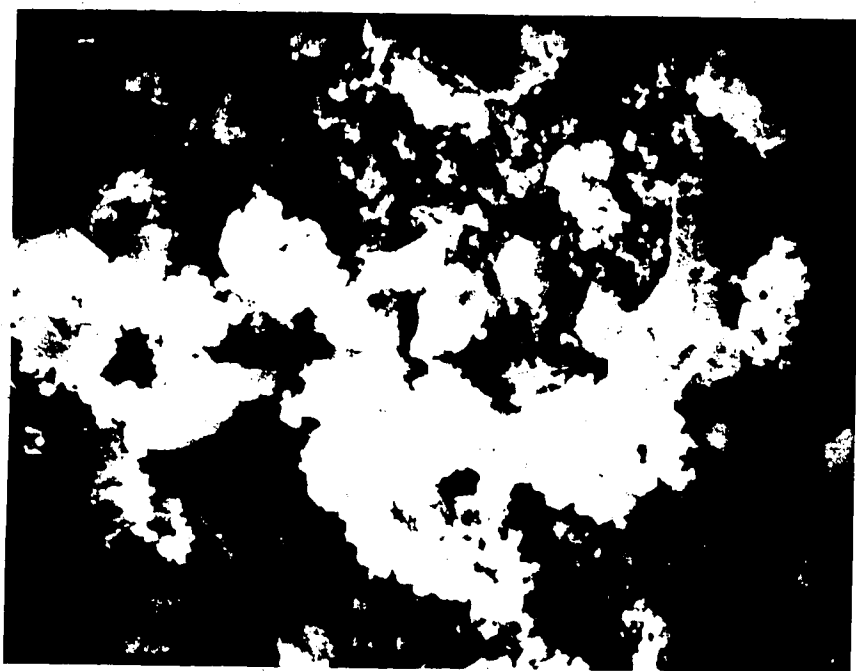


Fig. 47. Surface film in $\text{H}_2\text{O} + \text{CO}_2$ at 300°C after one week.

X1100

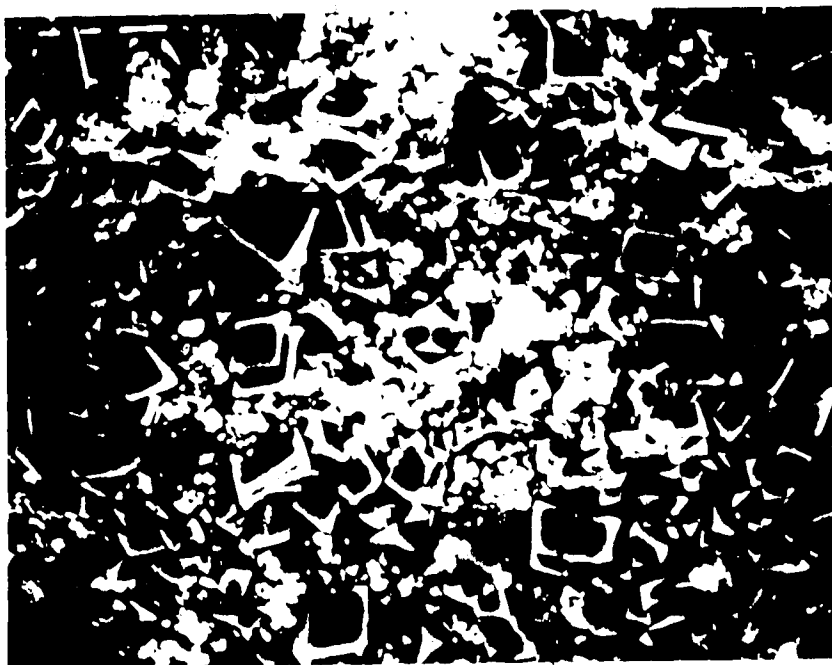


Fig. 48. Surface film in $\text{H}_2\text{O} + \text{CO}_2$ at 300°C after five weeks. X560



Fig. 49. Surface film in $\text{H}_2\text{O} + \text{CO}_2$ at 300°C after five weeks. X1100



Fig. 50. Surface film in 1 M NH_4HCO_3 + CO_2 at 300°C after one week. X560



Fig. 51. Surface film in 1 M NH_4HCO_3 + CO_2 at 300°C after one week. X1100

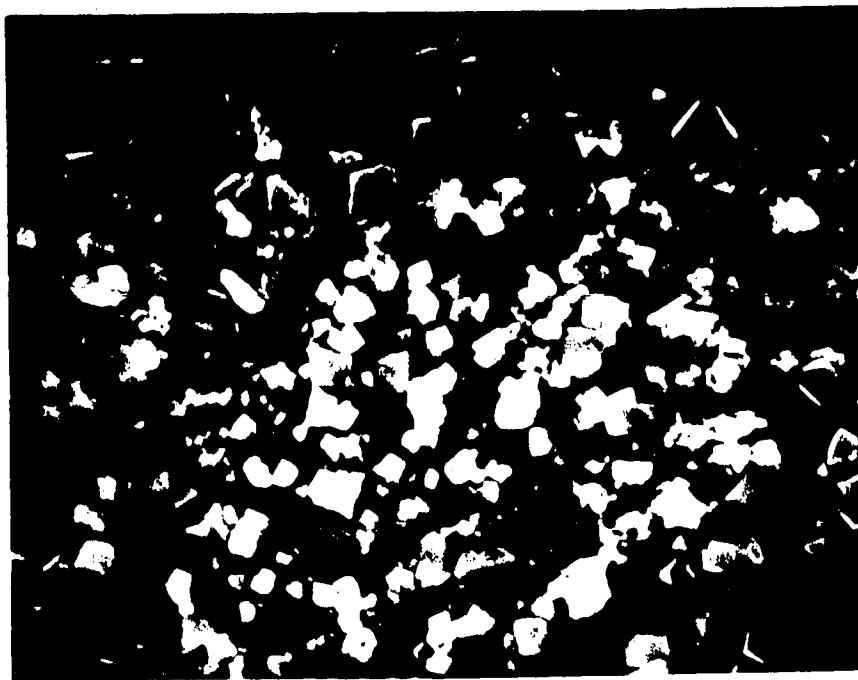


Fig. 52. Surface film in 1 M NH_4HCO_3 + CO_2 at 300°C after 3 weeks. X1100

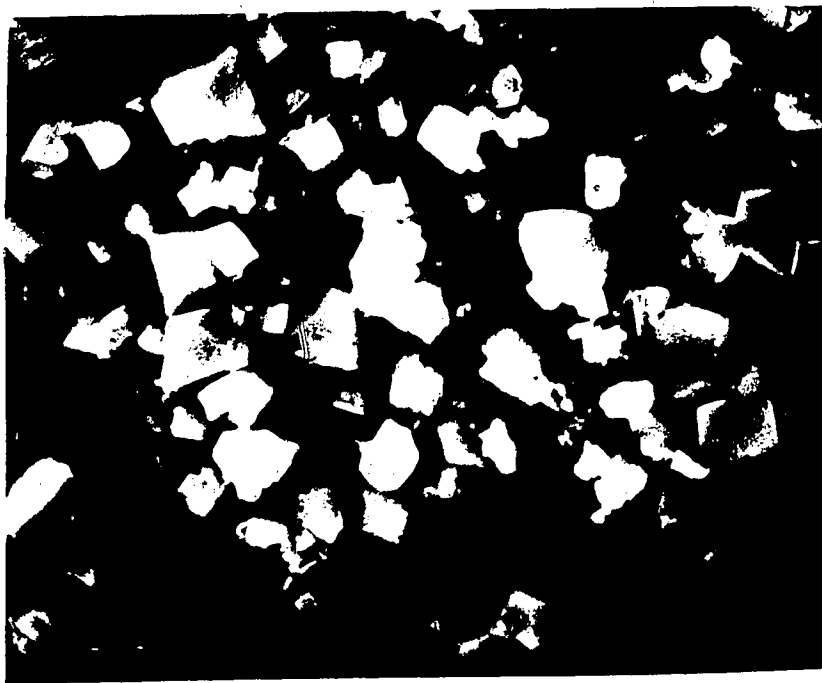


Fig. 53. Surface film in 1 M NH_4HCO_3 + CO_2 at 300°C after 3 weeks. X1800

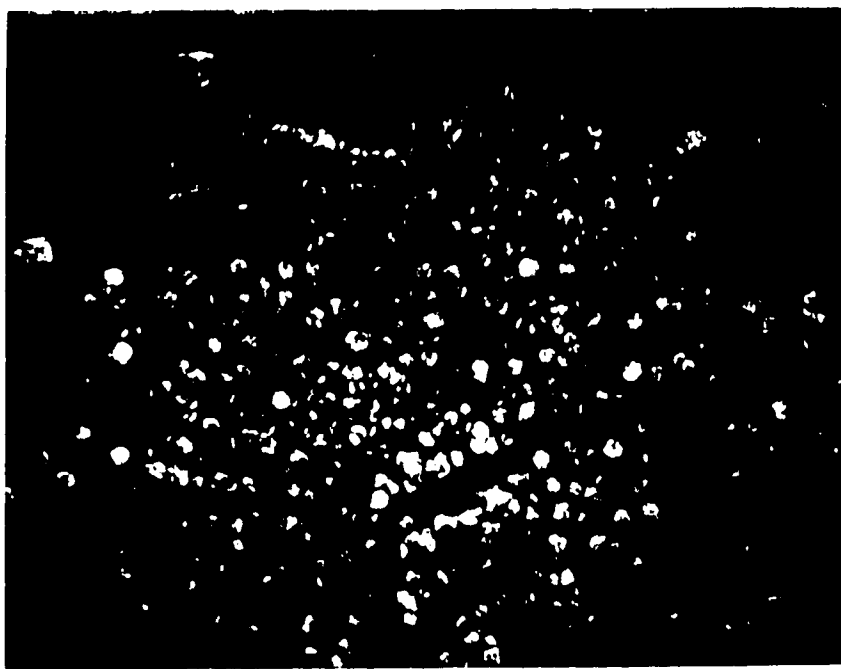


Fig. 54. Surface film in 1 M NH_4HCO_3 at 200°C after one week. X560

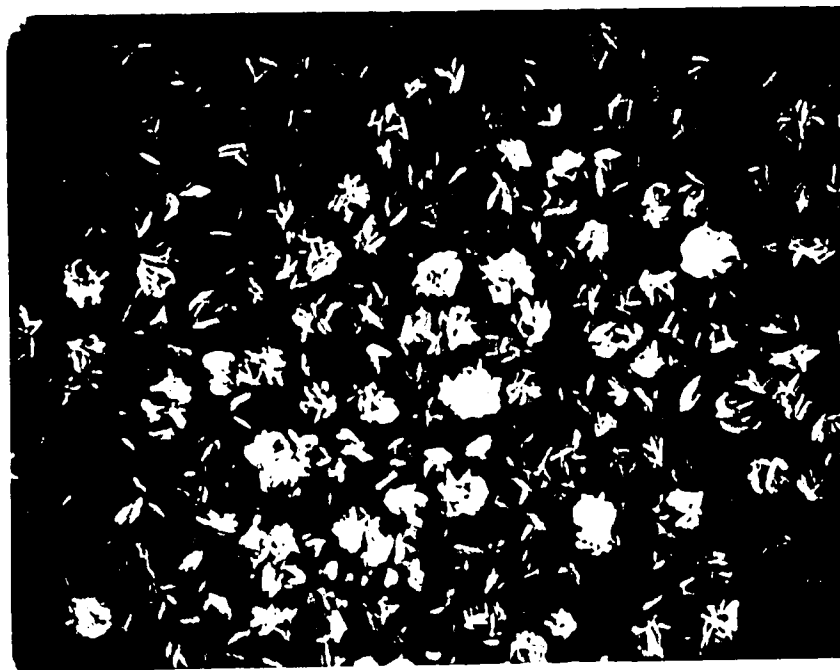


Fig. 55. Surface film in 1 M NH_4HCO_3 at 200°C after one week. X1100



Fig. 56. Surface film in 1 M NH_4HCO_3 at 200°C after 30 days.

X560

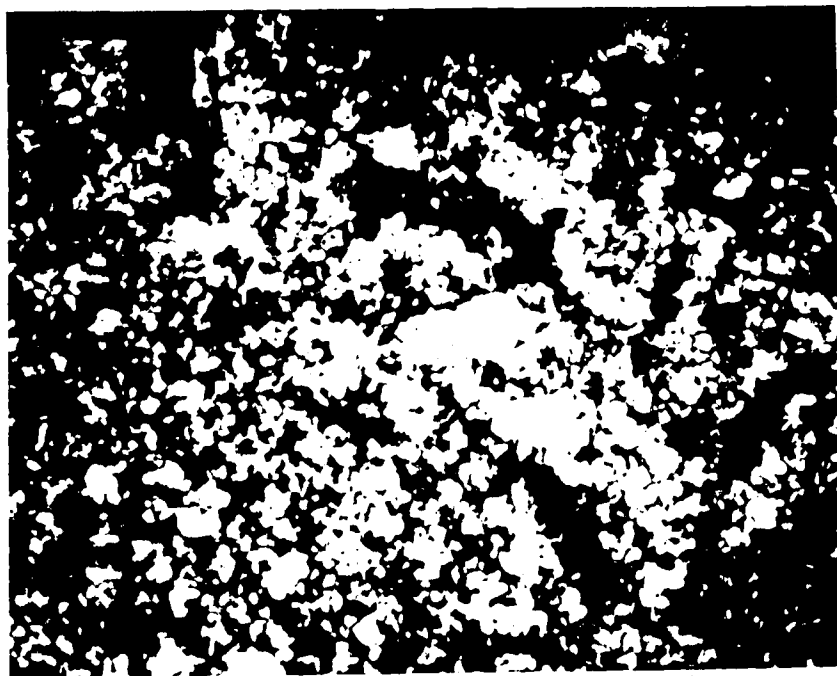


Fig. 57. Surface film in 1 M NH_4HCO_3 at 200°C after 30 days.

X1100

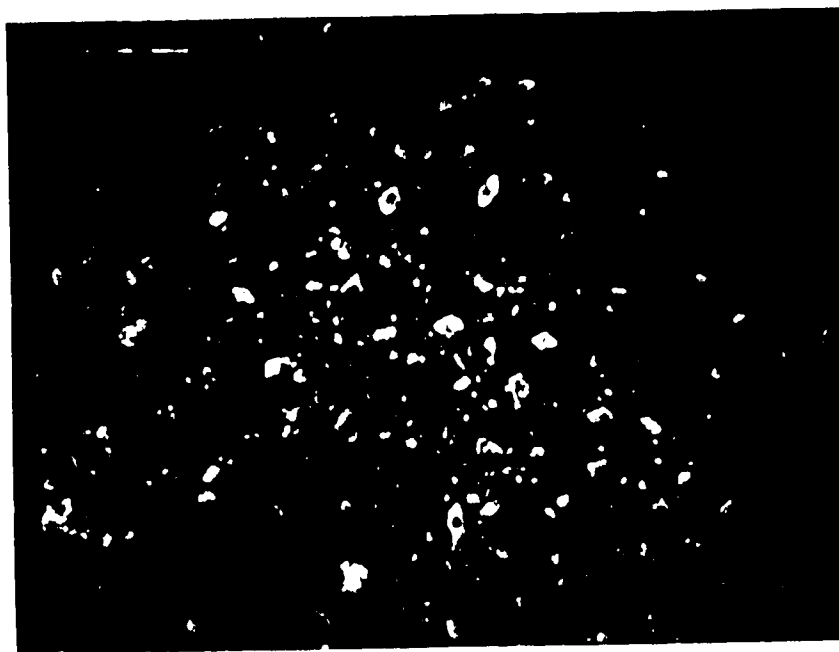


Fig. 58. Surface film in 1 M NH_4HCO_3 at 300°C after one week. X560



Fig. 59. Surface film in 1 M NH_4HCO_3 at 300°C after one week. X1100

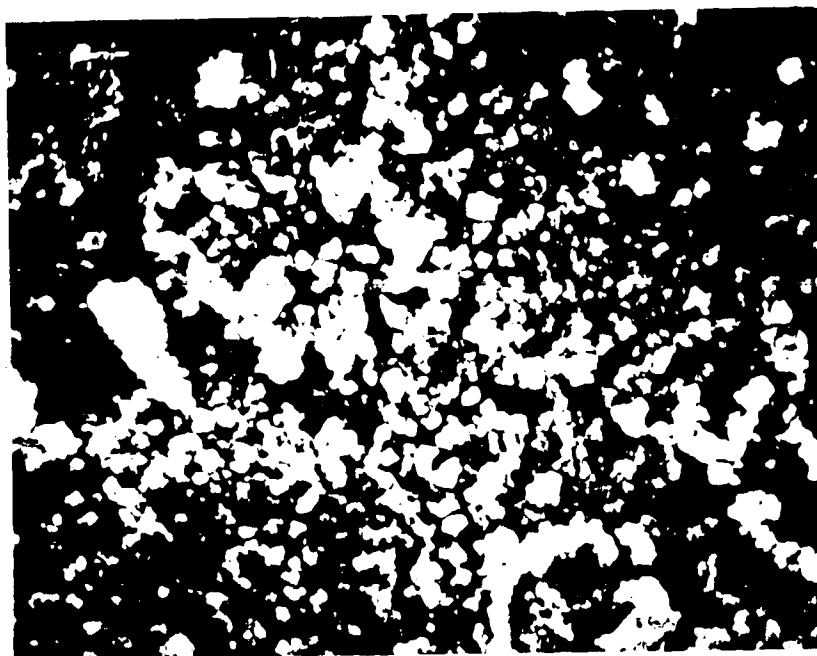


Fig. 60. Surface film in 1 M NH_4HCO_3 at 300°C after 2 weeks.

X1100

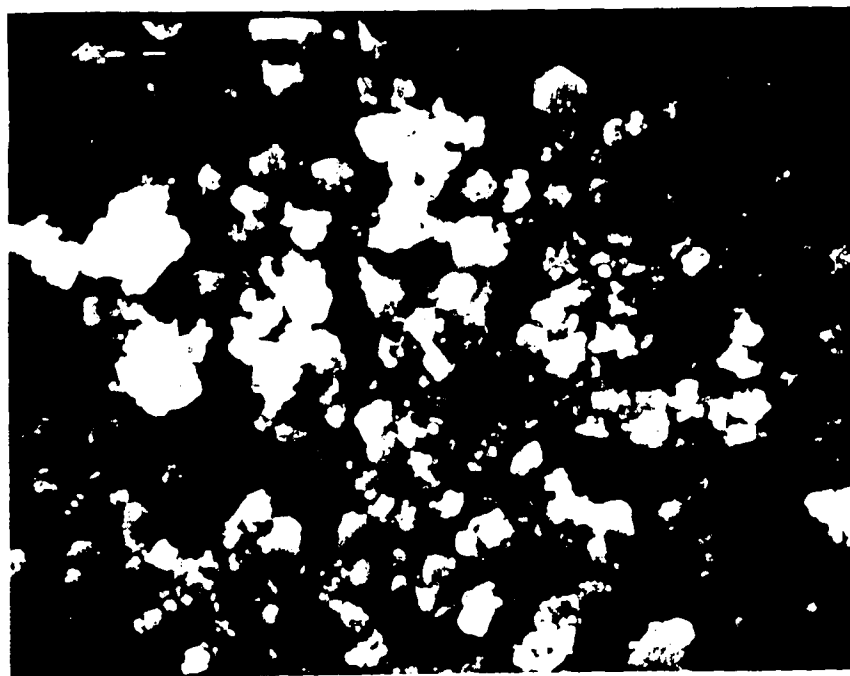


Fig. 61. Surface film in 1 M NH_4HCO_3 at 300°C after 2 weeks.

X1800

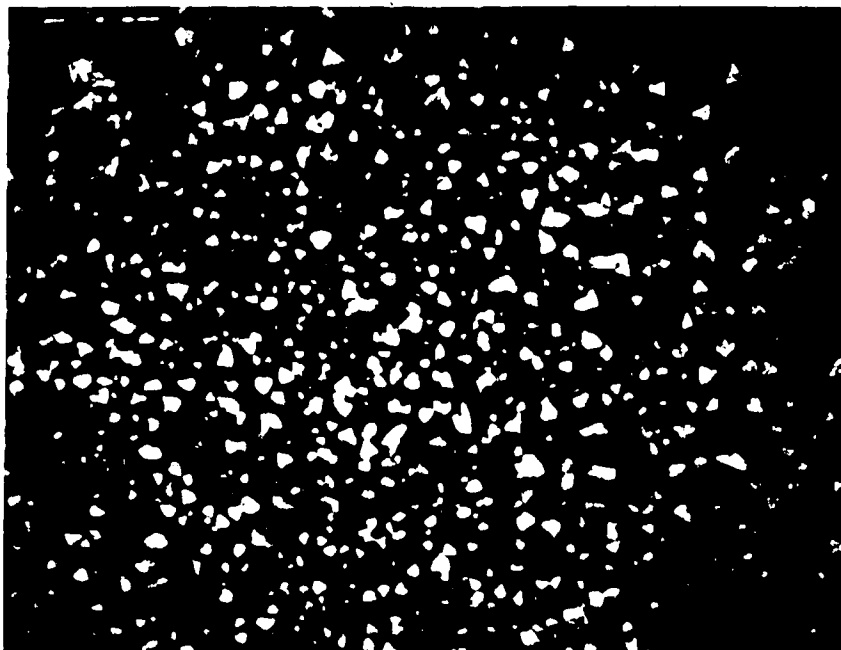


Fig. 62. Surface film in 1 M $(\text{NH}_4)_2\text{CO}_3$ at 200°C after 4 weeks. X560

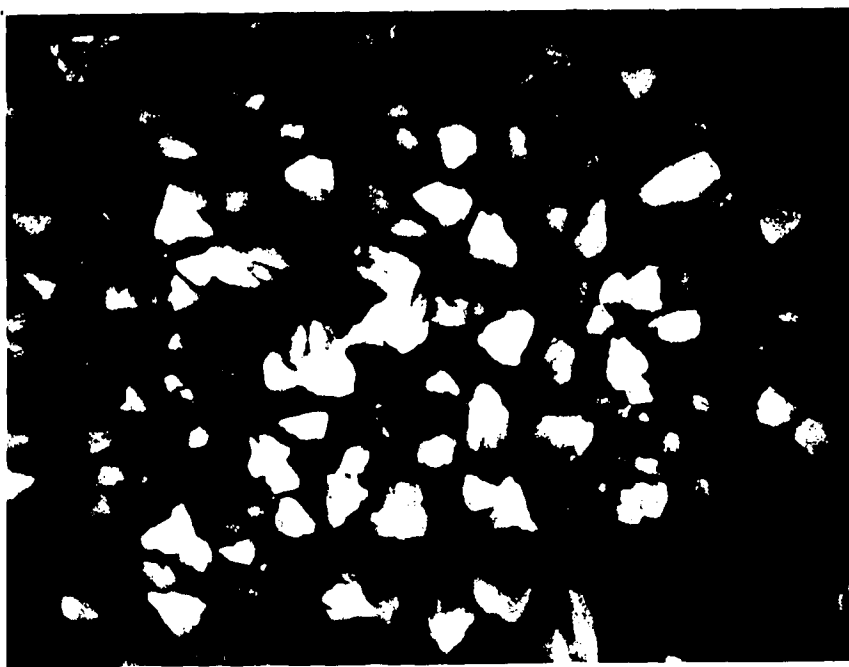


Fig. 63. Surface film in 1 M $(\text{NH}_4)_2\text{CO}_3$ at 200°C after 4 weeks. X1100

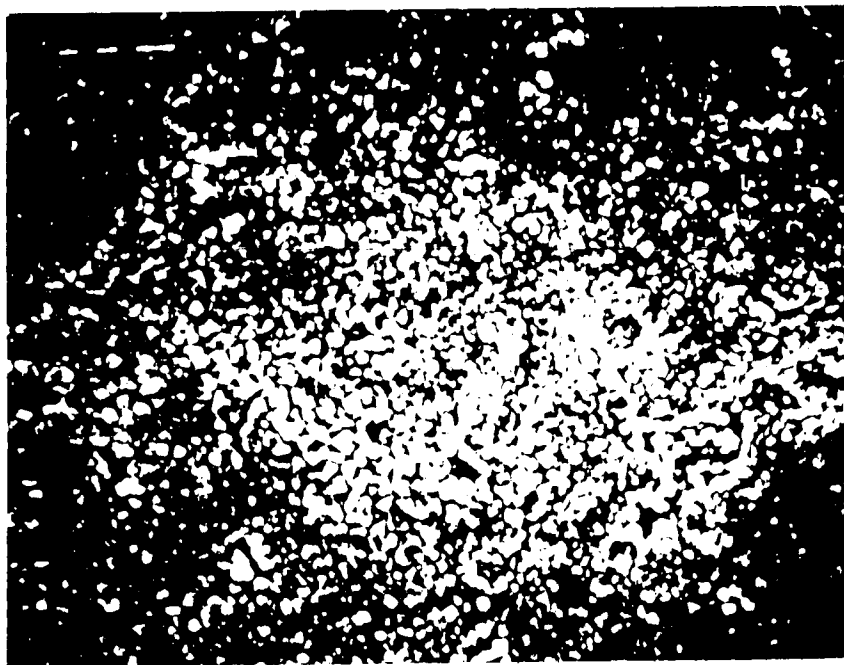


Fig. 64. Surface film in 1 M NH_4HCO_3 + 1 M NH_4OH at 200°C
after one week. X560

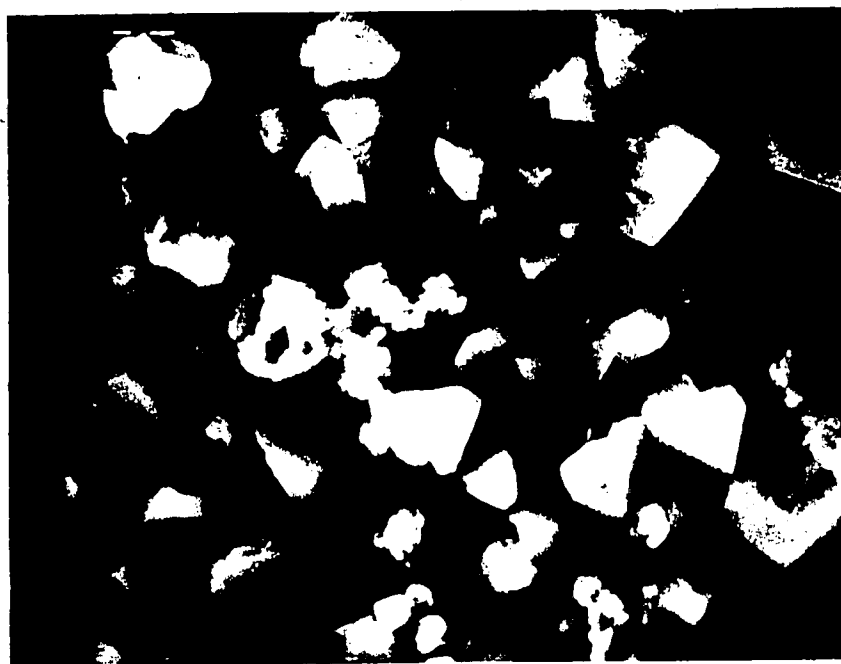


Fig. 65. Surface film in 1 M NH_4HCO_3 + 1 M NH_4OH at 200°C
after one week. X1800

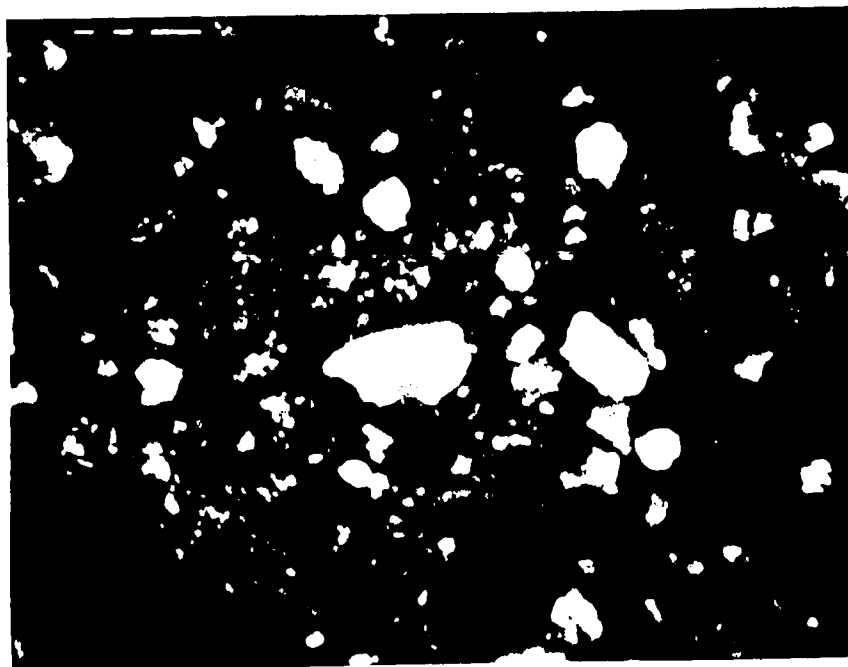


Fig. 66. Surface film in 1 M NH_4HCO_3 + 1 M NH_4OH at 200°C
after 4 weeks. X560

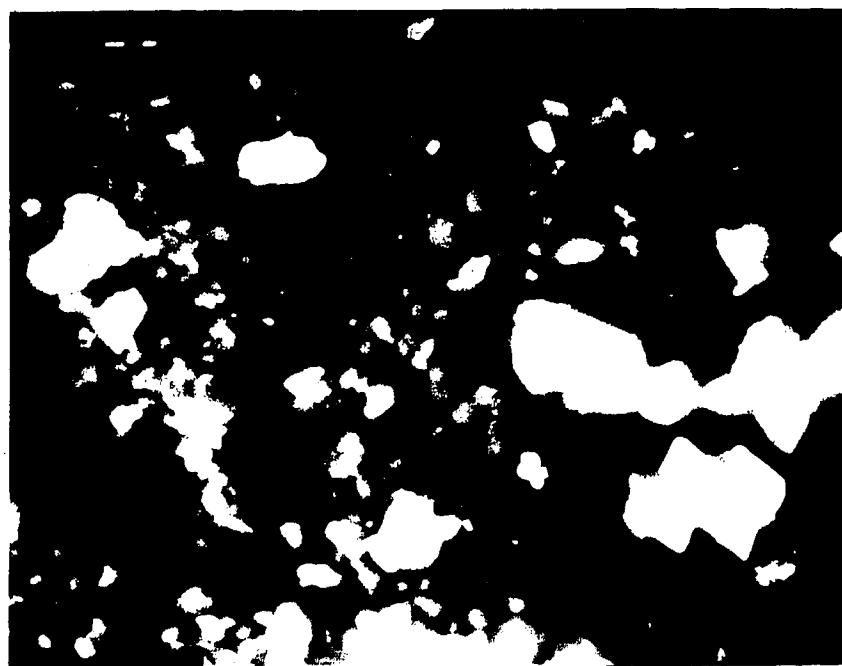


Fig. 67. Surface film in 1 M NH_4HCO_3 + 1-M NH_4OH at 200°C
after 4 weeks. X1100

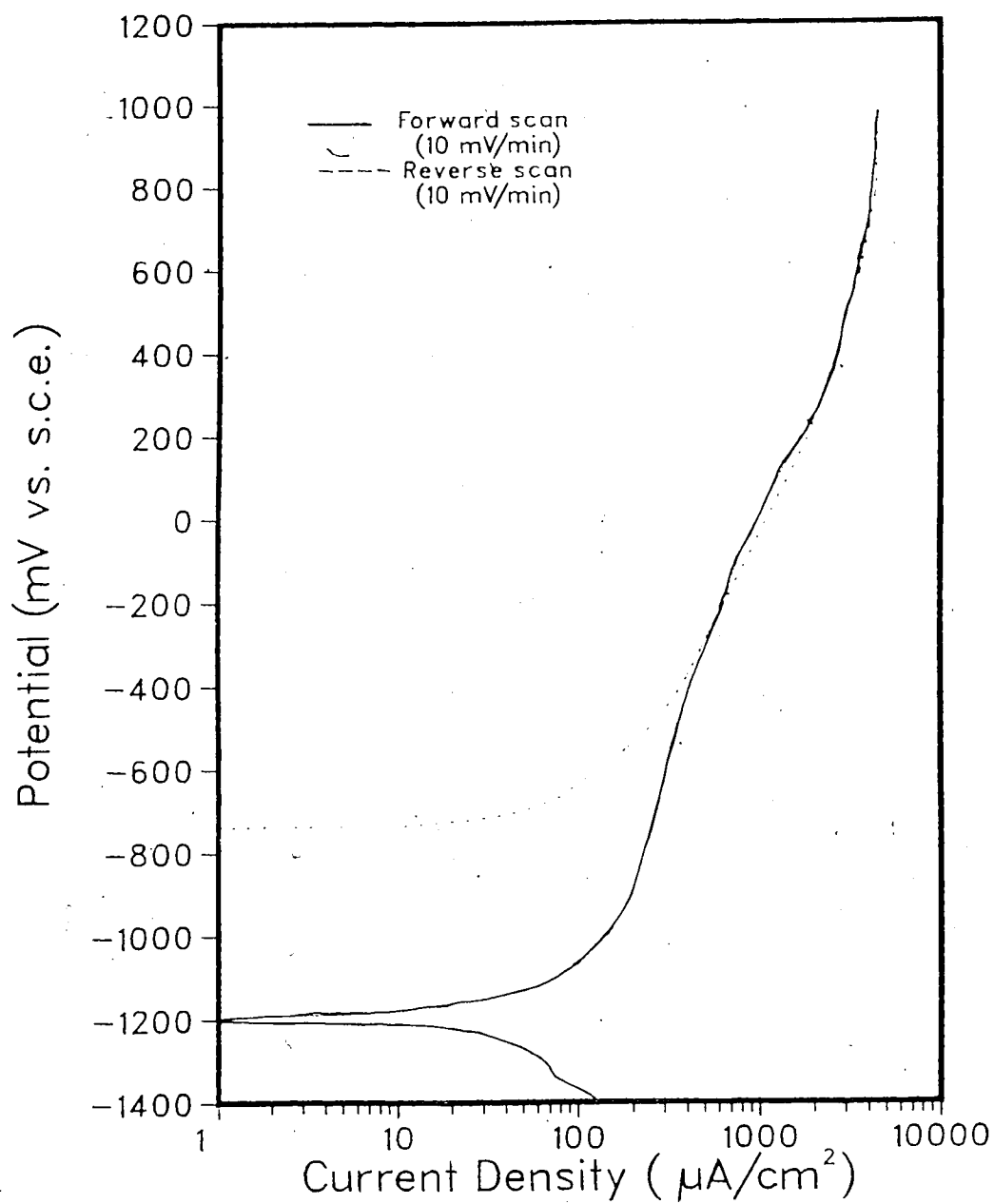


Fig. 68. Potentiodynamic polarization curve in $\text{H}_2\text{O} + \text{CO}_2$ at 100°C .

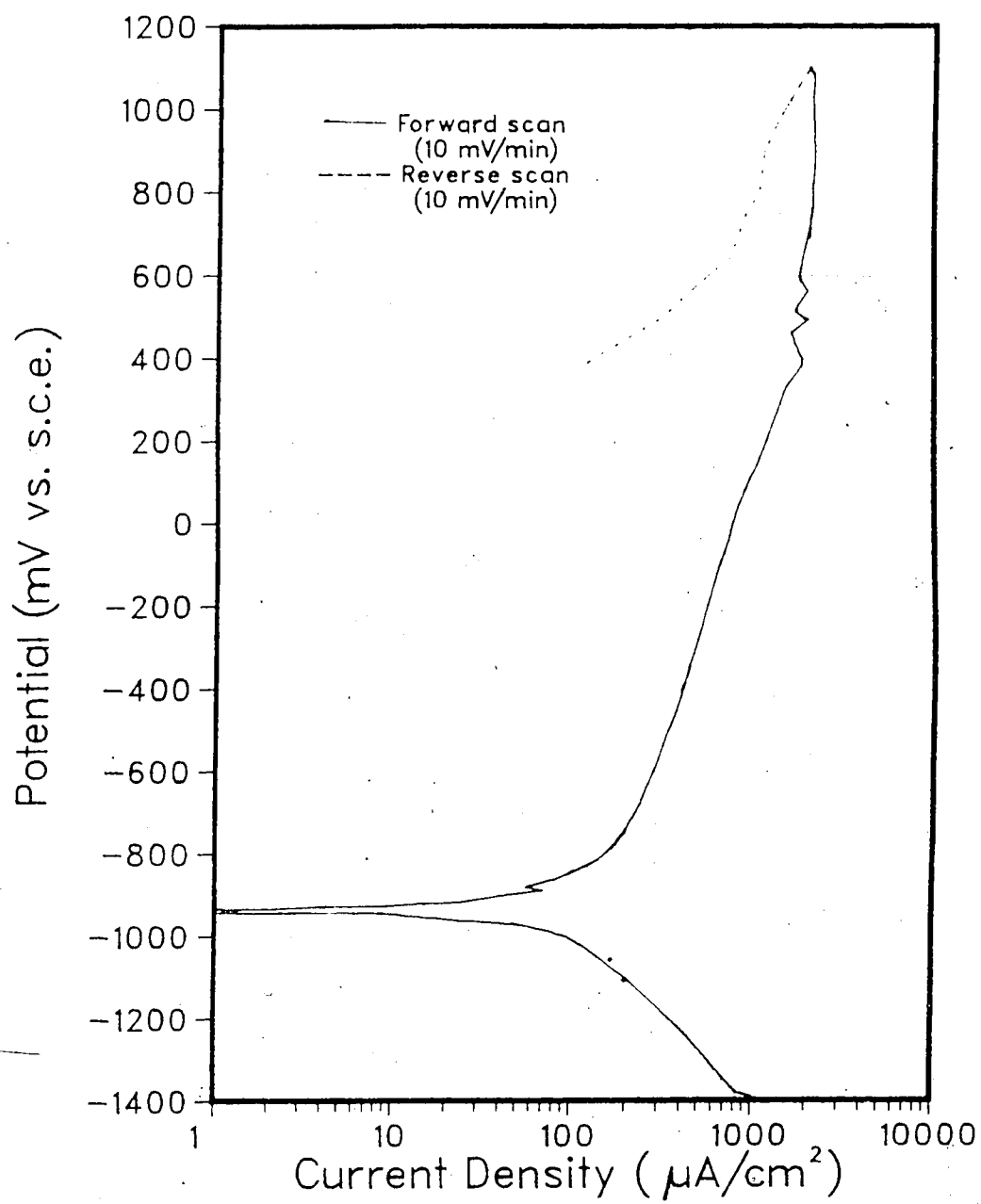


Fig. 69. Potentiodynamic polarization curve in $\text{H}_2\text{O} + \text{CO}_2$ at 150°C .

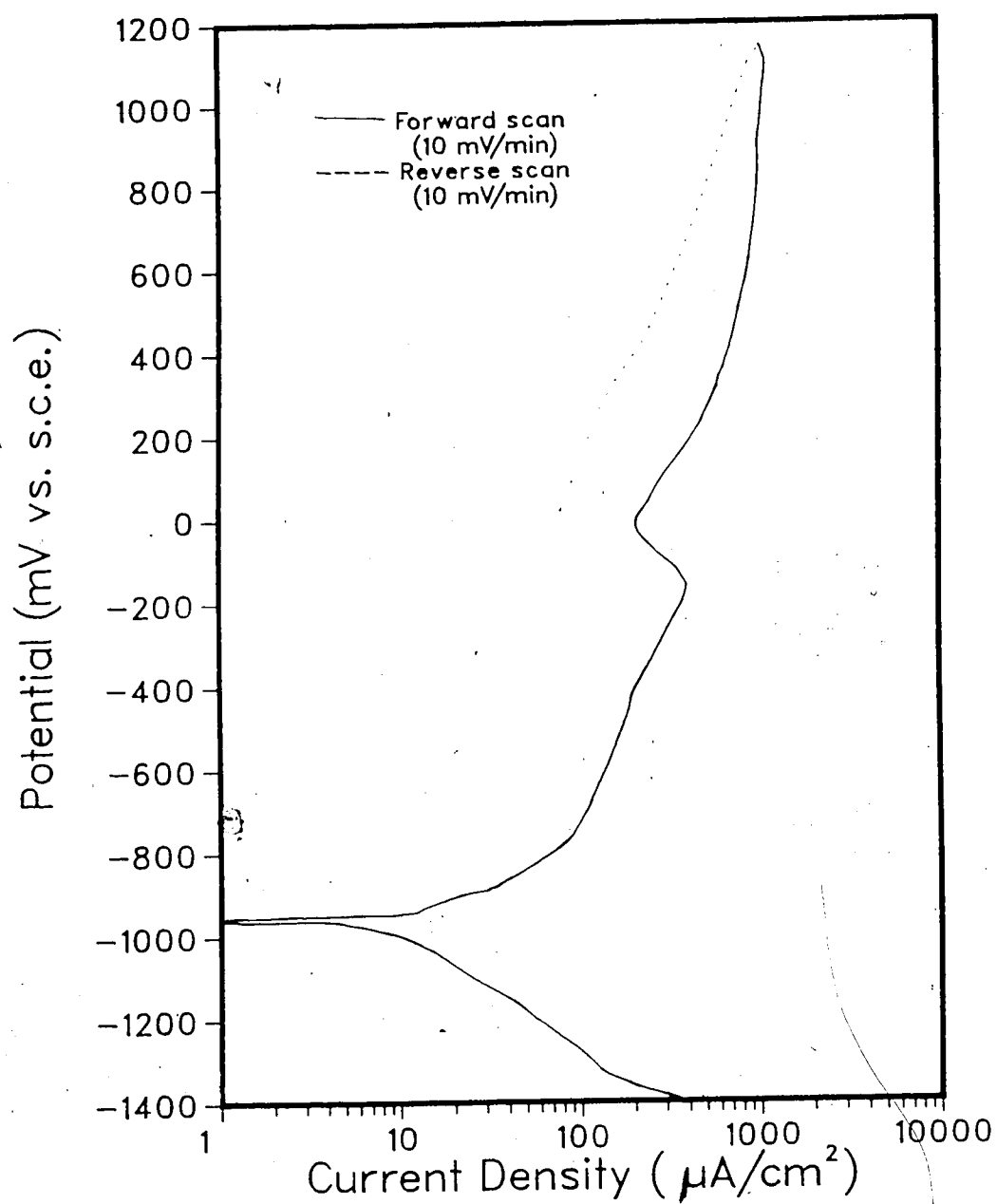


Fig. 70. Potentiodynamic polarization curve in $\text{H}_2\text{O} + \text{CO}_2$ at 200°C .

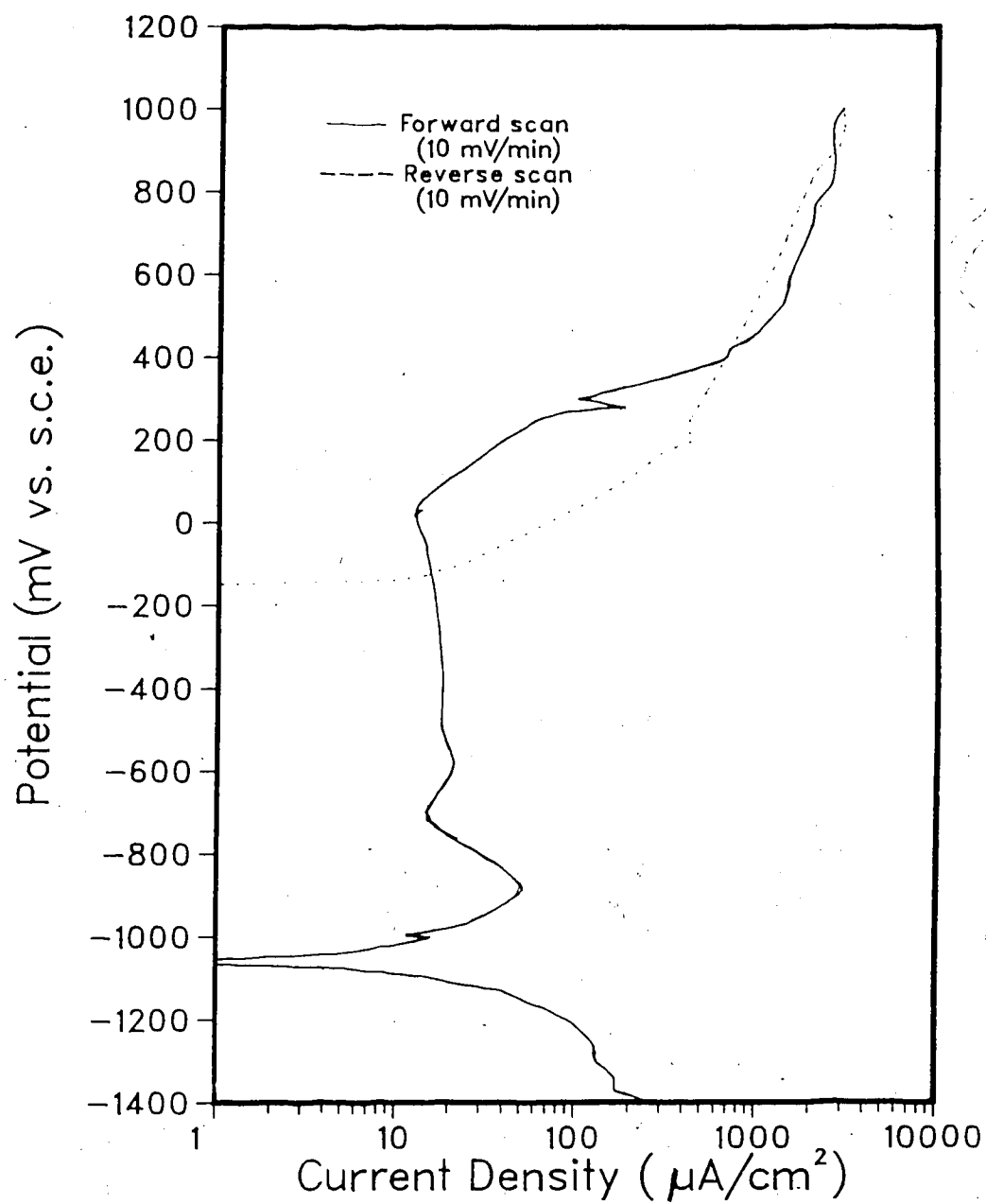


Fig. 71. Potentiodynamic polarization curve in $\text{H}_2\text{O} + \text{CO}_2$ at 250°C .

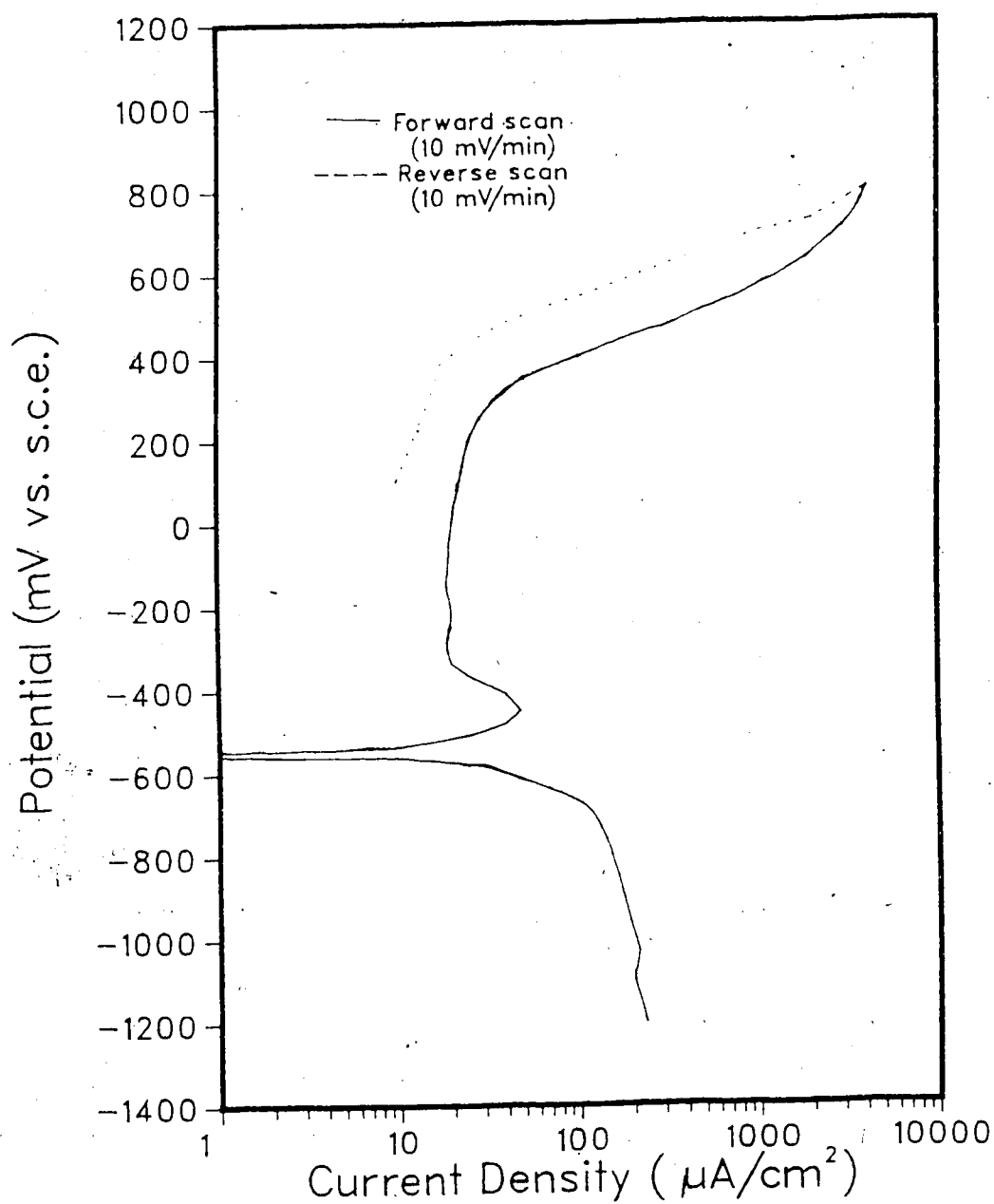


Fig. 72. Potentiodynamic polarization curve in 1 M NH_4HCO_3 + CO_2 at 100°C .

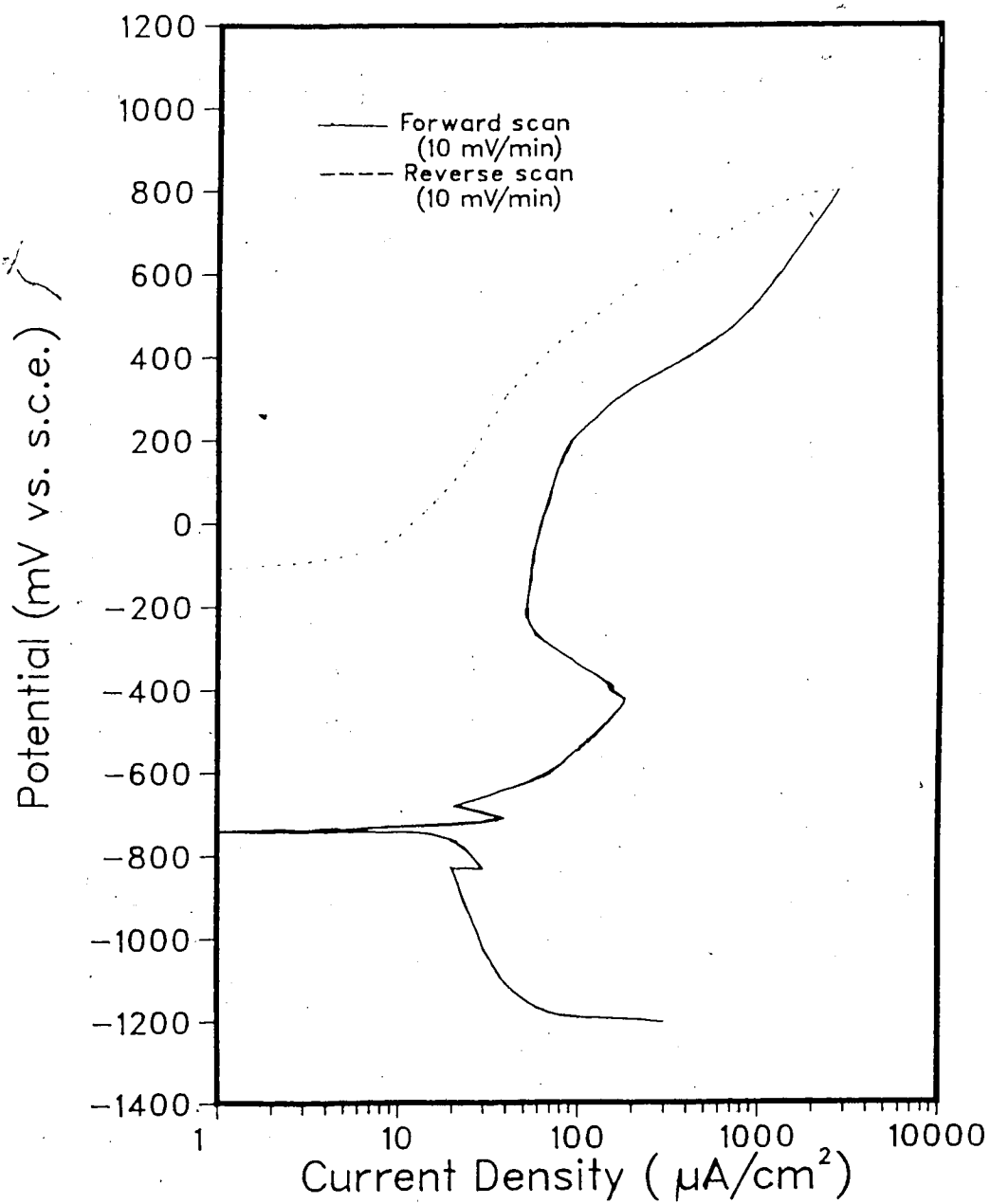


Fig. 73. Potentiodynamic polarization curve in 1 M NH_4HCO_3 + CO_2 at 150°C.

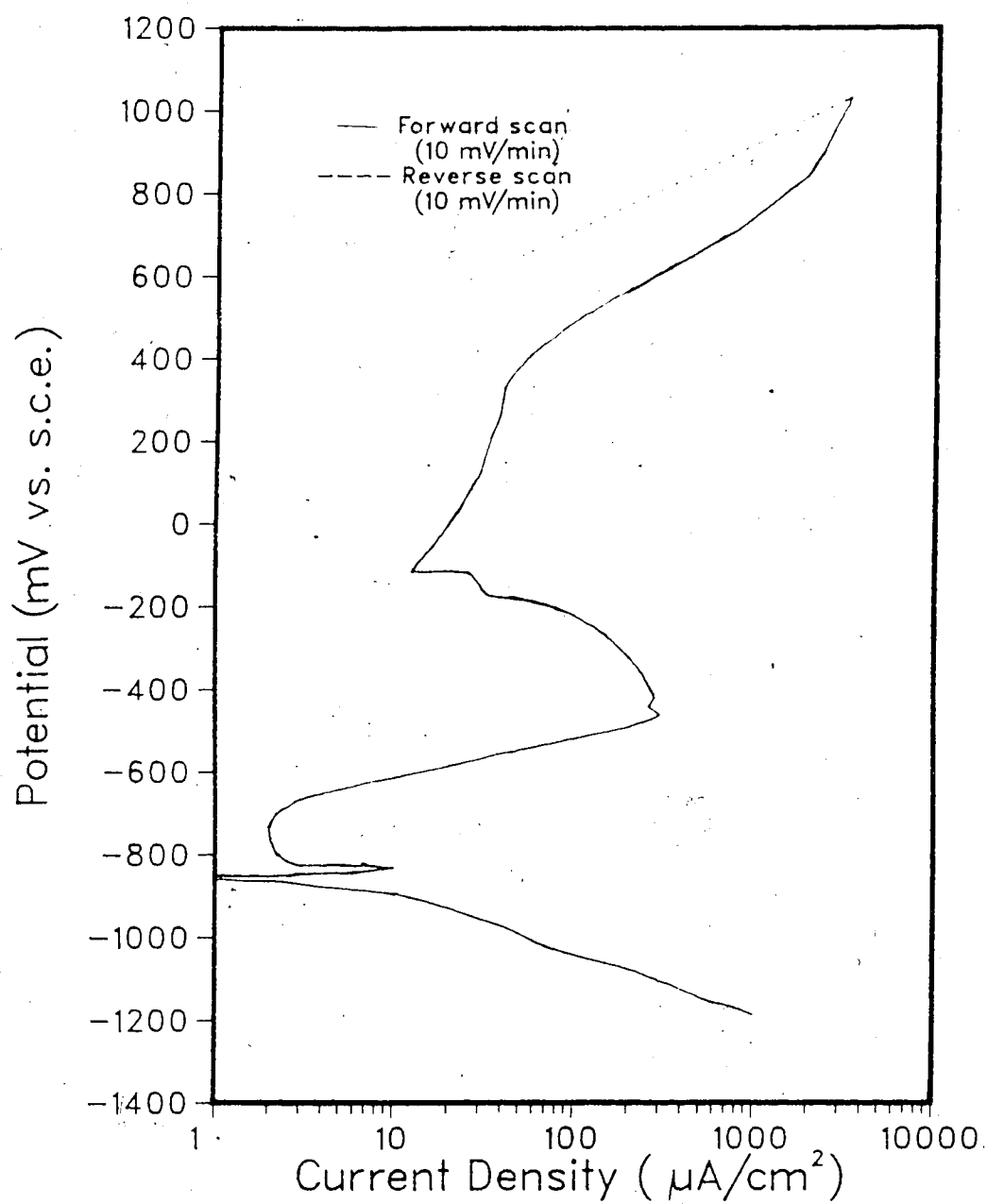


Fig. 74. Potentiodynamic polarization curve in 1 M NH_4HCO_3 + CO_2 at 200°C.

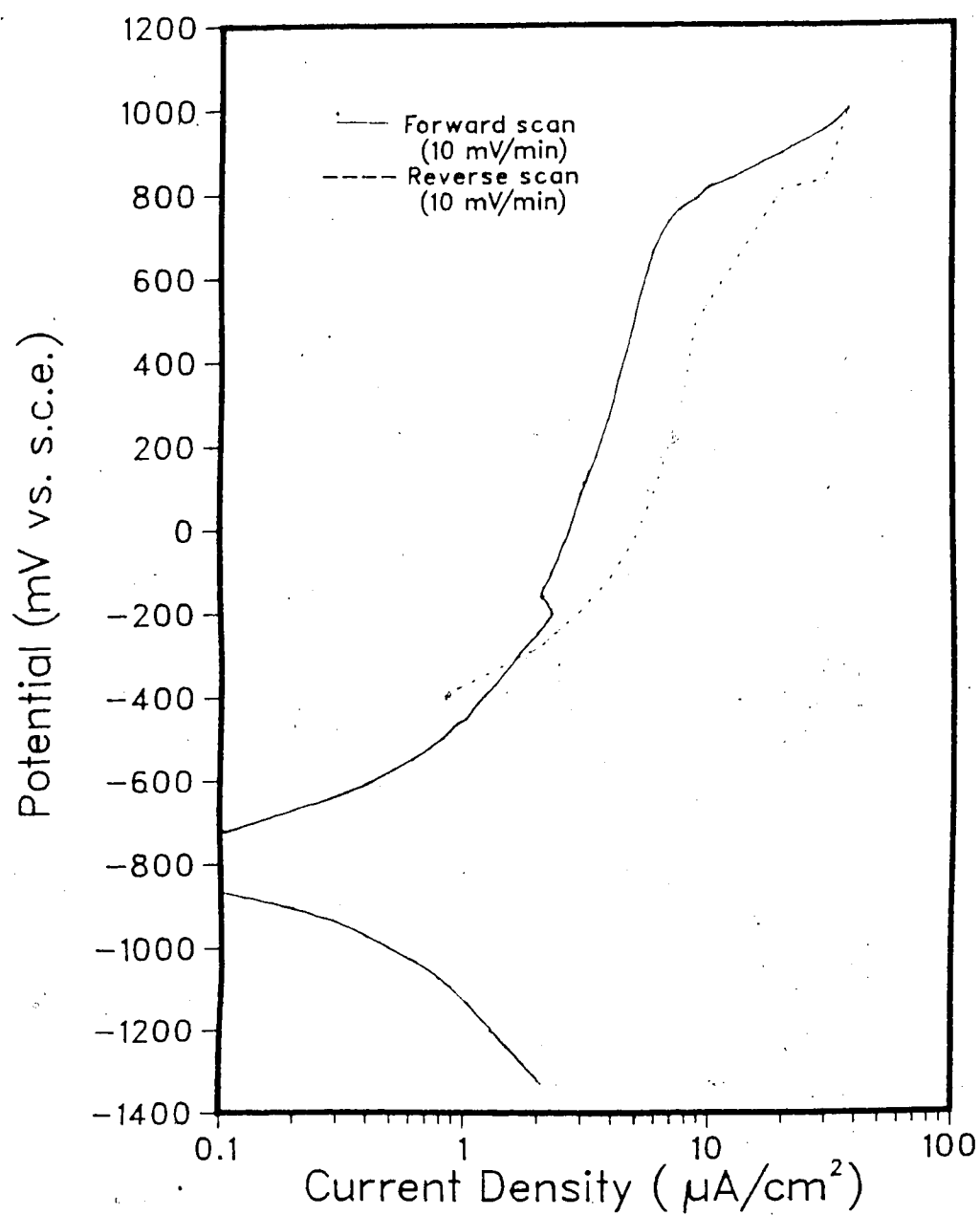


Fig. 75. Potentiodynamic polarization curve in 1 M NH_4HCO_3 + CO_2 at 250°C.

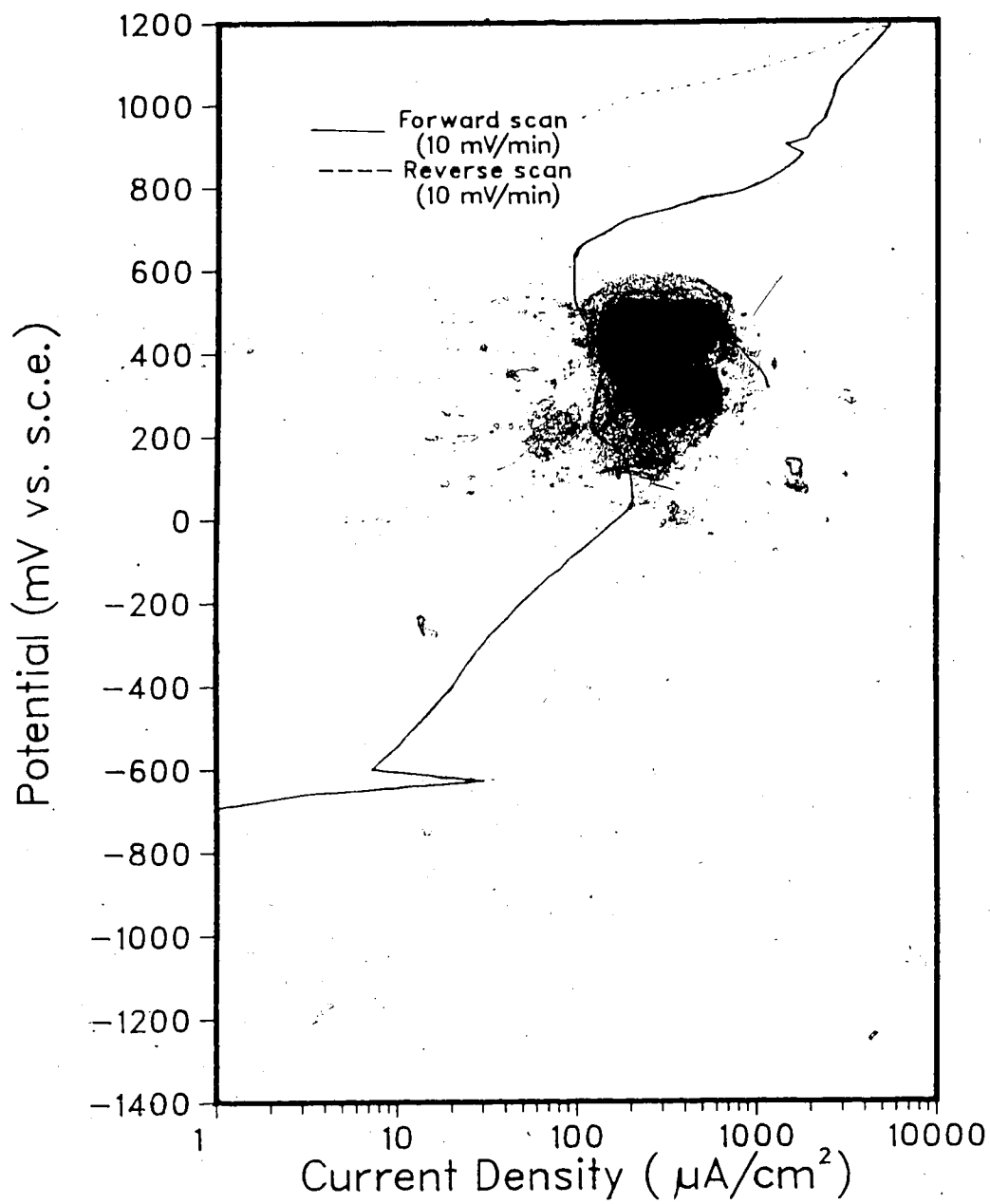


Fig. 76. Potentiodynamic polarization curve in 1 M NH_4HCO_3 at 100°C.

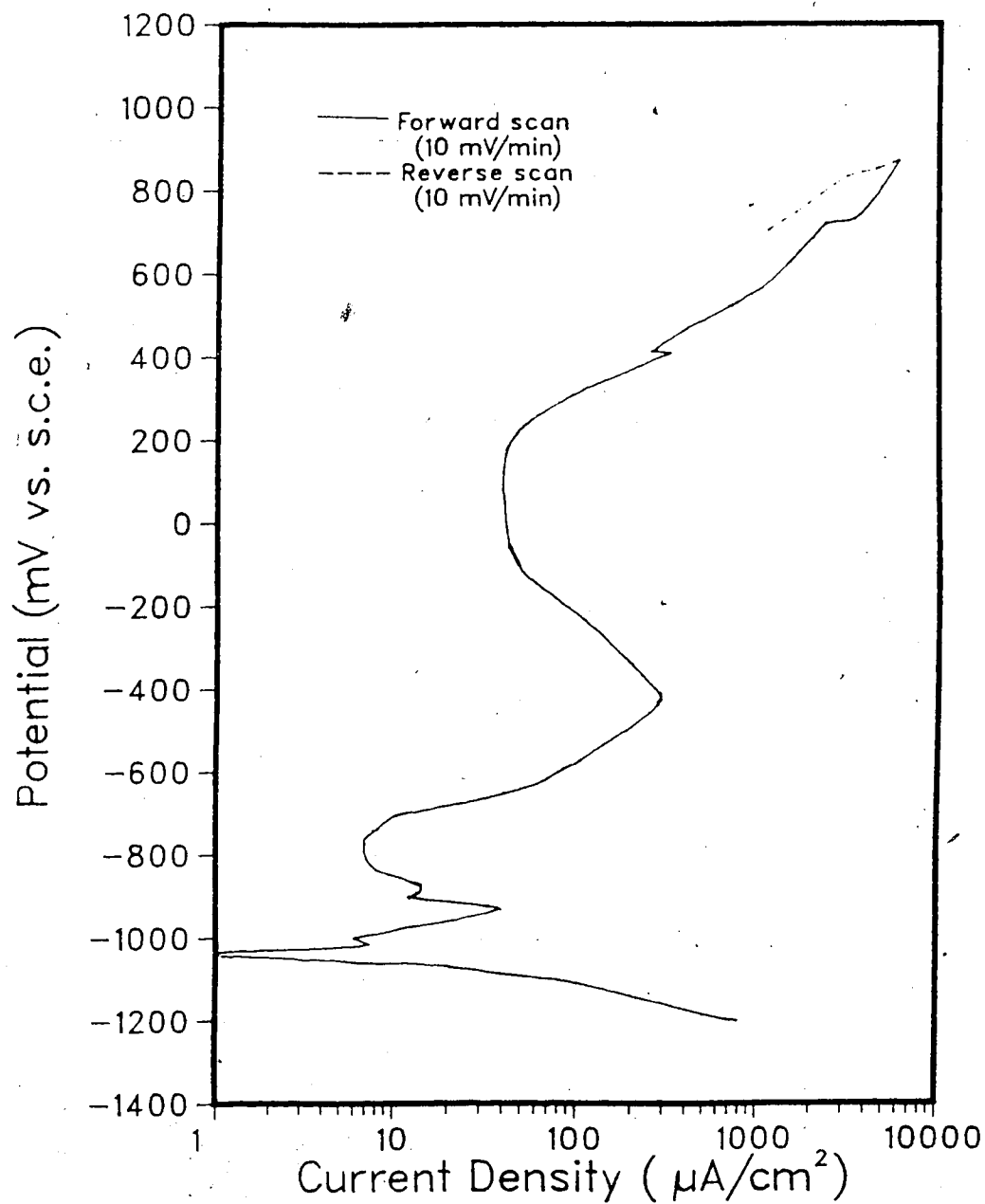


Fig. 77. Potentiodynamic polarization curve in 1 M NH_4HCO_3 at 150°C .

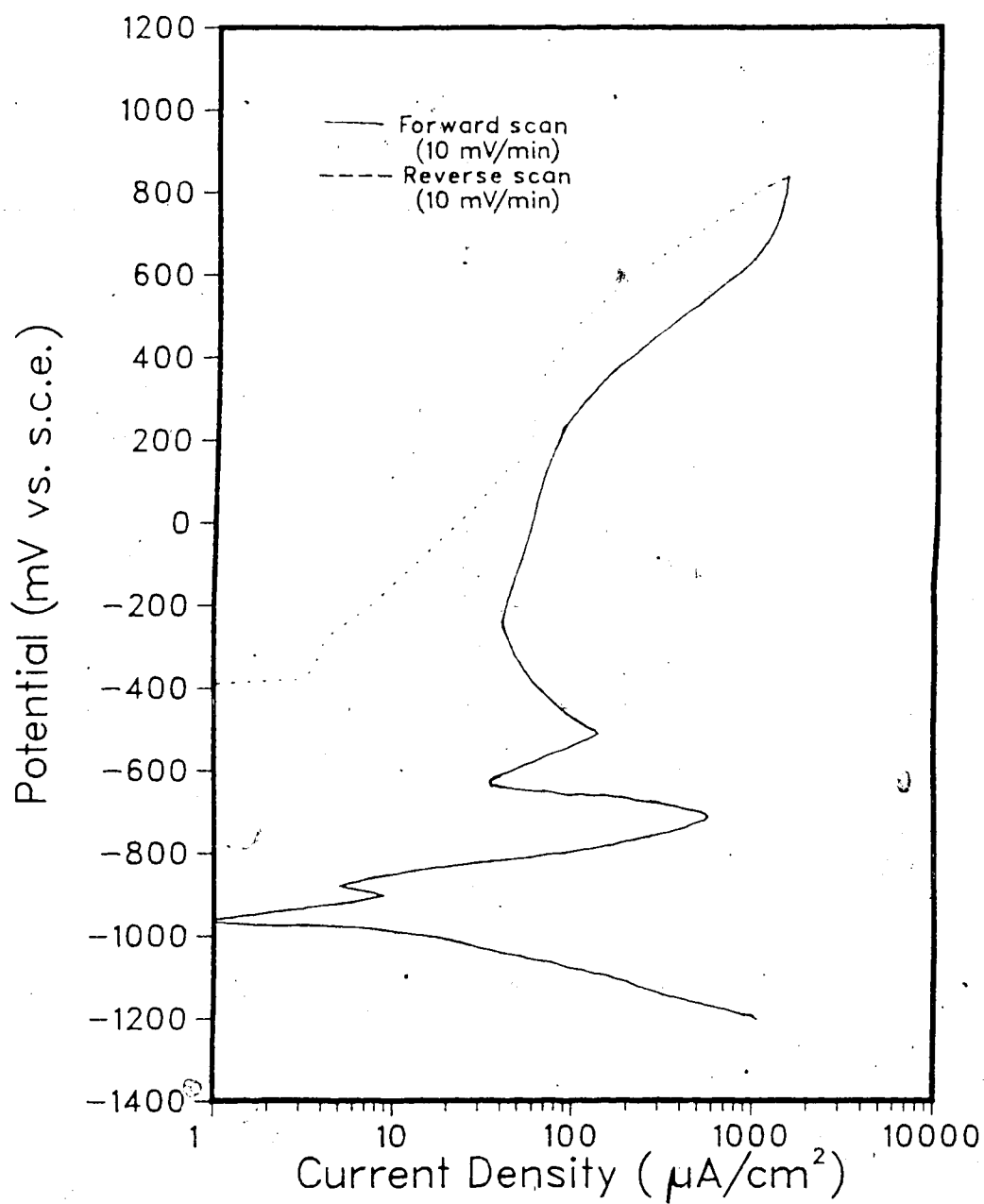


Fig. 78. Potentiodynamic polarization curve in 1 M NH_4HCO_3 at 200°C.

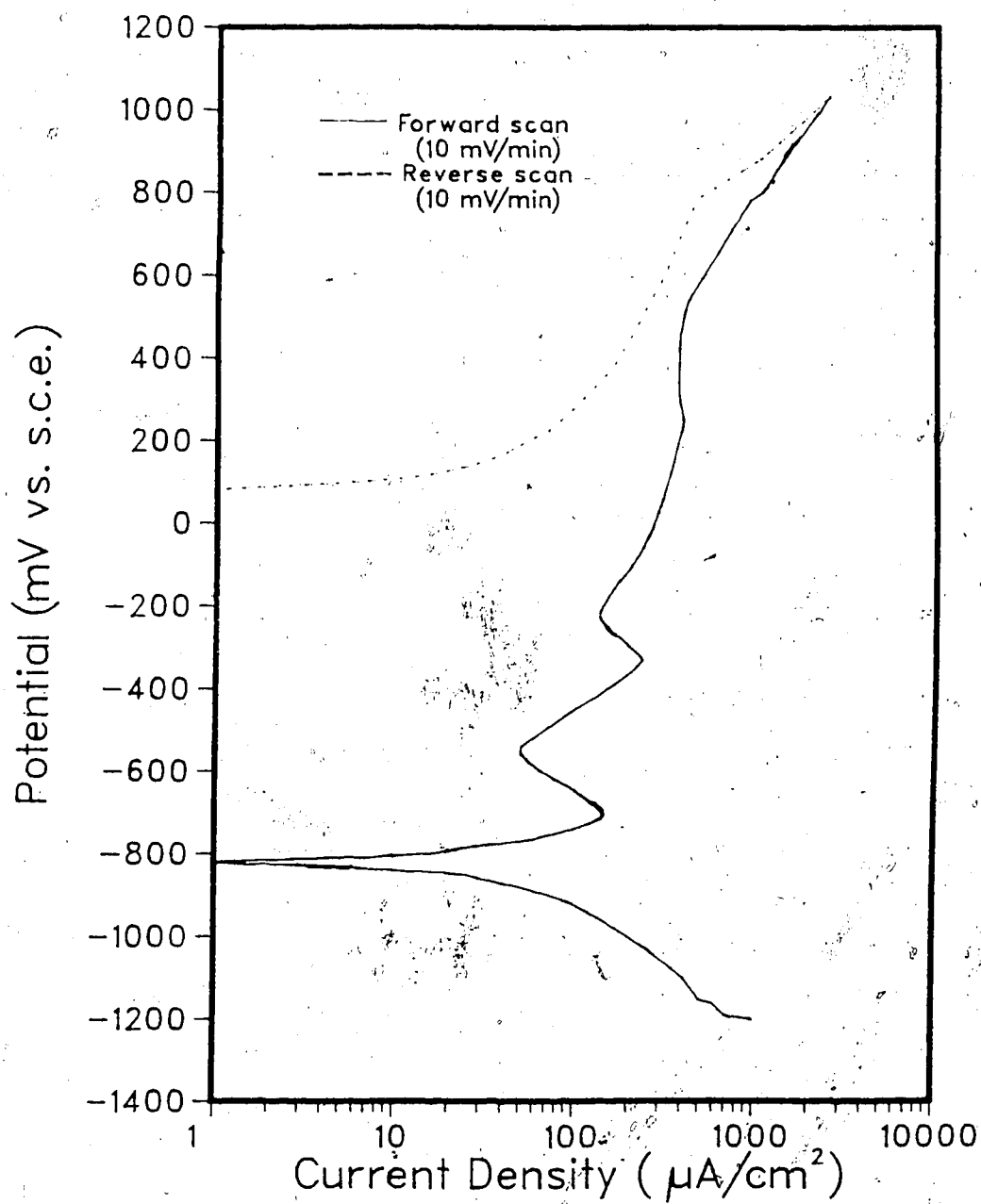


Fig. 79. Potentiodynamic polarization curve in 0.1 M NH_4HCO_3 at 250°C.

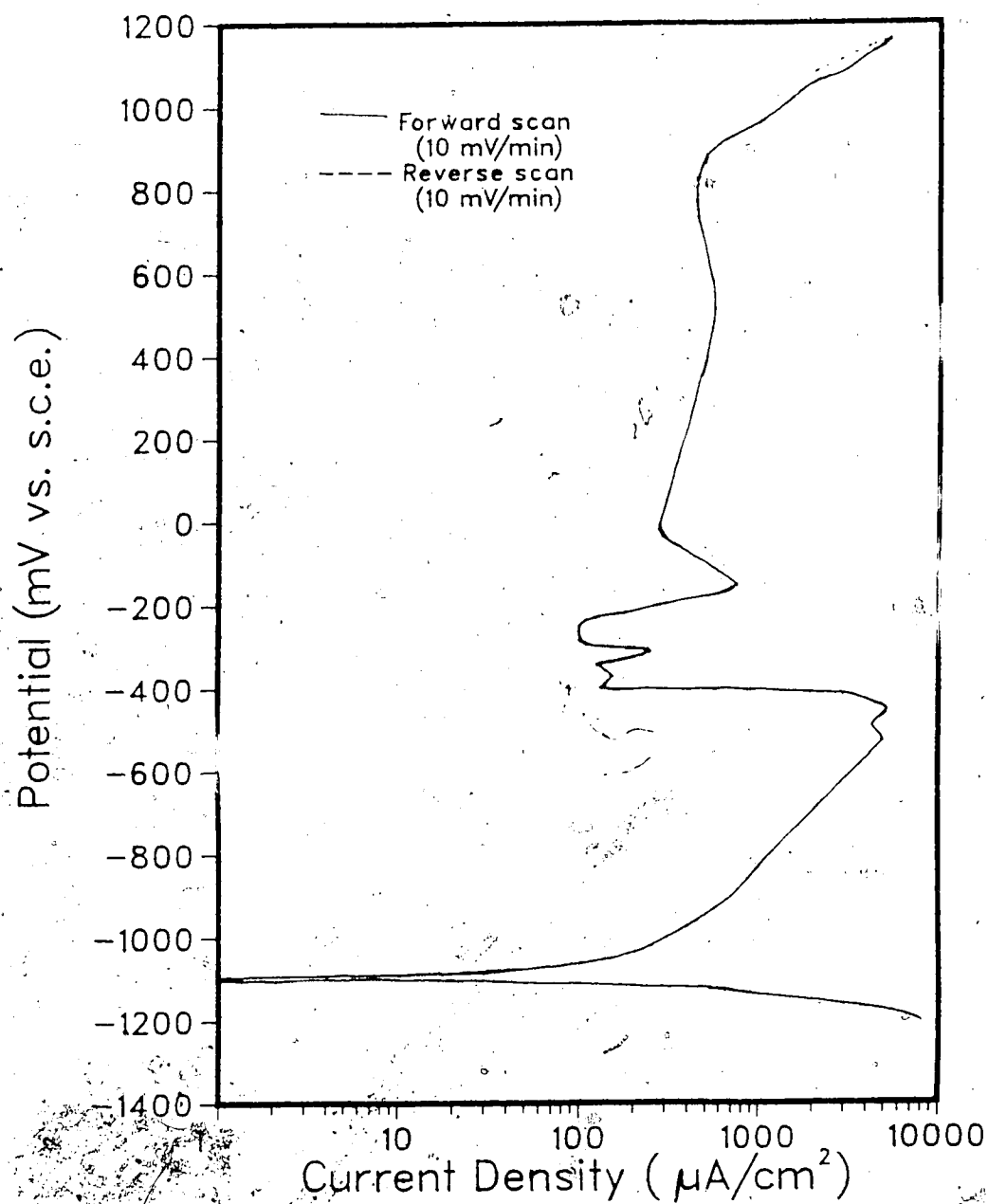


Fig. 80. Potentiodynamic polarization curve in 1 M NH_4HCO_3 + 1 M NH_4OH at 100°C.

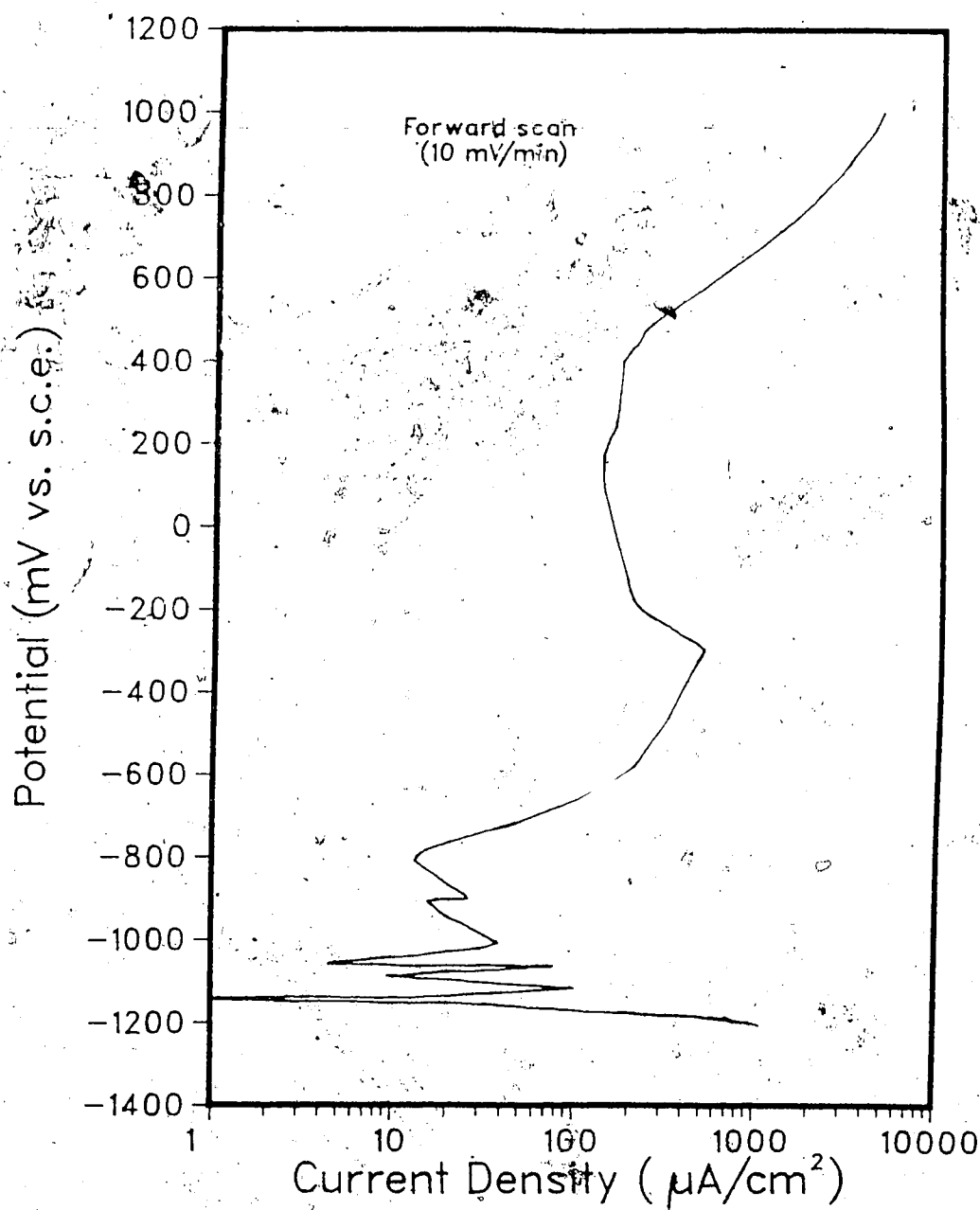


Fig. 81. Potentiodynamic polarization curve in 1 M NH_4HCO_3 +
1 M NH_4OH at 150°C .

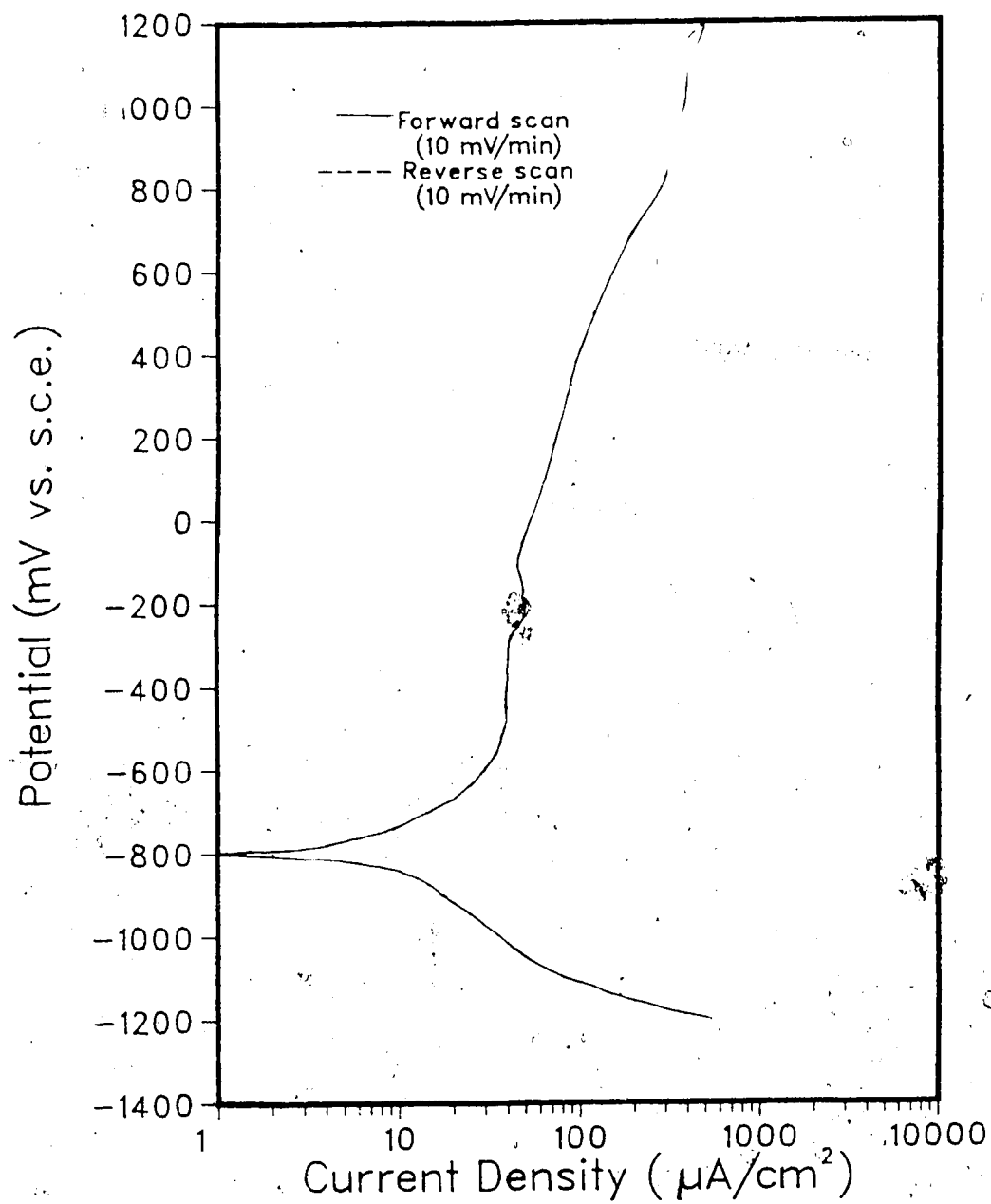


Fig. 82. Potentiodynamic polarization curve in 1 M NH_4HCO_3 +
1 M NH_4OH at 200°C.

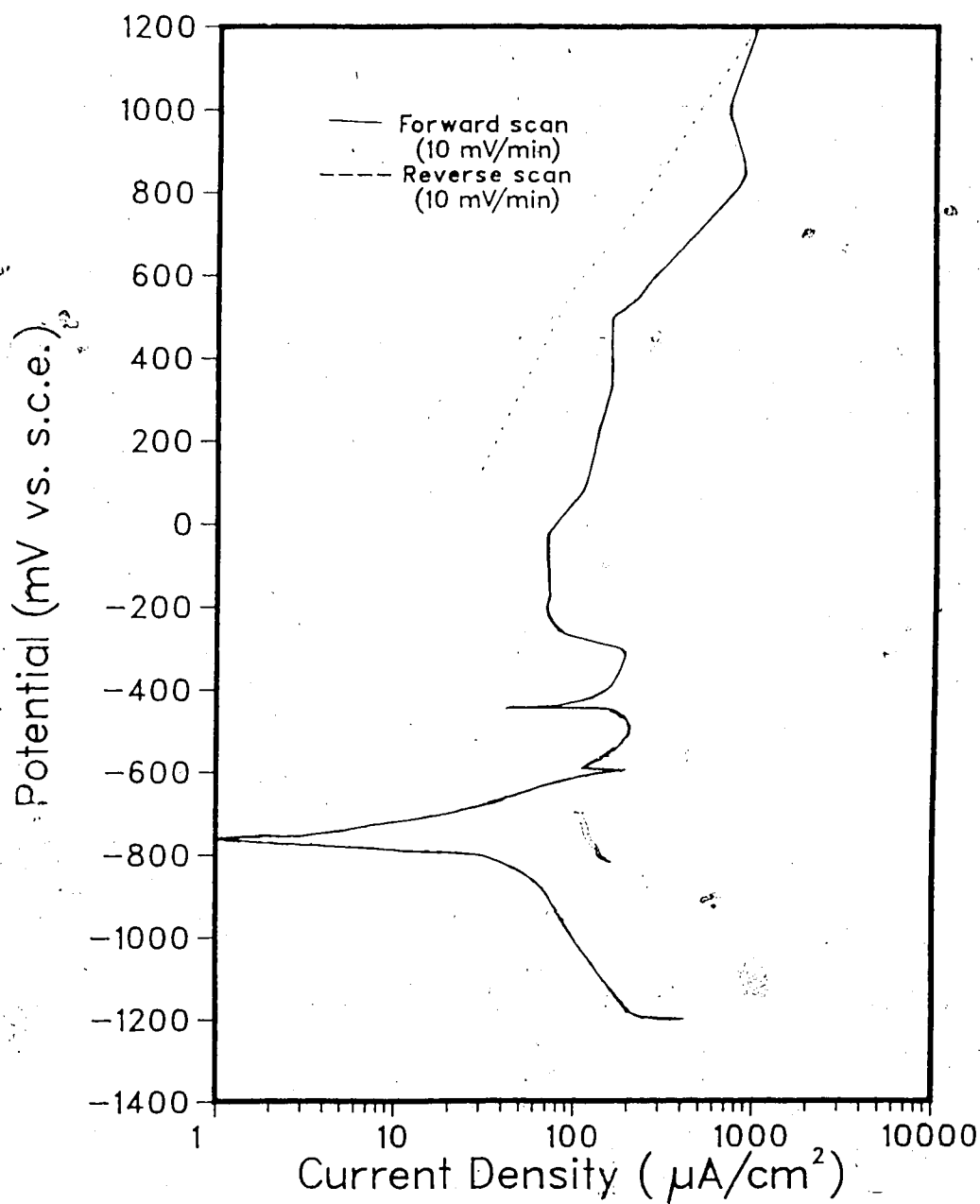


Fig. 83. Potentiodynamic polarization curve in 1 M NH_4HCO_3 +
1 M NH_4OH at 250°C.

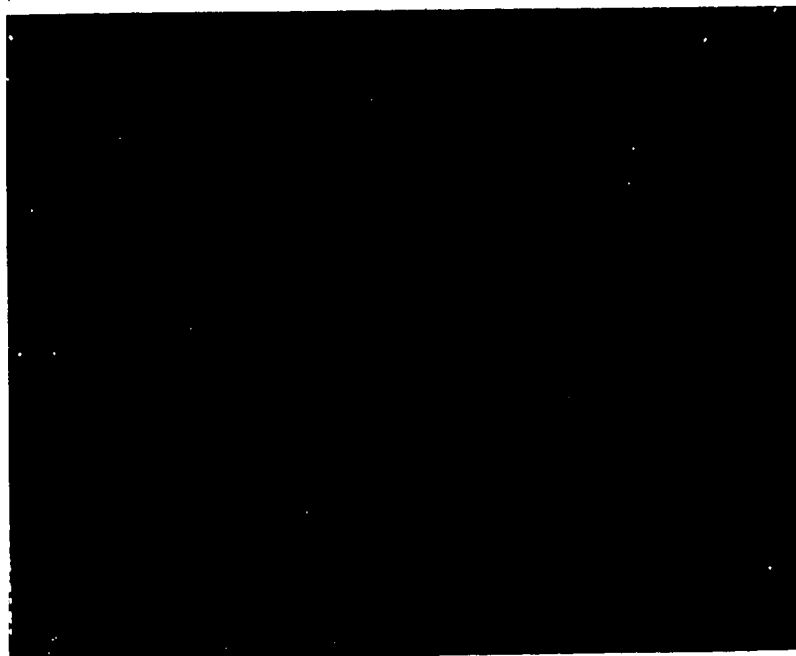


Fig. 84. Pitting on the sample after polarization run in H_2O
+ CO_2 at $100^\circ C$.

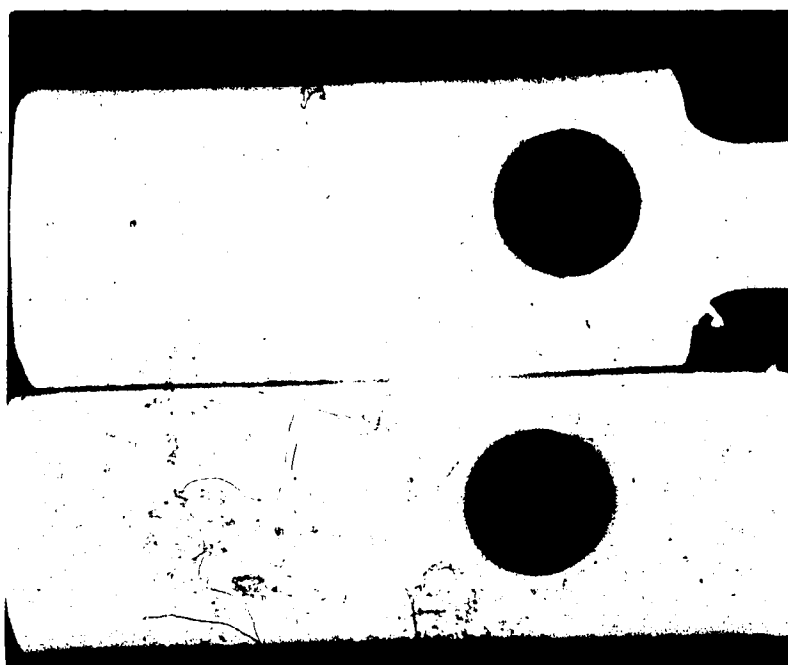


Fig. 85. Corrosion products at $150^\circ C$

- a. Top: mainly hematite at high potential
- b. Bottom: mainly magnetite at low potential.



Fig. 86. Pitting on the U-bend SCC sample in $H_2O + CO_2$ at $150^\circ C$ after one week.

References

1. Timothy Dowd, W., Preface, *Improved Oil Recovery*, Interstate Oil Compact Commission, Oklahoma, p. v (1983).
2. Farouq Ali S.M. and Meldau, R.F., Steam Injection, *Improved Oil Recovery*, Interstate Oil Compact Commission, Oklahoma, p. 311 (1983).
3. Fontana, M.G. and Greene, N.D., Modern Theory, Principles and Applications, Chap. 9 and 10, *Corrosion Engineering*, Second Edn., McGraw-Hill Book Company, p. 297-346 (1978).
4. West, J.M., Surface Films, Chap 4, *Electrodeposition And Corrosion Processes*, Second Edn., Van Nostrand Reinhold Company, p. 80 (1970).
5. Duby, P., Graphical Representation of Equilibria in Aq. Systems at Elevated Temp., *High Temp. and High Press. Electrochemistry in Aq. Solns.*, (Conf. Proc.), Eds.: Jones, D.de G., Slater, J. and Staehle, R.W., Vol. No. NACE-4, p. 353 (1976).
6. Lewis, D., *AE Report 432*, Studsvik, Sweden (1971).
7. Mann, G.M.W., Oxidation of Fe-Base Alloys Containing Less Than 12% Cr in High Temp Aq. Solns., *High Temp. and High Press. Electrochemistry in Aq. Solns.* (Conf. Proc.), Eds.: Jones, D.de G., Slater, J. and Staehle, R.W., Vol. No. NACE-4, p. 34 (1976).
8. Lumsden, J.B. and Staehle, R.W., Temp. Dependence of the Film Covered Electrode, *High Temp. and High Press.*

- Electrochemistry in Aq. Solns. (Conf. Proc.)*, Eds.: Jones, D.de G., Slater, J. and Staehle, R.W., Vol. No. NACE-4, p. 401 (1976).
9. Wagner, C. and Traud, W., *Elektrochem.*, Vol. 44, p. 391 (1938)
 10. Barnartt, S., Electrochemical Nature of Corrosion, *Electrochemical Techniques for Corrosion*, Ed.: Baboian, R., NACE, p. 1 (1977).
 11. Ford, F.P., Stress Corrosion Cracking, *Corrosion Processes*, Ed.: Parkins, R.N., Applied Science Publishers, p. 311 (1982).
 12. Logan, H.L., The Phenomena and Mechanism of SCC of Metals, Chap.1, *The Stress Corrosion of Metals*, John Wiley and Sons Inc. p. 1-42 (1966).
 13. Troiano, A.R., *Trans ASM*, 52, p. 54 (1960).
 14. Bernstein, I.M. and Thompson, A.W., An Evaluation of Hydrogen Embrittlement Mechanisms, *Mechanisms of Environmental Sensitive Cracking Of Materials (Conf. Proc.)*, Eds.: Swann, P.P., Ford, F.P. and Westwood, A.R.C., The Metals Society, p.412 (1977).
 15. Uhlig, H.H., Iron and Steel in Aq. Environments, Chap. 6, *Corrosion and Corrosion Control*, Second Edn., John Wiley & Sons Inc., p. 93-126 (1971).
 16. Uhlig, H.H., Iron and Steel, Section 2, Corrosion in Liquid Media, the Atmosphere and Gases, *The Corrosion Handbook*, Edr.: Uhlig, H.H., John Wiley & Sons Inc., p. 125-143 (1948).

17. Speller, F.N., Influence of Factors External to the Metal, Chap. 5, *Corrosion, Causes and Prevention*, Third Edn., McGraw-Hill Book Co., p. 187 (1951).
18. DeWaard, C. and Milliams, D.E., Carbonic Acid Corrosion of Steel, *Corrosion*, Vol. 31, No. 5, p. 157 (May 1975).
19. Kuznetsov, V.P., Effect of Temp. on Carbonic Acid Corrosion of Steel in the Simulated Condensate of Gas Wells, *Protection Of Metals*, Vol. 17, No. 3, p. 262 (May-June 1981).
20. Uhlig, H.H., Treatment of Water and Steam Systems, Chap. 17, *Corrosion and Corrosion Control*, Second Edn., John Wiley & Sons Inc., p. 272-291 (1971).
21. Hawkins, G.A. and Solberg, H.L., Corrosion by High Temp. Steam, *The Corrosion Handbook* Edr.: Uhlig, H.H., John Wiley & Sons Inc., p. 511-520 (1948).
22. Evans, R.U., Boilers and Condensers-Nuclear Power Plant, *The Corrosion and Oxidation of Metals*, Supplementary to Second Volume, Edwin Arnold, p. 243 (1976).
23. Catchpole, S., The Outlook for Nuclear Power Generation, *Chem. Ind.*, p. 592 (Aug 5, 1972).
24. Gibbs, G.B. and Popple, L.A., Oxidation of Structural Steels in CO₂ Reactors, *Nuclear Energy*, Vol. 21, No. 1, p. 51 (Feb. 1982).
25. Gadiyar, H.S. and Elayathu, N.S.D., Corrosion and Magnetite Growth on C-Steels in Water at 310°C, *Corrosion*, Vol. 36, No. 6, p. 306 (June 1980).

26. Ruther, W.E. and Hart, R.K., Influence of Oxygen on High Temp. Aq. Corrosion of Iron, *Corrosion*, Vol. 19, No. 4, p. 127t (1963).
27. Mungan, N., Carbon dioxide Flooding, Chap 1V, *Improved Oil Recovery*, Interstate Oil Compact Commission, Oklahoma, p. 128 (1983).
28. Nesbitt, H.W., Calculation of the Solubility of CO₂ in NaCl-rich Hydrothermal Solutions Using Regular Solution Equations, *Chemical Geology*, Vol. 43, No. 3/4, p. 319 (March. 1984).
29. Potter, E.C. and Mann, G.M.W., *Br. Corros. Journal*, Vol. 1, p. 26 (1965).
30. Fortune, H.J., Boiler Feed Water Treatment for Corrosion Control-Part2, *Corrosion Technology*, p. 154 (June 1962).
31. Bacon, T.S. and Brown, E.A., *Oil and Gas Journal*, Vol. 41, No. 49, p. 91 (April 15, 1943).
32. Carlson, H.A., *Oil and Gas Journal*, Vol. 45, p. 81 (Dec. 21, 1946).
33. Greenwell, H.E., Rado Loncaric and Byars, H.G., Use of Ammonia to Prevent Casing Corrosion, *Corrosion*, Vol. 11, p. 491t (1955).
34. Thomas, J.G.N., Nurse, T.J. and Walker, R., Anodic Passivation of Iron in Carbonate Solns., *Br. Corros. Journal*, Vol. 5, p. 87 (March 1970)
35. Thomas, J.G.N. and Davies, J.D., Influence of HCO₃⁻ and Cl⁻ Ions on the Stability of Oxide Films on Mild Steel

- in Near-Neutral Solutions, *Br. Corros. Journal*, Vol. 12, No. 2, p. 108 (1977).
36. Davies, D.H. and Burstein, G.T., The Effects of Bicarbonate on the Corrosion and Passivation of Iron *Corrosion*, Vol. 36, No. 8, p.416 (Aug. 1980).
37. Sutcliffe, J.M., Fessler, R.R., Boyd, W.K. and Parkins, R.N, SCC of Steel in Carbonate Solns., *Corrosion* , Vol. 28, No. 8, p. 313 (Aug. 1979).
38. Berry, W.E. and Payer, J.H., Internal Stress-Corrosion Cracking by Aqueous Solutions of CO and CO₂., *6th Symposium, Line Pipe Research (Oct.-Nov. 1979)*, AGA Catalogue No. L 30175.
39. Gerasimov, V.V., A Study of the Corrosion and Electrochemical Behavior of Al-Alloys in Aq. Media at Temp. to 300 C, *High Temp. and High Press. Electrochemistry in Aq. Solns. (Conf. Proc.)*, Eds.: Jones, D.de G., Slater, J. and Staehle, R.W., Vol. No. NACE-4, p. 106 (1976).
40. Bogearsts, W.F. and Van Haute, A.A. High. Temp. Corrosion Testing-A Breakthrough in Electrochemical Techniques for High Temp. Pressurized Solns., *International Conf. on Metallic Corrosion (Conf. Proc.)*, Vol. 4, p. 169 (June 1984).